ISSN 0711-6659

canadian acoustics
acoustique canadienne

Journal of the Canadian Acoustical Association - Journal de l'Association Canadienne d'Acoustique

MARCH 2012 | MARS 2012
Volume 40 -- Number 1 | Volume 40 -- Numéro 1

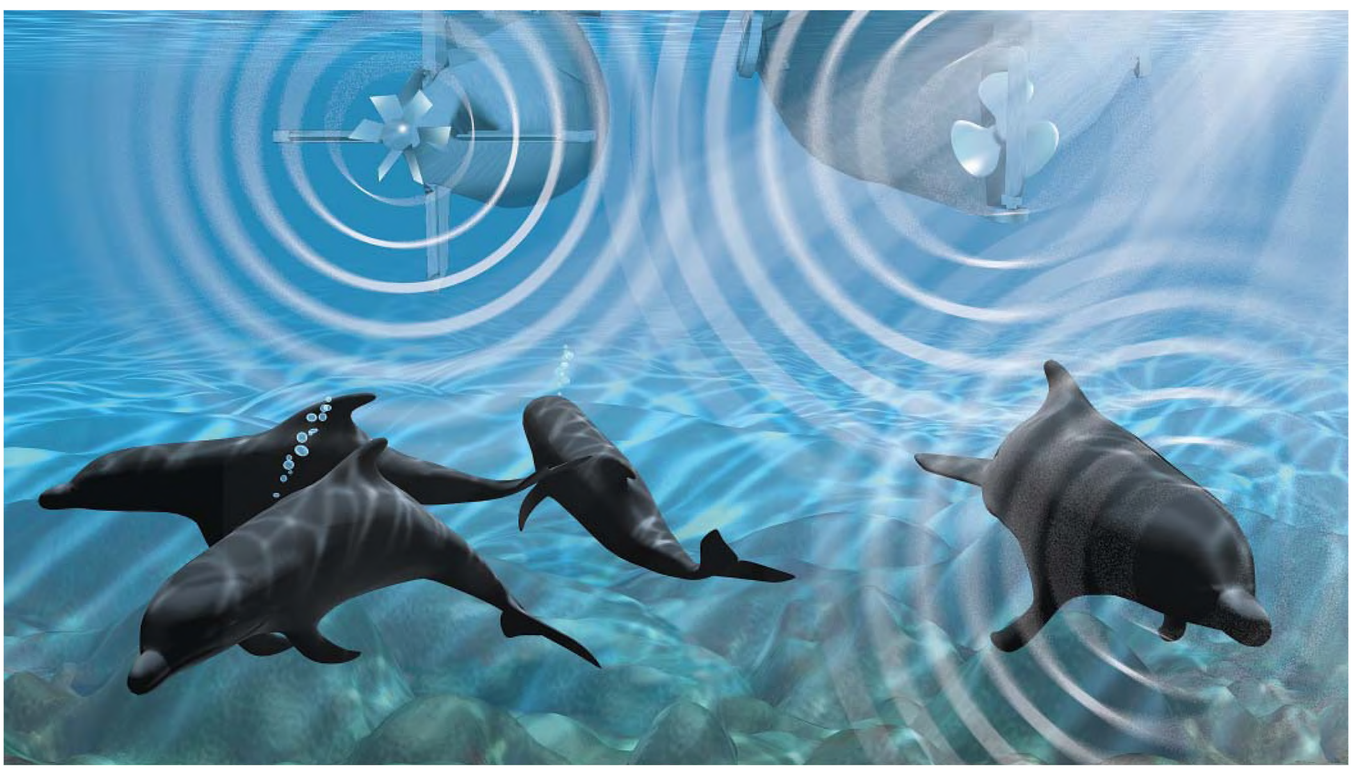

canadian acoustics
acoustique canadienne

THE CANADIAN ACOUSTICAL ASSOCIATION
P.O. BOX 1351, STATION "F"
TORONTO, ONTARIO M4Y 2V9

L'ASSOCIATION CANADIENNE D'ACOUSTIQUE
C.P. 1351, SUCCURSALE "F"
TORONTO, ONTARIO M4Y 2V9

CANADIAN ACOUSTICS publishes refereed articles and news items on all aspects of acoustics and vibration. Articles reporting new research or applications, as well as review or tutorial papers and shorter technical notes are welcomed, in English or in French. Submissions should be sent directly to the Editor-in-Chief. Complete instructions to authors concerning the required camera-ready copy are presented at the end of this issue.

CANADIAN ACOUSTICS is published four times a year - in March, June, September and December. The deadline for submission of material is the first day of the month preceeding the issue month. Copyright on articles is held by the author(s), who should be contacted regarding reproduction. Annual subscription: $35 (student); $80 (individual, institution); $350 (sustaining - see back cover). Back issues (when available) may be obtained from the CAA Secretary - price $20 including postage. Advertisement prices: $350 (full page- $1200 for four issues); $200 (half page - $700 for four issues); $150 (quarter page - $500 for four issues). Contact the Associate Editor (advertising) to place advertisements. Canadian Publication Mail Product Sales Agreement No. 0557188.

ACOUSTIQUE CANADIENNE publie des articles arbitrés et des informations sur tous les domaines de l'acoustique et des vibrations. On invite les auteurs à soumettre des manuscrits, rédigés en français ou en anglais, concernant des travaux inédits, des états de question ou des notes techniques. Les soumissions doivent être envoyées au rédacteur en chef. Les instructions pour la présentation des textes sont exposées à la fin de cette publication.

ACOUSTIQUE CANADIENNE est publiée quatre fois par année - en mars, juin, septembre et décembre. La date de tombée pour la soumission de matériel est fixée au premier jour du mois précédant la publication d'un numéro donné. Les droits d'auteur d'un article appartiennent à (aux) auteur(s). Toute demande de reproduction doit leur être acheminée. Abonnement annuel: $35 (étudiant); $80 (individuel, société); $350 (soutien - voir la couverture arrière). D'anciens numéros (non-épuisés) peuvent être obtenus du Secrétaire de l'ACA - prix: $20 (affranchissement inclus). Prix d'annonces publicitaires: $350 (page pleine - $1200 pour quatre publications); $200 (demi page - $700 pour quatre publications); $150 (quart de page - $500 pour quatre publications). Contacter le rédacteur associé (publicité) afin de placer des annonces. Société canadienne des postes - Envois de publications canadiennes - Numéro de convention 0557188.

GUEST EDITORIAL / EDITORIAL INVITÉ

This issue of Canadian Acoustics represents a special focus on Marine Acoustics. Acoustics plays a vital role in ocean science and technology since seawater is opaque to electromagnetic radiation (light, radio waves, microwaves), while sound is transmitted efficiently to long (in some cases, global) ranges. Hence, acoustics is used underwater for remote sensing, remote control, detection/localization, navigation, and communication, among many other applications. Further, there is an increasing realization that marine mammals and other sea life are sensitive to sound in the ocean and must be protected from disturbance and harm.

In Canada, marine acoustics activities are driven by environmental, technological, military, and geopolitical concerns, and involve research and development in government, industry, and academia. Of note is Canadian work in monitoring underwater industrial and shipping noise for marine mammal protection; acoustic fish stock assessment and tracking; acoustical oceanography to study ocean circulation and physical properties of the water column, seabed, and sea ice; and development of acoustic localization, tracking, and homing systems for autonomous underwater vehicles (AUVs). A noteworthy recent application of the latter is the use of AUVs under Arctic sea ice to map the seabed, in otherwise inaccessible regions, in support of Canadian sovereignty claims under the United Nations Convention on the Law of the Sea (work that set several world records for AUV use under ice in the process).

Although this special issue represents only an infinitesimal sample of marine acoustics efforts across Canada (and one paper from the U.S.), the authors and guest editors include representation from the three pillars of marine acoustics: Government (Garry Heard, Defence R&D Canada-Atlantic; Paul Gendron, Space and Naval Warfare Center Pacific, USA), Industry (Alexander MacGillivray and Melanie Austin, JASCO Applied Sciences; Duane Watson and Greg VanSlyke, Omnitech Electronics) and Academia (Stan Dosso, Dugald Thomson, Ross Chapman, et al., University of Victoria). Further, the six papers included here cover a wide range of topics including:

- mathematical advances in acoustic source localization,
- modelling the accuracy of AUV acoustic positioning systems,
- source characteristics of underwater air-gun arrays used in marine seismic exploration,
- long-range measurement and modelling of air-gun sound levels off the BC coast to investigate possible impacts on sea life,
- development of distributed digital sensor arrays for underwater acoustics applications using technology originally developed for hand-held computing devices and smart phones, and

Ce numéro de l'Acoustique Canadienne porte une attention particulière sur l'acoustique sous-marine. L'acoustique joue un rôle essentiel dans la science et les technologies océaniques puisque l'eau de mer est opaque au rayonnement électromagnétique (lumière, ondes radio, micro-ondes), tandis que le son est transmis de manière efficace sur de longues distances (dans certains cas, même globale). Par conséquent, l'acoustique sous-marine est utilisée pour la télédétection, le contrôle à distance, la détection et la localisation, la navigation et la communication, entre autres applications. En outre, il y a une prise de conscience croissante que les mammifères marins et autres animaux marins sont sensibles aux sons présents dans l'océan et qu'ils doivent être protégés contre ces perturbations et les dommages qui en résultent

Au Canada, les activités acoustiques sous-marines sont motivées par des préoccupations environnementales, technologiques, militaires et géopolitiques, et impliquent des activités de recherche et de développement au sein du gouvernement, de l'industrie et des universités. Mentionnons le travail du Canada pour la protection des mammifères marins via la surveillance sous-marine du bruit industriel ou lié au trafic maritime; les travaux acoustiques pour l'évaluation et le suivi des stocks de poissons; les travaux en acoustique océanographique pour l'étude de la circulation océanique et des propriétés physiques de la colonne d'eau, des fonds marins et des glaces marines ; les travaux pour le développement de la localisation acoustique et des systèmes de suivi à tête chercheuse pour les véhicules autonomes sous-marins (AUVs). Une application remarquable de ces AUVs est leur utilisation récente sous la banquise arctique pour la cartographie des fonds marins, dans les régions qui seraient autrement inaccessibles, servant ainsi d'appui aux revendications canadiennes de souveraineté en vertu de la Convention des Nations Unies sur le droit de la mer (tâche qui, soit dit en passant, a permis l'établissement de nouveaux records mondiaux pour l'utilisation d'AUV sous la glace).

Bien que ce numéro spécial ne représente qu'un échantillon infime des efforts entrepris en acoustique sous-marine à travers le Canada (complété par un article soumis depuis les États-Unis), les auteurs et les éditeurs invités incluent des représentants des trois acteurs de l'acoustique marine, soient les acteurs gouvernementaux (Garry Heard, Defence R&D Canada-Atlantic; Paul Gendron, Space and Naval Warfare Center Pacific, USA), industriels (Alexander MacGillivray et Melanie Austin, JASCO Applied Sciences; Duane Watson et Greg VanSlyke, Omnitech Electronics) et académiques (Stan Dosso, Dugald Thomson, Ross Chapman, et col., University of Victoria). En outre, les six documents inclus ici couvrent un large éventail de sujets, notamment:

- les avancées mathématiques en matière de localisation des sources acoustiques,
- la modélisation de la précision des systèmes de positionnement acoustique des AUVs,

- modelling the ocean acoustic response function for underwater acoustic communications.

The Marine Acoustics community in Canada has traditionally been a strong supporter of the CAA. Over the years, many members of this community have served on the CAA Board of Directors and Executive. The Canadian organizers of the 12th ICA Symposium on Underwater Acoustics donated the conference proceeds to the CAA to establish the Fessenden Student Prize in Underwater Acoustics, an annual award for the top graduate student in the field at a Canadian institution. The marine acoustics groups at UVic and JASCO were/are major organizers of the 2009 and 2012 CAA meetings in Victoria and Banff, respectively, while DRDC Atlantic hosted the 2006 meeting in Halifax. A previous special issue of Canadian Acoustics focused on Detection and Localization of Marine Mammals (June, 2004).

We hope that you will find this special issue on Marine Acoustics to be an interesting read, and that it will serve to illustrate the challenges and innovations in the field for our colleagues who practice acoustics on dry land!

Stan Dosso and Garry Heard
Guest Editors

- les caractéristiques de source des canons à air utilisés dans les explorations sismiques sous-marines,
- la mesure et la modélisation des niveaux sonores à grande distance des canons à air au large de la côte de la C.-B. afin d'en étudier les impacts possibles sur la vie marine,

  le développement, à l'aide de technologie développée à l'origine pour les appareils informatiques portatifs et les téléphones intelligents, de réseaux de capteurs numériques distribués pour des applications d'acoustique sous-marine
- la modélisation de la réponse acoustique de l'océan à des fins de communications acoustiques entre sous-marins.

La communauté d'acoustique sous-marine au Canada a toujours été un ardant partisan de l'ACA. Au fil des ans, de nombreux membres de cette communauté ont siégé aux conseil d'administration et comités exécutifs de l'ACA. Les organisateurs canadiens du 12e Symposium ICA sur l'Acoustique sous-marine ont fait don des recettes de conférence à l'ACA afin d'octroyer le Prix étudiant Fessenden en acoustique sous-marine, un prix annuel d'excellence pour étudiant diplômé dans ce domaine par une institution canadienne. Les groupes de recherche en acoustique sous-marine de l'Université de Victoria et de la compagnie JASCO ont été les principaux organisateurs des congrès de 2009 et 2012 de l'ACA à Victoria et à Banff, respectivement, tandis que DRDC Atlantique a accueilli la réunion de 2006 à Halifax. Un numéro thématique précédent du journal Acoustique Canadienne était consacré à la détection et à la localisation des mammifères marins (juin 2004).

Nous espérons que vous trouverez la lecture de ce numéro spécial sur l'acoustique sous-marine intéressante, et que ce numéro réussira à bien illustrer les défis et les innovations dans le domaine de collègues qui pratiquent, eux, l'acoustique sur la terre ferme!

Stan Dosso et Garry Heard
Rédacteurs invités

ACOUSTIC LOCALIZATION OF AN UNKNOWN NUMBER OF SOURCES IN AN UNCERTAIN OCEAN ENVIRONMENT

Stan E. Dosso
School of Earth and Ocean Sciences
University of Victoria, Victoria BC Canada V8W 3Y2
sdosso@uvic.ca

ABSTRACT

This paper develops a new approach to simultaneous localization of an unknown number of ocean acoustic sources when properties of the environment are poorly known, based on minimizing the Bayesian information criterion (BIC) over source and environmental parameters. A Bayesian formulation is developed in which water-column and seabed parameters, noise statistics, and the number, locations, and complex strengths (amplitudes and phases) of multiple sources are considered unknown random variables constrained by acoustic data and prior information. The BIC, which balances data misfit with a penalty for extraneous parameters, is minimized using hybrid optimization (adaptive simplex simulated annealing) over environmental parameters and Gibbs sampling over source locations. Closed-form maximum-likelihood expressions for source strength and noise variance at each frequency allow these parameters to be sampled implicitly, substantially reducing the dimensionality of the inversion. Gibbs sampling and the implicit formulation provide an efficient scheme for adding and deleting sources during the optimization. A simulated example is presented which considers localizing a quiet submerged source in the presence of two loud interfering sources in a poorly-known shallow-water environment.

SOMMAIRE

Cet article développe une nouvelle approche de localisation simultanée d'un nombre inconnu de sources acoustiques sous-marine lorsque les propriétés de l'environnement de l'océan sont mal connues, fondée sur la minimisation du Critére d'Information Baysien (CIB) sur la source et les paramètres environnementaux. Une formulation Bayésienne est développé pour que les paramètres de la colonne d'eau et des fonds marins, les statistiques du bruit, et le nombre, lieux et points forts complexes (amplitude et phase) de multiples sources sont considéré comme variables inconnues aléatoires forcée par les données acoustiques et information préexistante. Le CIB, qui stabilise les résultats inadapté avec une pénalité pour les paramètres erronés, est minimisé en utilisant l'optimisation adaptative hybrides simulation d'annelage adaptif simplex pour les paramètres environnementaux et l'échantillonnage de Gibbs pour les endroits de source. Des expressions de vraisemblance-maximal pour les intensités de source et la variance de bruit à chaque fréquence permet les paramètres à être échantillonnés implicitement, en réduisant la dimensionnalité de l'inversion. L'échantillonnage de Gibbs et la formulation implicite fournis une plateforme efficace pour l'ajout et la suppression des sources lors de l'optimisation. Un exemple simulé est présenté qui considère la localisation d'une source tranquille immergé dans la présence de deux sources d'interfrence forte.

1. INTRODUCTION

Matched-field processing methods have been applied extensively to localize an acoustic source in the ocean based on matching acoustic fields measured at an array of hydrophones with replica fields computed via a numerical propagation model for a grid of possible source locations [1]–[6]. Two challenging problems in matched-field processing involve source localization when properties of the environment (water column and seabed) are poorly known, and localization of multiple sources. Both issues are addressed in this paper.

The ability to localize an acoustic source is strongly affected by available knowledge of the ocean environment, such that environmental uncertainty often represents the limiting factor for localization in shallow water [7]–[9]. To account for environmental uncertainty in localization, unknown environmental parameters can be included, in addition to the source location, in an augmented inverse problem, and the misfit between measured and modelled fields minimized over all parameters, an approach referred to as focalization [10]–[14].

Considering multiple-source localization in a known environment, a number of variants of the matched-field method have been proposed based on eigenvector decompositions and/or specialized misfit functions [15]–[18]. In addition, iterative methods have been applied for localizing a weak source based on sequentially identifying and canceling stronger interfering sources [19]. An approach to simultaneously localize multiple sources in a known environment was developed by Michalopoulou [20] based on a Bayesian formulation and Gibbs sampling the posterior probability density over source locations, complex source strengths (amplitudes and phases), and noise variance, to provide a collection of models from which the best estimate can be selected. This approach was shown to be superior to coherent interference cancellation using a series of single-frequency Monte Carlo simulations. In addition, it was shown that the approach can be extended to sample over the number of sources. However, it was also shown that the approach is highly sensitive to environmental uncertainties, with even small environmental mismatch precluding successful localization.

Recently, Dosso and Wilmut [21] developed a Bayesian focalization approach for simultaneous localization of a fixed number of sources in an unknown environment. This is a computationally demanding problem, and the efficiency was improved greatly by applying analytic maximum-likelihood solutions for complex source strengths [15] and noise variance [22] at each frequency, which allow these parameters to be sampled implicitly (i.e., as a function of the source locations and environmental parameters) rather than explicitly. This substantially reduces the dimensionality and difficulty of the inversion, particularly for multi-frequency applications. The Bayesian focalization scheme is based on Gibbs sampling for source locations and applying hybrid optimization (adaptive simplex simulated annealing) [23] over environmental parameters. To determine the number of acoustic sources present, the focalization algorithm was run a series of times for an increasing numbers of sources, and the Bayesian information criterion (BIC) was computed from the results after the fact. (The BIC [24], [25] is an information measure used in model selection which trades off the ability to fit data with the number of free parameters in the model; the model that minimizes the BIC represents the smallest number of parameters which adequately fits the data, and is the preferred solution according to Occam's razor.)

This paper extends the multiple-source Bayesian focalization approach in [21] by sampling over the number of acoustic sources as part of the optimization process and directly minimizing the BIC, rather than the data misfit [26]. This requires only a single optimization run to determine the number and location of the sources, which is more convenient and can be more efficient than multiple runs with after-the-fact model selection. However, the manner in which sources are added to and deleted from the model during the optimization process represent crucial components of this algorithm. Purely random source additions and deletions generally have a very low probability of improving the solution and suffer a high rejection rate, which can lead to an algorithm that is in fact less efficient that the original [21]. It is shown here that Gibbs sampling from the conditional probability distribution given existing sources together with the implicit formulation for source strengths provides an efficient scheme to add sources, while applying a similar procedure to re-sample the remaining source locations provides efficient source deletion.

The remainder of this paper is organized as follows. Section 2 provides an overview of the theory and algorithms developed here, including the Bayesian formulation, likelihood function for implicit sampling, optimization algorithm, and model-selection procedure whereby sources are added and deleted. Section 3 illustrates localizing an unknown number of sources in a poorly-known environment using a simulation based on a quiet submerged source and two loud near-surface interferers. Finally, Section 4 summarizes and discusses this work.

2. THEORY AND ALGORITHMS

2.1 Bayesian Formulation

This section describes a Bayesian focalization approach for multiple-source localization in an uncertain ocean environment [21]. Let $\mathbf{d}$ be a vector of N data representing complex (frequency-domain) acoustic fields at an array of hydrophones. Let $\mathcal{M}$ denote the model specifying the choice of physical theory and parameterization for the problem, and let $\mathbf{m}$ be the vector of M free parameters representing a realization of $\mathcal{M}$ (e.g., source and environmental parameters). In a Bayesian formulation these quantities are considered random variables related by Bayes' rule

$$P(\mathbf{m}|\mathbf{d},\mathcal{M}) = \frac{P(\mathbf{d}|\mathbf{m},\mathcal{M})\,P(\mathbf{m}|\mathcal{M})}{P(\mathbf{d}|\mathcal{M})}. \quad (1)$$

In Eq. (1), $P(\mathbf{m}|\mathbf{d},\mathcal{M})$ is the posterior probability density (PPD) representing the state of information for the parameters including both data information, represented by $P(\mathbf{d}|\mathbf{m},\mathcal{M})$, and prior information, $P(\mathbf{m},\mathcal{M})$. Interpreting the conditional data probability density $P(\mathbf{d}|\mathbf{m},\mathcal{M})$ as a function of $\mathbf{m}$ for a fixed model $\mathcal{M}$ and measured data $\mathbf{d}$ defines the likelihood function, $L(\mathbf{m}) \propto \exp[-E(\mathbf{m})]$, where E is the data misfit function (discussed in Section 2.2). Hence, Eq. (1) can be written

$$P(\mathbf{m}|\mathbf{d},\mathcal{M}) = \frac{\exp[-\phi(\mathbf{m};\mathbf{d},\mathcal{M})]}{\int \exp[-\phi(\mathbf{m}';\mathbf{d},\mathcal{M})]\,d\mathbf{m}'}, \quad (2)$$

where a generalized misfit function, combining data and prior information, is defined

$$\phi(\mathbf{m};\mathbf{d},\mathcal{M}) = E(\mathbf{m};\mathbf{d},\mathcal{M}) - \log_e P(\mathbf{m}|\mathcal{M}). \quad (3)$$

This paper considers optimization approaches to compute the most-probable (optimal) model parameters, which maximize the PPD, or equivalent, minimizes ϕ:

$$\hat{\mathbf{m}} = \arg\max_{\mathbf{m}} P(\mathbf{m}|\mathbf{d},\mathcal{M}) = \arg\min_{\mathbf{m}} \phi(\mathbf{m};\mathbf{d},\mathcal{M}). \quad (4)$$

The optimization required in Eq. (4) is carried out numerically as described in Section 2.3. In this paper, prior information for source locations and environmental parameters consist of uniform distributions: the localization bounds delineate the source search region, while the environmental bounds define the range of physically-reasonable values for water-column and seabed parameters. However, it is also straightforward to apply non-uniform priors via Eqs. (2) and (3) if more specific information is available.

2.2 Likelihood Function

An insightful formulation of the likelihood function can greatly improve the efficiency of the optimization required in Eq. (4). In particular, the dimensionality of the inverse problem can be reduced significantly by applying a likelihood function which treats the source strengths and error statistics as implicit, rather than explicit, unknowns. To develop the implicit approach [21], consider data $\mathbf{d} = \{\mathbf{d}_f;\, f=1, N_F\}$ consisting of complex acoustic measurements at N_F frequencies and N_H hydrophones (i.e., $\mathbf{d}_f = \{[\mathbf{d}_f]_h;\, h=1, N_H\}$ is a complex vector with N_H elements, and there are N_F such vectors comprising the data set). The acoustic field at each frequency is assumed to be due to N_S sources at locations (ranges and depths) $\mathbf{x} = \{\mathbf{x}_s = (r_s, z_s);\, s=1, N_S\}$ with complex source strengths $\mathbf{a} = \{[\mathbf{a}_f]_s\}$. The data errors are considered complex Gaussian-distributed random variables with unknown variances $\boldsymbol{\nu} = \{\nu_f\}$, and the unknown environmental parameters are represented by $\mathbf{e}$. In this case the set of model parameters is $\mathbf{m} = \{\mathbf{x}, \mathbf{e}, \mathbf{a}, \boldsymbol{\nu}\}$, and (suppressing the dependence on $\mathcal{M}$ for simplicity) the likelihood function is

$$\begin{aligned} L(\mathbf{x}, \mathbf{e}, \mathbf{a}, \boldsymbol{\nu}; \mathbf{d}) &= \prod_{f=1}^{N_F} \frac{1}{(\pi\nu_f)^{N_H}} \exp[-|\mathbf{d}_f - \sum_{s=1}^{N_S} [\mathbf{a}_f]_s\, \mathbf{d}_f(\mathbf{x}_s, \mathbf{e})|^2/\nu_f] \\ &= \frac{1}{\prod_{f=1}^{N_F} (\pi\nu_f)^{N_H}} \exp[-\sum_{f=1}^{N_F} |\mathbf{d}_f - \mathbf{D}_f\, \mathbf{a}_f|^2/\nu_f], \end{aligned} \tag{5}$$

where $\mathbf{d}_f(\mathbf{x}_s, \mathbf{e})$ represents the modelled acoustic fields computed for a unit-amplitude, zero-phase source at location $\mathbf{x}_s$, and $\mathbf{D}_f$ is an $N_H \times N_S$ complex matrix defined

$$[\mathbf{D}_f]_{hs} \equiv [\mathbf{d}_f]_h(\mathbf{x}_s, \mathbf{e}). \tag{6}$$

Equation (5) can be written $L \propto \exp[-E]$ where the data misfit (negative log-likelihood) function is given by

$$E(\mathbf{x}, \mathbf{e}, \mathbf{a}, \boldsymbol{\nu}; \mathbf{d}) = \sum_{f=1}^{N_F} |\mathbf{d}_f - \mathbf{D}_f\, \mathbf{a}_f|^2 / \nu_f + N_H \log_e \nu_f. \tag{7}$$

Considering first source strengths, the maximum-likelihood (ML) estimate is obtained by setting $\partial E/\partial \mathbf{a}_f = 0$ leading to

$$\mathbf{d}_f = \mathbf{D}_f\, \mathbf{a}_f. \tag{8}$$

Provided there are more hydrophones than sources, the complex system of equations (8) is over-determined and can be written as an $N_S \times N_S$ system

$$\mathbf{D}_f^\dagger\, \mathbf{d}_f = \mathbf{D}_f^\dagger\, \mathbf{D}_f\, \mathbf{a}_f, \tag{9}$$

where † indicates conjugate transpose. The system of equations (9) represent the least-squares normal equations, which are straightforward to solve for the ML estimate $\hat{\mathbf{a}}$ (singular-value decomposition is applied here to ensure a stable solution [27]). Writing this solution in terms of matrix inversion,

$$\hat{\mathbf{a}}_f = \mathbf{D}_f^{-g}\, \mathbf{d}_f, \tag{10}$$

where the generalized inverse is defined

$$\mathbf{D}_f^{-g} = \left(\mathbf{D}_f^\dagger\, \mathbf{D}_f\right)^{-1} \mathbf{D}_f^\dagger. \tag{11}$$

Substituting Eq. (10) into (7) leads to

$$E(\mathbf{x}, \mathbf{e}, \boldsymbol{\nu}; \mathbf{d}) = \sum_{f=1}^{N_F} \left| \left(\mathbf{I} - \mathbf{D}_f\, \mathbf{D}_f^{-g}\right) \mathbf{d}_f \right|^2 / \nu_f + N_H \log_e \nu_f, \tag{12}$$

where $\mathbf{I}$ is the identity matrix. Considering next the data errors, applying $\partial E/\partial \nu_f = 0$ to Eq. (12) leads to ML solution

$$\hat{\nu}_f = \frac{1}{N_H} \left| \left(\mathbf{I} - \mathbf{D}_f\, \mathbf{D}_f^{-g}\right) \mathbf{d}_f \right|^2. \tag{13}$$

Substituting Eq. (13) into (12) and neglecting additive constants leads to

$$E(\mathbf{x}, \mathbf{e}; \mathbf{d}) = N_H \sum_{f=1}^{N_F} \log_e \left| \left(\mathbf{I} - \mathbf{D}_f\, \mathbf{D}_f^{-g}\right) \mathbf{d}_f \right|^2. \tag{14}$$

Evaluating Eq. (14) for specific $\mathbf{x}$ and $\mathbf{e}$ automatically applies the ML estimates for $\mathbf{a}$ and $\boldsymbol{\nu}$. Hence, using this equation in focalization, the corresponding variability in source strengths and variance's is accounted for implicitly. This implicit sampling replaces explicit sampling over these parameters, substantially reducing the dimensionality of the inversion. For an environmental model with N_E parameters, explicit sampling of all parameters involves solving an optimization problem of dimension $2N_S N_F + N_F + 2N_S + N_E$, whereas implicit sampling reduces this to $2N_S + N_E$. For example, in the test case considered in Section 3 which involves 3 sources at 3 frequencies and 8 environmental parameters, the dimensionality is reduced from 35 to 14. If desired, the values for the source strengths assumed during implicit sampling can be obtained via Eq. (10).

2.3 Optimization

The optimization algorithm developed for Bayesian focalization represents a hybrid approach that adaptively combines elements of the global-search method of simulated annealing (SA) with the local downhill simplex (DHS) method. SA [28] is based on an analogy with statistical thermodynamics, according to which the probability that a system of atoms at absolute temperature T is in a state $\mathbf{m}$ with free energy $\phi(\mathbf{m})$ is given by the Gibbs distribution, which can be written

$$P_T(\mathbf{m};T) = \frac{\exp\left[-\phi(\mathbf{m})/T\right]}{\int \exp\left[-\phi(\mathbf{m})/T\right] d\mathbf{m}}. \tag{15}$$

Unlike in classical physics, the probability distribution for non-zero T extends over all states, and system transitions which increase ϕ are allowed, although these are less probable than transitions which decrease ϕ. SA is based on sampling the Gibbs distribution P_T while gradually lowering T to simulate the system in near-equilibrium as it evolves to its ground state (global minimum-energy configuration). In an optimization problem, ϕ represents an objective function to be minimized over a set of parameters $\mathbf{m}$ (the correspondence is clear for inversion: the PPD, Eq. (2), represents a Gibbs distribution at unit temperature).

Two sampling approaches are commonly used in SA. Metropolis sampling [29], [30] simulates Gibbs equilibrium by repeatedly perturbing parameters and accepting perturbations for which a random number ξ drawn from a uniform distribution on $[0,1]$ satisfies

$$\xi \leq \exp\left[-\Delta\phi/T\right]; \tag{16}$$

if this condition is not met, the perturbation is rejected. Alternatively, Gibbs sampling [29], [30] (also called heat-bath SA), draws a perturbed parameter at random from the (non-normalized) conditional probability distribution for that parameter, with other parameters held fixed at their current values, and the new value is accepted unconditionally. For example, in Gibbs sampling a new value for parameter m_i is drawn from the conditional distribution

$$P_T(m_i) = \exp\left[-\phi(m_i|m_1,\ldots,m_{i-1},m_{i+1},\ldots,m_M)\right]/T. \tag{17}$$

Gibbs sampling can be much more efficient than Metropolis sampling if the conditional distribution can be computed for all values of m_i in a single calculation. This is the case for source range and depth in focalization, as the acoustic field can be computed over the search region from a single computation of the normal mode functions and wave-numbers given fixed environmental parameters [31]. However, Gibbs sampling cannot be applied efficiently to optimize over environmental parameters, and Metropolis sampling must be used for these.

In Metropolis sampling, the type of perturbations is an important factor determining efficiency. In particular, perturbations along the parameter axes can be inefficient for correlated parameters, and perturbation size is an important factor. While large perturbations are required at early stages (high T) to widely search the space, at later stages (low T) these have a high rejection rate. The method of very-fast simulated re-annealing (VFSR) draws perturbations from Cauchy distributions and reduces the distribution width for each parameter linearly with temperature, applying a different rate of temperature reduction (chosen arbitrarily) for each parameter [32]. However, selecting appropriate temperature reduction factors can be difficult.

The method of adaptive simplex simulated annealing (ASSA) combines components of VFSR and DHS in an adaptive hybrid algorithm [23]. DHS operates on a simplex of $M+1$ models in an M-dimensional model space, and generates local downhill steps using a geometric scheme based on reflections and contractions of the highest-misfit model relative to the remainder of the models in the simplex [27], [33]. ASSA applies perturbations consisting of a DHS step followed by a Cauchy-distributed random variation, which are accepted or rejected according to the Metropolis criterion (16). The trade-off between randomness and determinism (i.e., gradient information) is controlled by adaptively scaling the Cauchy distribution width for each parameter based on the idea that the size of the recently-accepted perturbations provides an effective scaling for new perturbations. In particular, ASSA draws random parameter perturbations using Cauchy distributions scaled adaptively by the running average of the accepted random perturbations for that parameter over the last several temperature steps. Incorporating DHS in a SA framework provides gradient information that speeds convergence, overcomes parameter correlations, and provides an effective memory for the algorithm (since the simplex contains the M best models encountered to that point in the search). ASSA has proved to be a highly effective optimization algorithm in a number of applications [34]–[36], and is used here for optimizing over environmental parameters in multiple-source focalization.

2.4 Model Selection: Number of Sources

Determining the number of sources that contribute significantly to the total acoustic field is an important but challenging issue in multiple-source localization. In a Bayesian formulation this can be considered an application of model selection, i.e., seeking the most appropriate model $\mathcal{M}$ given the measured data $\mathbf{d}$. In Bayes' rule (1), the conditional probability $P(\mathbf{d}|\mathcal{M})$ of the data for a particular model parameterization can be considered the likelihood of the parameterization given the data, referred to as the Bayesian evidence for $\mathcal{M}$. Since the evidence serves as a normalizing factor in Bayes' rule, it can be written

$$P(\mathbf{d}|\mathcal{M}) = \int P(\mathbf{d}|\mathbf{m},\mathcal{M})\, P(\mathbf{m}|\mathcal{M})\, d\mathbf{m}. \tag{18}$$

Unfortunately, this integral is particularly difficult to evaluate [37], [38], and cannot be solved repeatedly within a numerical optimization algorithm. Alternatively, the BIC [24], [25], an asymptotic point estimate of evidence, is applied here:

$$-2\log_e P(\mathbf{d}|\mathcal{M}) \approx \mathrm{BIC} = -2\log_e L(\hat{\mathbf{m}};\mathbf{d},\mathcal{M}) + M\log_e N, \quad (19)$$

where $\hat{\mathbf{m}}$ is the optimal model, and M and N are the total number of parameters and data, respectively. For the development here, this can be written, within an additive constant, as

$$\begin{aligned}\mathrm{BIC} \;=\; & 2E(\hat{\mathbf{m}};\mathbf{d},\mathcal{M}) + \\ & (2N_S N_F + N_F + 2N_S + N_E)\log_e 2N_F N_H, \quad (20)\end{aligned}$$

where the factor of two in the expression for N results from complex data. Because the BIC is based on the negative log likelihood, low BIC values are preferred. The first term on the right of Eq. (20) favors models with low misfits; however, this is balanced by the second term which applies a penalty for additional free parameters. The data misfit can always be decreased by including more parameters; however, at some point this decrease is not justified and the model is over-parameterized and the data over-fit. Minimizing the BIC provides the model with the smallest number of parameters required to fit the data, or, conversely, the largest number of parameters resolved by the data. This provides the preferred solution according to Occam's razor (hypotheses/models should be as simple as possible).

Earlier work on multiple-source localization [21] was based on an algorithm that minimized $E(\mathbf{m})$ for a fixed number of sources. This algorithm was run a series of times for an increasing numbers of sources ($N_S = 1, 2, \ldots$), and the BIC computed from the optimization results after the fact to identify the preferred solution. The present paper develops a localization approach which samples over the number of sources as part of the optimization, and directly minimizes the BIC. In this approach a single optimization run determines the number and location of the sources. Adding and deleting sources during the optimization are examples of what are referred to as "birth" and "death" moves, respectively, in trans-dimensional inversion [39], [40], in which these moves are accepted or rejected according to the Metropolis criterion, Eq. (16). As such, the manner in which sources are added to and deleted from the model is vitally important. Adding sources of random strength at locations drawn from a uniform random distribution over the search region has a very low probability of improving the solution, and suffers a high rejection rate. Likewise, deleting sources purely at random is an inefficient procedure.

In the multiple-source focalization algorithm developed here, the range and depth for a new source to be added to the model are drawn by applying two-dimensional (2-D) Gibbs sampling, i.e., drawn from the 2-D conditional probability distribution for the location of a new source, given the current values of the locations and strengths of all existing sources and of the environmental parameters. Further, the complex strength for the new source is assigned the ML value as given by Eq. (10). Assigning the location and strength of a new additional source in this manner has a far higher probability of producing a good fit to the acoustic data, and hence being accepted according to the Metropolis criterion, than uniform random draws. Further, the probability of selecting a good source location increases as the temperature decreases according to Eq. (17), in keeping with a wide search of the parameter space at high T, and a more-focused local search to ensure convergence at low T.

To improve the acceptance rate of deleting a source from the model, the procedure developed here is to re-sample the locations of the existing sources by 2-D Gibbs sampling, again applying the ML source strength estimates. This allows the remaining sources to re-distribute themselves so as to best accommodate the change in the total acoustic field due to the deleted source.

The above procedures have been found to provide an efficient scheme to add or delete a source during focalization. Focalization for an unknown number of sources is based on a series of perturbation cycles at each temperature step, with each cycle consisting of: (1) perturbing and accepting/rejecting environmental parameters via ASSA, (2) perturbing existing source locations via Gibbs sampling, and (3) attempting either a source addition or a deletion (chosen randomly with 0.5 probability each). If a source deletion is attempted, the source to be deleted is chosen uniformly at random from the existing sources.

3. EXAMPLE

This section illustrates multiple-source focalization with a simulated example involving two relatively strong near-surface sources and a third quieter submerged source in a poorly-known environment. The scenario is illustrated in Fig. 1 and parameter values and prior bounds for source locations and environmental parameters are summarized in Table 1. The locations of the three sources are $(r_1, z_1) = (7$ km, 4 m$)$, $(r_2, z_2) = (3$ km, 2 m$)$, and $(r_3, z_3) = (5.4$ km, 50 m$)$, with corresponding signal-to-noise ratios (SNRs) at the receiver array of 10, 5, and 0 dB at each of three frequencies of 200, 300, and 400 Hz. Simulated acoustic data were computed at a vertical line array comprised of 24 hydrophones at 4-m spacing from 4- to 100-m depth in 100 m of water using the normal-mode propagation model ORCA [31]. Random complex Gaussian errors were added to the synthetic data with variances and source amplitudes set at each frequency to achieve the SNRs given above. The resulting source amplitudes $A_{sf} = |[\mathbf{a}_f]_s|$ are approximately 1.00, 0.60, and 0.2 for sources s = 1, 2, and 3, respectively (amplitudes vary slightly with frequency). For simplicity, source phases, $\theta_{sf} = \tan^{-1}(\Re\{[\mathbf{a}_f]_s\}/\Im\{[\mathbf{a}_f]_s\})$, were set independent of frequency as $\pi/4$, $\pi/2$, and $-\pi/2$ radians for sources s = 1, 2, and 3, respectively. Note, however, that the localization algorithms consider independent complex source strengths for each source and frequency. The prior information for all source locations is a

Table 1: Parameter values and prior bounds for source and environmental parameters (in the units for attenuation, λ represents wavelength).

Parameters	True values	Bounds
N_S	3	$[1, 4]$
r_1 (km)	7	$[0, 10]$
r_2 (km)	3	$[0, 10]$
r_3 (km)	5	$[0, 10]$
z_1 (m)	4	$[0, 100]$
z_2 (m)	2	$[0, 100]$
z_3 (m)	50	$[0, 100]$
D (m)	100	$[98, 102]$
c_b (m/s)	1580	$[1500, 1700]$
ρ_b (g/cm^3)	1.5	$[1.2, 2.2]$
α_b (dB/λ)	0.1	$[0, ,0.5\ ]$
c_1 (m/s)	1520	$[1515, 1525]$
c_2 (m/s)	1517	$[1514, 1522]$
c_3 (m/s)	1513	$[1510, 1516]$
c_4 (m/s)	1510	$[1508, 1512]$

uniform distribution over 0–100 m in depth and 0–10 km range, and the number of sources, N_S, was constrained to be 1–4. The numerical grid applied for localization involves depth and range increments of 2 m and 0.05 km, respectively (other parameters are treated as continuous variables). Unknown geoacoustic parameters include the sound speed, c_b, density, ρ_b, and attenuation, α_b, of a uniform bottom. Water-column unknowns include the water depth, D, and the sound-speed profile represented by four parameters, c_1–c_4, at depths of 0, 10, 50, and D m. Prior information for the environmental parameters consists of uniform distributions over bounded intervals representing large uncertainties, as given in Table 1.

The multiple-source focalization algorithm described in Section 2 was applied to the above problem as follows. The temperature was initiated at a value T_0 high enough so that essentially all perturbations were accepted initially, and reduced logarithmically according to $T_i = \beta^i T_0$ where i represents the temperature step and $\beta =$

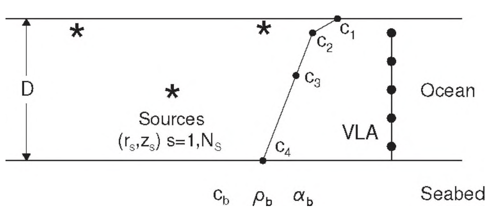

Figure 1. Schematic diagram of the multiple-source localization problem, including unknown environmental parameters (defined in text), source locations, and vertical line array (VLA) of hydrophones.

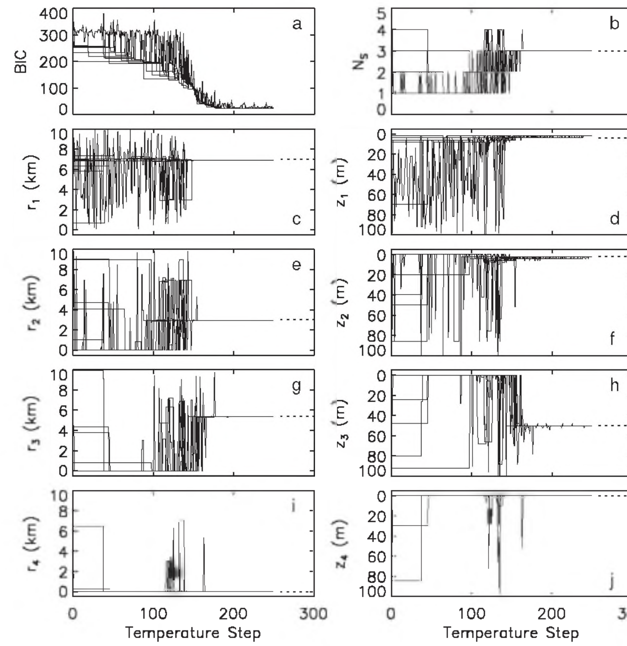

Figure 2. Focalization process for the BIC, number of sources, N_S, and source ranges and depths, r_1–r_4 and z_1–z_4, respectively. Dotted lines at right indicate true values.

0.99. At each temperature step 10 accepted perturbations of the environmental parameters were required, and the running-average perturbation sizes used in ASSA were computed from 3 temperature steps (30 accepted models). As described in Section 2.4, after each environmental perturbation via ASSA, source locations were sampled via Gibbs sampling, and source additions or deletions were attempted.

Figure 2 shows the focalization process in terms of the BIC, number of sources, N_S, and source ranges and depths for the 4 possible sources as a function of temperature step (when a source is not present, its range and depth are set to zero). Parameter values for all models in the simplex are shown; however, for clarity, only one realization of the simplex for each temperature step is included (i.e., the total number of models plotted is down-sampled by a factor of 10). For graphical purposes, the BIC values have been shifted arbitrarily since only the relative variation in is relevant.

The BIC, shown in Fig. 2(a), decreases by approximately 300 in value during the focalization procedure. The number of sources, N_S, shown in Fig. 2(b), initially favours smaller numbers, since early in the inversion when the data are poorly fit the penalty for extra parameters tends to dominate the misfit. As the model parameters improve with temperature step (shown in this and subsequent figures), the data misfit becomes a more important component of the BIC, and the number of sources tends to increase, varying from 1–4 between about temperature steps 100–150. Above about temperature step 150 the variability decreases, and N_S ultimately converges to the correct value of 3 sources for all models in the simplex. Figure 2(c)–(j) shows that, after initial wide variation, the source ranges and depths

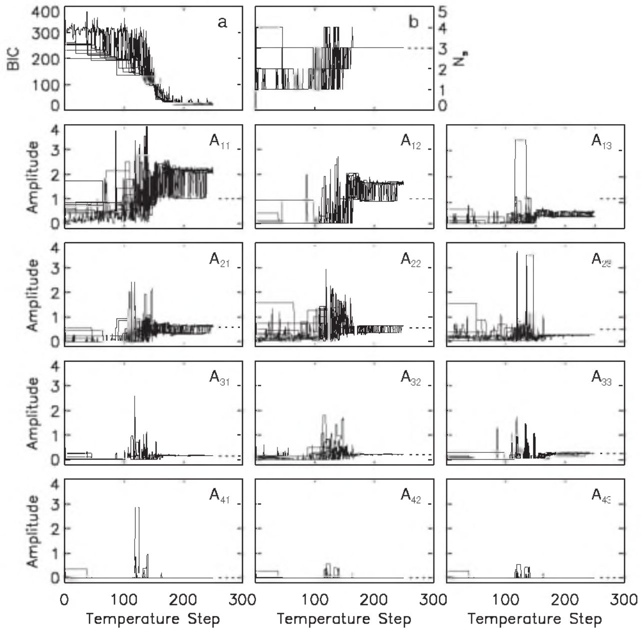

Figure 3. Focalization process for the BIC, number of sources, N_S, and source amplitudes, A_{sf}, where indices s and f identify the source and frequency, respectively. Dotted lines at right indicate true values.

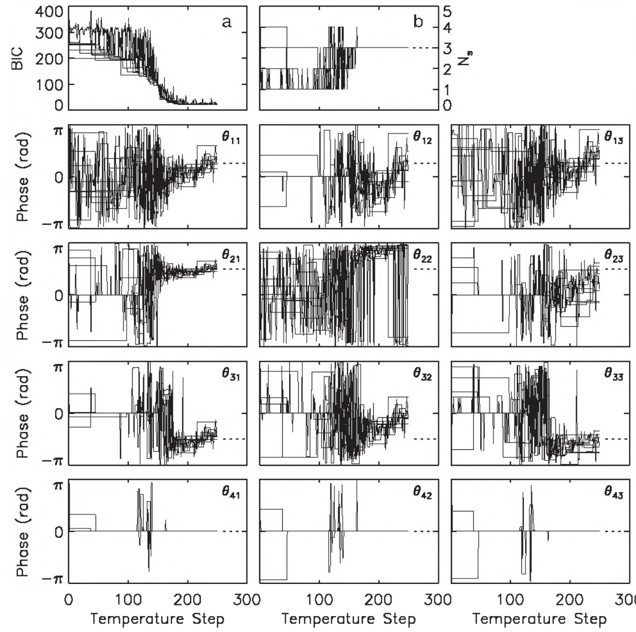

Figure 4. Focalization process for the BIC, number of sources, N_S, and source phases, θ_{sf}, where indices s and f identify the source and frequency, respectively. Dotted lines at right indicate true values.

converge to excellent estimates of the true values. The rate of convergence appears to be in order of SNR, with source 1 (SNR = 10 dB) converging slight earlier than source 2 (5 dB), which in turn converges slightly earlier than source 3 (0 dB).

While successful estimation of the number and location of the acoustic sources, as shown in Fig. 2, is the goal of multiple-source focalization, it is interesting to also consider the results in terms of complex source strengths and geoacoustic parameters. Figure 3 shows the source amplitudes sampled during the focalization process. In general, the final amplitude estimates represent reasonable approximations of the true values, with the poorest results for the first (strongest) source at each of the 3 frequencies (i.e., A_{11}–A_{13}). Further, the amplitudes at each frequency are correctly ordered in magnitude, with $A_{1f} > A_{2f} > A_{3f}$, $f = 1, \ldots, 3$. Figure 4 shows the source phases sampled during focalization. Rough approximations to the true phases are obtained in most cases, although considerable variability persists to the lowest temperatures.

Finally, Fig. 5 shows the environmental parameters throughout the focalization process. Figure 5(d) shows that the seabed sound speed c_b is particularly well estimated within the search bounds, and good results are also obtained for seabed density and attenuation, ρ_b and α_b, in Fig. 5(e) and (f), respectively. Figure 5(c) shows that the water depth D is somewhat under-estimated; this is likely due to correlations with the water-column sound speeds c_1–c_4 in Fig. 5(g)–(j) which are also under-estimated, as it is the water depth divided by sound speed that determines the acoustic transit time over the water column affecting modal properties.

4. SUMMARY AND DISCUSSION

This paper developed and illustrated Bayesian focalization for the simultaneous localization of an unknown number of acoustic sources in an uncertain ocean environment. The approach is based on formulating the posterior probability density over the source locations and complex source strengths (amplitudes and phases) as well as unknown environmental properties and noise variances. The Bayesian information criterion was minimized over all these parameters, as well as over the number of sources, providing the optimal trade-off between data misfit and model parameterization and identifying the number of sources resolved by the data. The minimization was carried out efficiently by applying adaptive hybrid optimization (ASSA) over environmental parameters and Gibbs sampling over source locations. Analytic maximum-likelihood solutions were applied for source strengths and noise variances, which allow these parameters to be sampled implicitly. Sources were added to the model during inversion using Gibbs sampling and ML source strengths to provide a reasonable acceptance rate. Similarly, when a source was deleted, Gibbs sampling was applied to re-position the remaining sources for reasonable acceptance.

The Bayesian focalization approach was illustrated for a 3-source, 3-frequency example involving two relatively strong near-surfaces sources (SNRs of 10 and 5 dB) and a quieter submerged source (SNR = 0 dB) with substantial uncertainties in water-column and seabed properties. Minimizing the BIC determined the correct number of sources present, and all sources were successfully localized. The example showed that multiple-frequency acoustic data at these SNRs provide sufficient information to estimate the number and locations of multiple

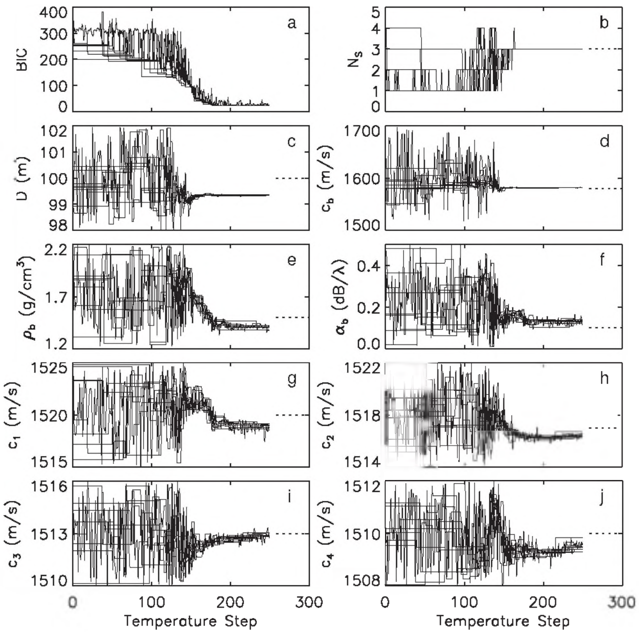

Figure 5. Focalization process for the BIC, number of sources, N_S, and environmental parameters (identified in Table 1). Dotted lines at right indicate true values.

sources, as well as to approximate source amplitudes and phases and unknown environmental parameters.

Finally, it is worth noting that repeated runs of a similar inversion algorithm which varied the number of sources but minimized the data misfit, rather than the BIC, always selected 4 sources (the upper bound) for the 3-source test case. Further, while the two strong sources were always correctly localized, the quiet submerged source was generally not, although the acoustic data were well fit. Hence, minimizing an objective function which combines data misfit with a penalty for overparameterization, as in the BIC, appears to be necessary to reliably localize an unknown number of sources in applications such as this.

ACKNOWLEDGEMENTS

The author thanks Michael Wilmut, Jan Dettmer, and Gavin Steininger for interesting and helpful discussions on Bayesian inversion methods.

REFERENCES

[1] H. P. Bucker, "Use of calculated sound fields and matched field detection to locate sound sources in shallow water," J. Acoust. Soc. Am., **59**, 368–373 (1976).

[2] A. B. Baggeroer, W. A. Kuperman, and H. Schmidt, "Matched field processing: Source localization in correlated noise as an optimum parameter estimation problem," J. Acoust. Soc. Am., **83**, 571–587 (1988).

[3] J. M. Ozard, "Matched field processing in shallow water for range, depth, and bearing determination: Results of experiment and simulation," J. Acoust. Soc. Am., **86**, 744–753 (1989).

[4] A. Tolstoy, "Computational aspects of matched field processing in underwater acoustics," *Computational Acoustics*, edited by D. Lee, A. Cakmak, and R. Vichnevetsky (North Holland, Amsterdam, 1990), Vol. 3, pp. 303–310.

[5] A. Tolstoy, *Matched Field Processing for Underwater Acoustics* (World Scientific Pub., Singapore, 1993) pp. 1–228.

[6] A. B. Baggeroer, W. A. Kuperman, and P. N. Mikhalevsky, "An overview of matched field methods in ocean acoustics," IEEE J. Oceanic Eng., **18**, 401–424 (1993).

[7] D. R. Del Balzo, C. Feuillade, and M. R. Rowe, "Effects of water-depth mismatch on matched-field localization in shallow water," J. Acoust. Soc. Am., **83**, 2180–2185 (1988).

[8] A. Tolstoy, "Sensitivity of matched field processing to sound-speed prone mismatch for vertical arrays in a deep water Pacific environment," J. Acoust. Soc. Am., **85**, 2394–2404 (1989).

[9] E. C. Shang and Y. Y. Wang, "Environmental mismatching effects on source localization processing in mode space," J. Acoust. Soc. Am., **89**, 2285–2290 (1991).

[10] M. D. Collins and W. A. Kuperman, "Focalization: Environmental focusing and source localization," J. Acoust. Soc. Am., **90**, 1410–1422 (1991).

[11] S. E. Dosso, "Matched-field inversion for source localization with uncertain bathymetry," J. Acoust. Soc. Am., **94**, 1160–1163 (1993).

[12] P. Zakarauskas, S. E. Dosso, and J. A. Fawcett, "Matched-field inversion for source location and optimal equivalent bathymetry," J. Acoust. Soc. Am., **100**, 1493–1500 (1996).

[13] R. N. Baer and M. D. Collins, "Source localization in the presence of gross sediment uncertainties," J. Acoust. Soc. Am., **120**, 870–874 (2006).

[14] S. E. Dosso and M. J. Wilmut, "Bayesian focalization: Quantifying source localization with environmental uncertainty," J. Acoust. Soc. Am., **121**, 2567–2574 (2007).

[15] A. N. Mirkin and L. H. Sibul, "Maximum likelihood estimation of the location of multiple sources in an acoustic waveguide," J. Acoust. Soc. Am., **95**, 877–888 (1994).

[16] M. D. Collins, L. T. Fialkowski, W. A. Kuperman, and J. S. Perkins, "The multi-value Bartlett processor and source tracking," J. Acoust. Soc. Am., **97**, 235–241 (1995).

[17] L. Zurk, N. Lee, and J. Ward, "Source motion mitigation for adaptive matched field processing," J. Acoust. Soc. Am., **113**, 2719–2731 (2003).

[18] T. B. Nielson, "Localization of multiple acoustic sources in the shallow ocean," J. Acoust. Soc. Am., **118**, 2944–2953 (2005).

[19] H. C. Song, J. de Rosny, and W. A. Kuperman, "Improvement in matched field processing using the CLEAN algorithm," J. Acoust. Soc. Am., **113**, 1379–1386 (2003).

[20] Z.-H. Michalopoulou, "Multiple source localization using a maximum *a posteriori* Gibbs sampling approach," J. Acoust. Soc. Am., **120**, 2627–2634 (2006).

[21] S. E. Dosso and M. J. Wilmut, "Bayesian multiple source localization in an uncertain environment," J. Acoust. Soc. Am., **129**, 3577–3589 (2011).

[22] S. E. Dosso and M. J. Wilmut, "Estimating data uncertainty in matched-field geoacoustic inversion," IEEE J. Oceanic Eng., **31**, 470–479 (2006).

[23] S. E. Dosso, M. J. Wilmut, and A. L. Lapinski, "An adaptive hybrid algorithm for geoacoustic inversion," IEEE J. Oceanic Eng., **26**, 324–336 (2001).

[24] G. Schwarz, "Estimating the dimension of a model," Ann. Stat., **6**, 461–464 (1978).

[25] J. Dettmer, S. E. Dosso, and C. W. Holland, "Model selection and Bayesian inference for high-resolution seabed reflection inversion," J. Acoust. Soc. Am., **125**, 706–716 (2009).

[26] S. P. Brooks, N. Friel, and R. King, "Classical model selection via simulated annealing," J. R. Statist. Soc., **65**, 503–520 (2003).

[27] W. H. Press, S. A. Teukolsky, W. T. Vetterling, and B. P. Flannery, *Numerical Recipes in Fortran 77*, 2nd Ed (Cambridge University Press, Cambridge, 1992).

[28] S. Kirkpatrick, C. D. Gelatt, and M. Vecchi,"Optimization by simulated annealing," Science, **220**, 671–680 (1983).

[29] W. R. Gilks, S. Richardson, and G. J. Spiegelhalter, *Markov Chain Monte Carlo in Practice* (Chapman and Hall, London,

1996).

[30] J. J. K. Ó Ruanaidh and W. J. Fitzgerald, *Numerical Bayesian Methods Applied to Signal Processing* (Springer-Verlag, New York, 1996).

[31] E. K. Westwood, C. T. Tindle, and N. R. Chapman, "A normal mode model for acousto-elastic ocean environments," J. Acoust. Soc. Am., **100**, 3631–3645 (1996).

[32] L. Ingber, "Very fast simulated reannealing," Mathl. Comput. Modeling, **12**, 967–993 (1989).

[33] J. Nelder and R. Mead, "A simplex method for function minimization," Computer Journal, **7**, 308–313 (1965).

[34] S. E. Dosso and B. J. Sotirin, "Optimal array element localization, J. Acoust. Soc. Am., **106**, 3445–3459 (1999).

[35] A. S. Lapinski and S. E. Dosso, "Bayesian geoacoustic inversion for the Inversion Techniques 2001 Workshop," IEEE J. Oceanic Eng., **28**, 380–399 (2003).

[36] S. Molnar, S. E. Dosso, and J. F. Cassidy, "Bayesian inversion of microtremor array dispersion data in Southwestern British Columbia," Geophys. J. Int., **183**, 923–940 (2010).

[37] S. Chib, "Marginal likelihood from the Gibbs output," J. Am. Stat. Assoc., **90**, 1313–1321 (1995).

[38] J. R. Shaw, M. Bridges, and M. P. Hobson, "Efficient Bayesian inference for multimodal problems in cosmology," Mon. Not. R. Astron. Soc., **378**, 1365–1370 (2006).

[39] P. J. Green, "Trans-dimensional Markov chain Monte Carlo," in *Highly Structured Stochastic Systems*, Oxford Statistical Science Series (Oxford University Press, Oxford, 2003), pp. 179–198.

[40] J. Dettmer and S. E. Dosso, "Trans-dimensional geoacoustic inversion," J. Acoust. Soc. Am., **128**, 3393–3405 (2010).


Concerto
4-Channel Multi-Function Acoustic Measuring System
All you need in one system:
- 4-channel SLM Class 1
- RT60, EDT, C80, D50 & Ts
- 4-channel Data Logger
- 4-channel Spectrum Analyzer
- Building and Human Vibration
- Monitoring Station with Remote Access
Custom Modules Available
See demo : www.softdb.com/concerto.php
Remote access via
iPhone or PC


I-Track
Automatic Real-Time Sound Mapping
Automotive
Industrial
Laboratory
Architectural
See demo : www.softdb.com/itrack.php
5-Minute Mapping
Freehand Scanning Without Grid

MODELLING UNCERTAINTY IN AN UNDERWATER ACOUSTIC POSITIONING SYSTEM

Dugald Thomson[1], Stan E. Dosso[1], Emmett Gamroth[2] and Colin Bradley[2]
[1]School of Earth & Ocean Sciences and [2]Department of Mechanical Engineering
University of Victoria, Victoria, BC, Canada, V8P 5C2, dugald@uvic.ca

ABSTRACT

This paper develops a ray-based travel-time inversion to simulate the accuracy of an active underwater acoustic localization system, and examines the localization accuracy as a function of various sources of error and geometric and environmental factors. The system considered here simulates localizing an autonomous underwater vehicle using arrival times of acoustic transmissions from an onboard source as measured at hydrophones distributed spatially over a test range. Since localization uncertainty is a function of source location, uncertainties are calculated for the source at a grid of locations over the areas of the test bed. Localization accuracy is considered as a function of timing errors, uncertainty in hydrophone locations, target depth, variations in sound-speed profile, and hydrophone geometry.

SOMMAIRE

Cet article développe un inversion de temps d'arrivée en traçant des rayons pour simuler la précision d'un système actif de localisation acoustiques sous-marins, et examine la précision de localisation en fonction de diverses sources d'erreur et de facteurs géométriques et environnementale. Le système considéré ici simule la localisation d'un véhicule autonome sous-marin en utilisant les instants d'arrivés des transmissions acoustiques provenant d'une source à bord tel que mesuré à partir d'hydrophones répartis spatialement sur une plage de test. Puisque l'incertitude de localisation est fonction de l'emplacement de la source, les incertitudes sont calculées pour la source à une grille de lieux sur les zones du banc d'essai. La précision de localisation est considérée comme une fonction de synchronisation des erreurs, l'incertitude dans l'emplacement des hydrophones, la profondeur des cibles, les variations du profile vitesse-son, et la géométrie des hydrophones.

1. INTRODUCTION

Precise positioning of autonomous underwater vehicles (AUVs) is an important problem for the ocean science community as it attempts to extend its reach further into the deeps. Terrestrial Global Positioning Systems (GPS) are of little use for an underwater target as the high-frequency/low-power signals they employ are unable to penetrate beyond the surface layers of the ocean due to reflection and absorption by the seawater. The Integrated Acoustic System (IAS) being designed by the University of Victoria's Ocean Technology Test Bed (OTTB) team aims to overcome this obstacle by developing a high-precision underwater acoustic positioning system. The goal is to produce a system, similar to a commercial Long Baseline unit, capable of positioning a target within the OTTB range to a sufficient accuracy for use as a ground truth for testing onboard navigation systems.

The range itself covers an area of approximately 1.5 km by 1.5 km, with five hydrophones moored to 3-m towers on the seabed at depths of 60 m to 130 m and located in the four corners of the range plus one near the centre, as depicted in Fig. 1. The N-S axis is referred to as y while the E-W axis is aligned to x, with z being depth below surface. The AUV will be outfitted with a generic 'pinger', a transducer that periodically emits an acoustic pulse in the 5-80 kHz frequency range as it moves about the range. The pulse travels through the underwater medium, and is received at the five hydrophones stations (Gamroth, Kennedy & Bradley, 2011).

The received ping arrival instants represent the data, which are used to estimate the source position using the time difference of arrival through a ray-based linearized inversion technique. The error in the source position estimate is a function of clock error in the Precision Time Protocol (PTP) system (±10 µs), tower position survey error (±0.40 m in each of three dimensions expected), and errors in the measured sound-speed profile (due to instrument bias). Positional uncertainty is also affected to a large degree by the source/hydrophone geometry.

The sound-speed profiles used in this investigation are shown in Fig. 2. The solid-line profile was obtained from direct sound-speed measurements using a velocimeter cast at the range in Saanich Inlet, on November 8, 2011, a day with calm winds. The dashed-line profile was derived from temperature and salinity data collected by Zaikova et al. (2010) within Saanich Inlet but outside the OTTB range during February, 2008. Once the range is operational, the protocol will call for collection of a sound-speed profile within a few hours of data collection for use in target positioning.

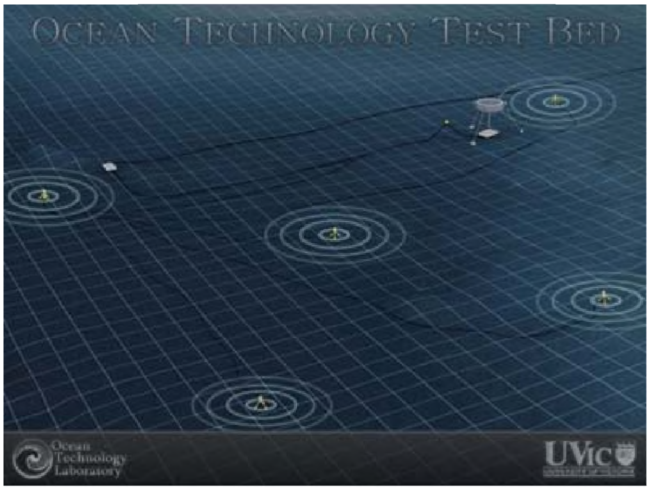

Figure 1: Conceptual image of the OTTB range located in Saanich Inlet, near Victoria, BC, showing the five hydrophone tower locations and a grid representing the simulated target positions (Ocean Technology Test Bed, 2005).

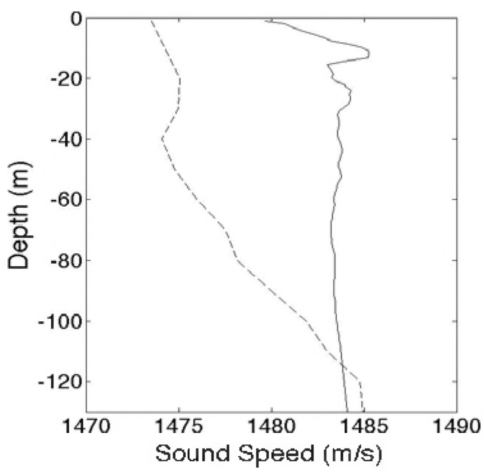

Figure 2: Sound-speed profiles used in the simulations. The solid-line profile was collected during November, 2011. The dashed-line profile was collected by Hallam & Tortell (2008) during February, 2008.

To examine the anticipated localization accuracy of the system, a simulation procedure was developed which calculates uncertainties for a series of positions about the range. The remainder of this paper describes the inversion algorithm used to compute localization uncertainties (Section 2) and gives a series of examples considering a variety of factors that affect the accuracy (Section 3).

2. METHOD

The modelling study carried out here to estimate the localization accuracy for a target located within the range is based on estimating the posterior uncertainties of the source-location in *x*, *y*, and *z*. Since the source-location uncertainty varies with source location, uncertainties are calculated for the source at each point within a grid of positions over the area of the test bed. At each grid point, the source-location uncertainties are estimated using a linearized Bayesian approach that includes the effects of arrival-time errors as well as uncertainties in hydrophone locations and sound speed. A complete description of these methods can be found in Dosso & Ebbeson (2006). The lateral (r) uncertainty is calculated as the square root of the L_2 norm of the horizontal (x and y) uncertainty components.

The OTTB range is modelled as a range-independent, layered ocean using a measured sound-speed profile. The data set $\mathbf{t}$ is the vector of $N = H$ measured ray arrival times at the $H = 5$ hydrophone stations, while the model $\mathbf{m}$ is a vector of $M = 3H + 5$ parameters representing source locations (x, y, z), hydrophone positions (X_i, Y_i, Z_i $i = 1, \ldots, 5$), source instant (t_0), and an unknown constant bias to the sound-speed profile (Δc) as

$$\mathbf{m} = \begin{bmatrix} x, y, z, \bar{c}t_0, X_1, Y_1, Z_1, \ldots, X_i, Y_i, Z_i, \Delta c \\ for \;\; i = 1{:}H \end{bmatrix}^T, \tag{1}$$

where the source instant t_0 is multiplied by $\bar{c}$, a representative sound speed, to provide the same units and scale as positional parameters.

The observed data $\mathbf{t}$ are the arrival times of pings originating from the target and received at the five hydrophone stations for each given source transmission. These data contain noise (errors) as discussed in Section 1, and the direct path ray arrival times $\mathbf{t}$ can be written in general vector form as

$$\mathbf{t} = \mathbf{t}(\mathbf{m}) + \mathbf{n}, \tag{2}$$

where $\mathbf{t}(\mathbf{m})$ are the predicted data based on the model parameters $\mathbf{m}$, i.e., the calculated travel times along eigenrays connecting source and receivers, and $\mathbf{n}$ are errors on the data. The error n_i on datum t_i is assumed to be an independent Gaussian-distributed random process with zero mean and standard deviation σ.

Expanding $\mathbf{t}(\mathbf{m})$ in a Taylor series to first order about an arbitrary starting model $\mathbf{m_0}$, the result can be written

$$\mathbf{d} = \mathbf{Jm}, \tag{3}$$

where

$$\mathbf{d} = \mathbf{t}(\mathbf{m}) - \mathbf{t}(\mathbf{m_0}) + \mathbf{Jm_0} \tag{4}$$

are modified data and $\mathbf{J}$ is the Jacobian matrix of partial derivatives of the data functionals with respect to the model parameters evaluated at $\mathbf{m_0}$:

$$J_{ij} = \partial d_i(\mathbf{m_0}) / \partial m_j. \tag{5}$$

This matrix is sometimes called the sensitivity matrix as it quantifies the sensitivity of the data to the model, and contains the physics and geometry of the forward problem.

Prior information about the model parameters is also considered in the problem. Assuming this prior information represents a Gaussian uncertainty distribution with expected values $\widehat{m}_k$ (the prior estimate for the kth parameter) and standard deviations ξ_k, the maximum *a posteriori* (MAP) solution is given by

$$\mathbf{m}_{\mathrm{MAP}} = \hat{\mathbf{m}} + \left[\mathbf{J}^{\mathrm{T}}\mathbf{C_d}^{-1}\mathbf{J} + \mathbf{C_p}^{-1}\right]^{-1}\mathbf{J}^{\mathrm{T}}\mathbf{C_d}^{-1}(\mathbf{d} - \mathbf{J}\hat{\mathbf{m}}), \quad (6)$$

where $\mathbf{C_d} = \sigma^2\mathbf{I}$ is the data covariance matrix and $\mathbf{C_p} = diag\{\xi_k{}^2\}$ is the prior model covariance matrix. Further, the posterior probability density is a Gaussian distribution about $\mathbf{m}_{\mathrm{MAP}}$ with posterior model covariance matrix

$$\mathbf{C_m} = \left[\mathbf{J}^{\mathrm{T}}\mathbf{C_d}^{-1}\mathbf{J} + \mathbf{C_p}^{-1}\right]^{-1}. \quad (7)$$

The square root of the diagonal elements of $\mathbf{C_m}$ provide posterior standard deviation (uncertainty) estimates for the model parameters.

Equation (7) represents a linearized approximation in this problem; however, comparison to non-linear solutions from Monte Carlo analysis (Dosso & Sotirin, 1999) indicates that linearization errors are small if $\mathbf{m_0}$ is close to the true model. When inverting measured data this is usually realized by iterating the linearized solution to convergence.

The inversion techniques described above are based on a fast ray-tracing algorithm that uses Newton's method to determine eigenrays; analytic expressions for the ray derivatives are available for the Jacobian matrix (Dosso & Ebbeson, 2006).

In this paper, uncertainties in x, y, z, and $r = \sqrt{x^2 + y^2}$ are taken from Eq. (7) and used to quantify the expected localization accuracy.

3. RESULTS

A series of simulations are presented here to compare the effects on localization accuracy of several factors: hydrophone positioning and sound-speed uncertainty, different source depths, and the effect of reducing target vertical positioning uncertainty through the addition of a depth sensor. The results of increased and decreased timing errors are also considered, as well as different sound-speed profiles and hydrophone geometric configurations.

The first simulation considers what is referred here to as the 'ideal-case' scenario, where the hydrophone positional uncertainty and the sound-speed profile bias are both assumed to be zero, with the timing uncertainty set to the PTP limit of 10 µs. The source depth is 10 m, and the sound-speed profile is the solid line from Fig. 2 (common to all simulations unless otherwise noted). This represents the simplest case where only the uncertainty due to the system timing error is considered. The results of this simulation are shown in Fig. 3 in terms of x, y, r, and z uncertainties (colour contours) over the area of the range.

The effects of source/hydrophone geometry are immediately visible in Fig. 3. The smallest uncertainty in x is found for a source located between two or more hydrophones in x; similarly, the lowest uncertainty in y occurs for a source between two or more hydrophones in y. The most accurate vertical positioning tends to occur for the source locations nearest a hydrophone, where the acoustic ray travels nearly vertically. The greatest horizontal uncertainty occurs for a source in the corners of the range, where the source/hydrophone geometry is poor; the greatest vertical uncertainty tends to occur for a source furthest from a hydrophone, because the greatest amount of vertical information is contained in rays that arrive at steep vertical angles at the hydrophone.

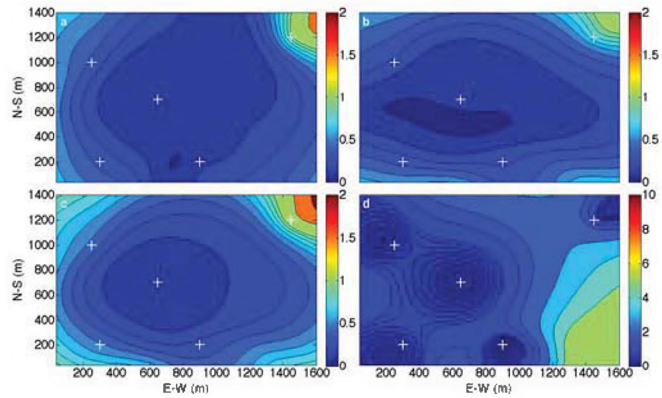

Figure 3: Localization uncertainties for the 'ideal case' of perfectly known hydrophone locations and sound-speed profile. Panels (a)-(d) show absolute errors in *x*, *y*, *r*, and *z*, respectively, for a source at 10-m depth. contours represent uncertainty in metres. Hydrophone locations are depicted as white crosses.

In the second example, the uncertainty from the 'standard case' is examined, where the timing uncertainties remain at 10 µs, the hydrophones have positional uncertainties of 0.40 m in x, y, and z, and the sound-speed profile has an uncertainty (bias) of 1 m/s. The target depth is again set to 10 m. The results of the simulation are shown in Fig. 4. The uncertainties are much greater than in the 'ideal case', indicating that relatively small uncertainties in hydrophone location and sound-speed profile can have a significant effect on AUV localization accuracy and must be taken into account in a meaningful modelling study.

The smallest uncertainties for the x component in Fig. 4(a) are found in the middle of the range and aligned N-S, as these locations produce the most favourable hydrophone geometry for estimating the position in x, due to the rays arriving with large x components. Similarly for the y component, in Fig. 4(b), the smallest uncertainties also tend to the centre but the alignment is E-W. Additionally, the horizontal uncertainty components tend to be lower in the southern and western regions of the range, as the northeastern hydrophone is asymmetrically located at a longer interval than the typical spacing between other hydrophones. This greater span increases the region of poor geometry within the range, whereas in the south and west regions, a higher proportion of the area produces favourable geometric alignments in x and y.

Figure 4(c) shows the uncertainty in r, which combines the uncertainty of x and y. The region of small uncertainty has a rounded symmetrical shape as opposed to the linear shape in the individual x and y components, and the combined uncertainty is always greater than either constituent component. The vertical uncertainty in Fig. 4(d) is lowest for a target located close to any hydrophone, with increasing uncertainty for targets that are further away from a hydrophone.

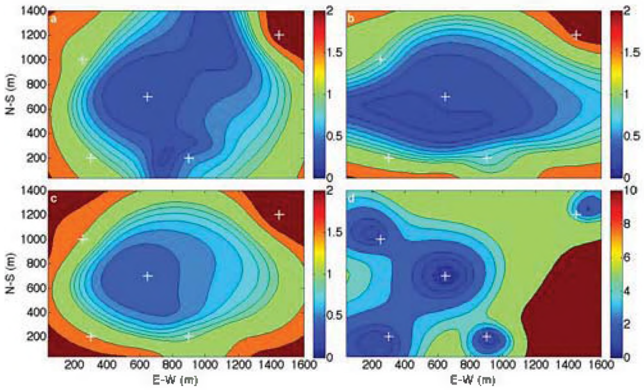

Figure 4: Localization uncertainties for the 'standard-case' scenario. Panels (a)-(d) show absolute errors in *x*, *y*, *r*, and *z*, respectively, for a source at 10-m depth. Colour contours represent uncertainty in metres. Hydrophone locations are depicted as white crosses.

The effect of varying target depth is presented in Fig. 5, which shows the result for the same simulation parameters but with a target at 40-m depth. The horizontal results are similar to the 10-m depth case shown in Fig. 4; however, the geometric effects are more pronounced with the deeper target, due to the reduced vertical extent between source and receiver. In *z*, the uncertainty increases for the deeper target especially in areas of the range distant from a hydrophone, where uncertainty is relatively high. This scenario was repeated for multiple source depths (not shown). For targets at greater depths, the vertical uncertainty increases, since the ray arrives at the hydrophone more horizontally, providing less vertical information about the target position. Hence, the IAS system is ineffective at estimating the depth of a deep source.

In investigating ways to overcome this limitation and to improve overall uncertainty, a scenario was simulated where the target is outfitted with a depth sensor, so that its vertical positioning is always known to within 0.03 m, shown in Fig 6. In this simulation the posterior uncertainty in z is $\leq$ 0.03 m throughout the range. The effect of this improved uncertainty on the lateral uncertainty varies depending on the location within the range. For the locations with relatively low uncertainty (those with the most favourable geometry), the uncertainty is improved only slightly, typically on the order of 2%. However, in the regions where uncertainty is high, as well as locations near a hydrophone, the improvement is much more significant: as much as 70%.

To consider next the effect of timing errors, a simulation was run where the timing uncertainty was increased by a factor of 100 to 1 ms. The results are presented in Fig. 7, and show that uncertainty is substantially increased for all components, indicating that timing uncertainty is an important contributor to overall target positional uncertainty. The 1 ms error was chosen because this is a representative timing accuracy in a typical system employing Network Timing Protocol, as opposed to the 10 μs accuracy achieved in a PTP network (Lentz & Lecroart, 2009). This finding indicates that a high-precision acoustic positioning system would not be feasible without a PTP network.

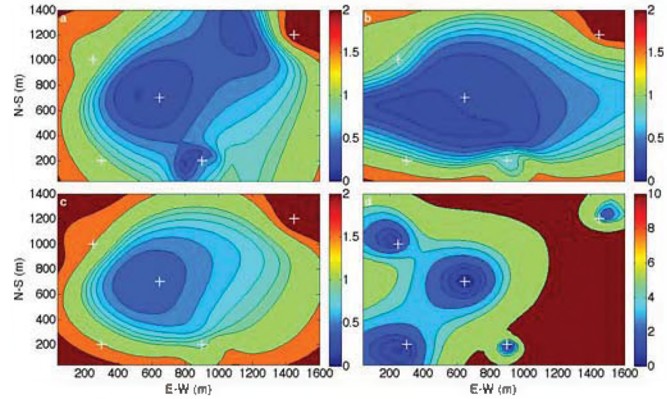

Figure 5: Localization uncertainties for the 'standard-case' scenario. Panels (a)-(d) show absolute errors in *x*, *y*, *r*, and *z*, respectively, for a source at 40-m depth. Colour contours represent uncertainty in metres. Hydrophone locations are depicted as white crosses.

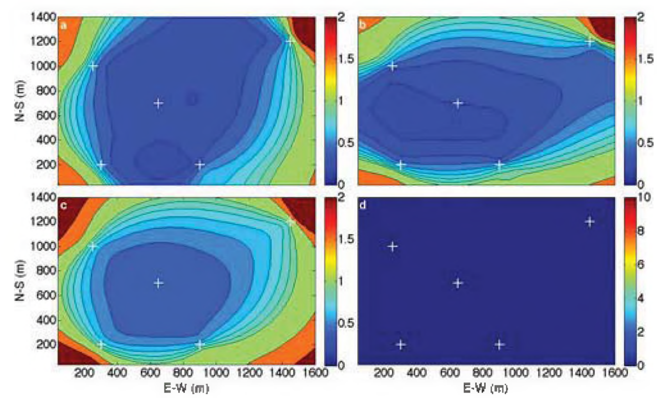

Figure 6: Localization uncertainties for the 'depth-sensor case' scenario with target position in *z* assumed to be known to within 0.03 m uncertainty due to a depth sensor. Panels (a)-(d) show absolute errors in *x*, *y*, *r*, and *z*, respectively, for a source at 10-m depth. Colour contours represent uncertainty in metres. Hydrophone locations are depicted as white crosses.

Another aspect of the PTP network is the potential to further increase the timing precision; it is anticipated that further development in network timing protocols will allow for timing precision to within 100s of nanoseconds (Lentz & Lecroart, 2009). These improvements could be incorporated into the IAS in the future, so a simulation was carried out reducing timing uncertainty by a factor of 100 to 100 ns, shown in Fig. 8. The results are virtually identical to the 'standard case' (Fig. 4) with timing uncertainty 100 times greater, indicating that there exists a limit, near the PTP timing uncertainty of 10 μs, beyond which the overall positional uncertainty is not impacted by further improvement; rather, the uncertainty in hydrophone positions becomes the limiting factor.

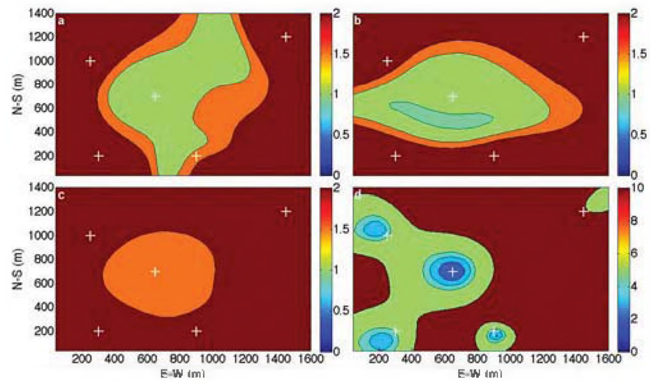

Figure 7: Localization uncertainties for the 'standard-case' scenario with a timing error of 1 ms. Panels (a)-(d) show absolute errors in *x*, *y*, *r*, and *z*, respectively, for a source at 10-m depth. Colour contours represent uncertainty in metres. Hydrophone locations are depicted as white crosses.

To determine whether the localization accuracy would be expected to vary significantly during the year as a function of seasonal variations to the sound-speed profile, Fig. 9 shows the 'standard-case' scenario run using the upward-refracting February profile shown in Fig. 2. The most notable difference from the standard-profile results (Fig. 4) is the increased uncertainty in the *x* and *y* components for target locations furthest from a hydrophone, and in *z* for target locations nearer a hydrophone. However, the variation in uncertainty due to sound-speed profile difference is generally small, indicating that the IAS should function consistently throughout the year.

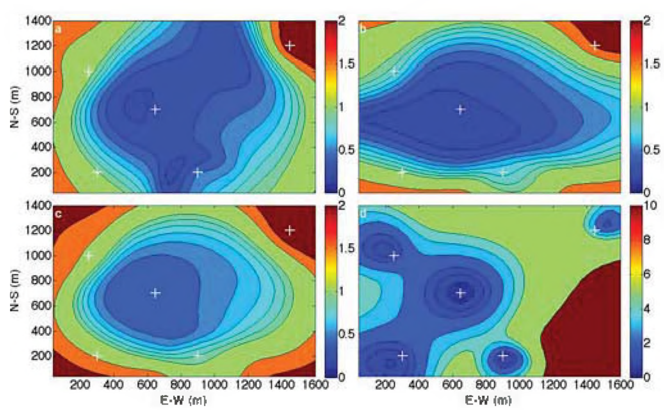

Figure 8: Localization uncertainties for the 'standard-case' scenario with a timing error of 100 ns. Panels (a)-(d) show absolute errors in *x*, *y*, *r*, and *z*, respectively, for a source at 10-m depth. Colour contours represent uncertainty in metres. Hydrophone locations are depicted as white crosses.

Finally, a simulation was carried out investigating the effects of moving the NE hydrophone tower in line with the other hydrophones to create a more symmetric range. The results are presented in Fig. 10, and show that by moving this hydrophone closer to the others, the uncertainty improves slightly for target locations contained within the perimeter of hydrophones, but becomes substantially worse outside this perimeter.

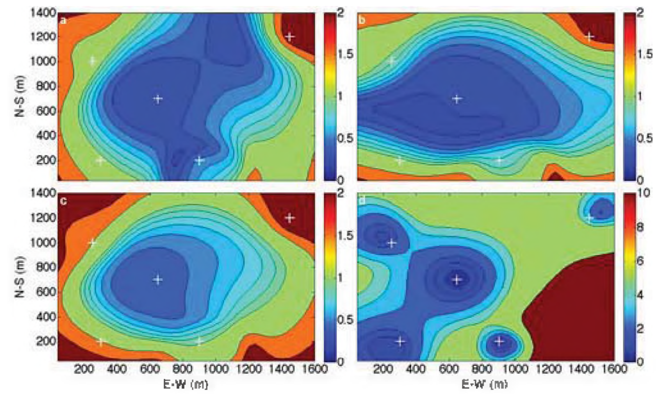

Figure 9: Localization uncertainties for the 'standard-case' scenario using a February sound-speed profile. Panels (a)-(d) show absolute errors in *x*, *y*, *r*, and *z*, respectively, for a source at 10-m depth. Colour contours represent uncertainty in metres. Hydrophone locations are depicted as white crosses.

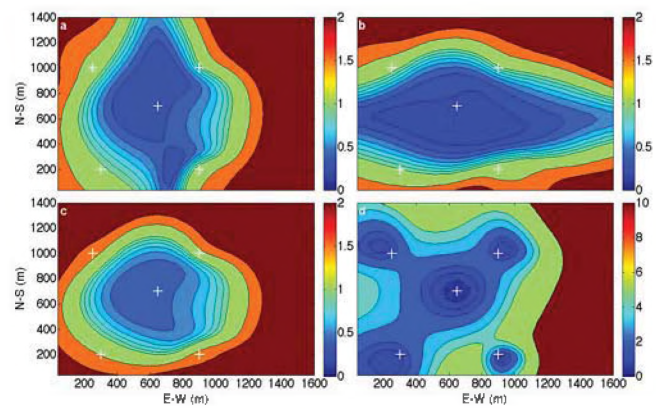

Figure 10: Localization uncertainties for the 'standard-case' scenario, relocating the NE hydrophone tower closer to the others. Panels (a)-(d) show absolute errors in *x*, *y*, *r*, and *z*, respectively, for a source at 10-m depth. Colour contours represent uncertainty in metres. Hydrophone locations are depicted as white crosses.

4. DISCUSSION

This paper developed and illustrated a simulation procedure to investigate localization accuracy for an underwater target (AUV) in an acoustic test range. The simulation procedure allows examination of the effects of several factors, which are integral to the overall system performance, and is a valuable tool for predicting localization accuracy in a variety of situations. In this paper, localization uncertainty is examined as a function of hydrophone positional uncertainty, sound-speed uncertainty, timing errors, and source depth. The effect of reducing target positional uncertainty by employing an AUV-mounted depth sensor is also considered. Finally, different sound-speed profiles and hydrophone geometric configurations are examined.

The simulation is especially beneficial for determining the expected baseline uncertainty for the range given specific values for the system factors (e.g. timing errors, hydrophone-positional and sound-speed uncertainties). In determining whether a certain static accuracy throughout the range is a realizable goal, localization uncertainties can be computed using realistic values for these system factors. Further, the effect of varying these factors on localization accuracies can be quantified.

It was shown that for the standard case (timing uncertainties of 0.1 ms, hydrophone location uncertainties of 0.4 m, sound-speed uncertainties of 1 m/s, 10 m source depth) the minimum positional uncertainty at any point in the range was on the order of 40 cm laterally, and 70 cm vertically. These smallest lateral uncertainties occur near the centre of the range, while the smallest vertical uncertainties are generally found above hydrophones. The largest uncertainties, extending well above 1 m, occur towards the periphery of the range due to less favourable source/hydrophone geometry.

Simulations show that for the existing range infrastructure, a high-precision acoustic positioning system is not feasible using standard network protocol due to the timing uncertainty. Using the PTP network timing, the timing accuracy is sufficient to allow high-precision positioning. However, the improvement in positional uncertainty from further development of the PTP timing uncertainty is negligible, indicating that the operational limit has been met for timing error improvement and improvement in hydrophone localization would be required.

While the methods described here are applied to the specific case of the University of Victoria's OTTB, the approach is general and can be applied to model and examine the accuracy of any underwater acoustic positioning system.

REFERENCES

[1] Ocean Technology Test Bed (2005). *Integrated Acoustic System*. Retrieved Janurary 24, 2011, from LACIR: Ocean Technology: http://web.uvic.ca/~lacir/ocean/acoustics.php.

[2] Gamroth, E., Kennedy, J. & Bradley, C. (2011). Design and testing of an acoustic ranging technique applicable for an underwater positioning system. *Underwater Technology*, 29 (4), 183-193.

[3] Zaikova, E., Walsh, D., Stilwell, C., Mohn, W., Tortell, P. & Hallam, S. (2010). Microbial community dynamics in a seasonally anoxic fjord: Saanich Inlet, British Columbia. *Environmental Microbiology* , 12 (1), 172-191.

[4] Dosso, S.E. & Ebbeson, G. (2006). Array element localization accuracy and survey design. *Canadian Acoustics*, 34(4), 1-11.

[5] Dosso, S.E. & Sotirin, B. (1999). Optimal array element localization. *Journal of the Acoustical Society of America*, 106, 3445-3459.

[6] Lentz, S. & Lecroart, A. (2009). Precision timing in the NEPTUNE Canada network. *OCEANS 2009-EUROPE*, 1-5.

Modeling underwater sound propagation from an airgun array using the parabolic equation method

Alexander O. MacGillivray[1] and N. Ross Chapman[2]
[1]JASCO Applied Sciences, Victoria, BC, Canada
[2]School of Earth and Ocean Sciences, University of Victoria, Victoria, BC, Canada
alex@jasco.com, chapman@uvic.ca

ABSTRACT

This article presents a technique for modeling sound propagation from an airgun array, using the parabolic equation (PE) method, that takes into full account the far-field, angle-dependent radiation pattern of the array. This is achieved by generating a PE starting field for the array by summing together shaded, phase-shifted replicas of the PE self-starter. The array starter has been implemented using the RAM parabolic equation model. A validation comparison is presented of field predictions generated using the array starter against exact normal mode solutions for an array source computed using the ORCA model. Examples of synthetic waveform airgun array calculations performed using the array starter are also provided. The method presented in this article can be used to accurately predict pressure waveforms from an airgun array in the ocean environment provided that the modeler knows (or can compute) far-field source signatures for individual airguns in the array.

SOMMAIRE

Cet article présente une technique permettant de modéliser la propagation du son provenant dun réseau de canons à air, en utilisant la méthode de léquation parabolique (EP), qui prend en compte le patron de directivité du réseau en champ lointain. Cette approche est réalisée en créant un champ initial pour la globalité du réseau défini comme la somme des réplicats de départ (pondérés et déphasés) de chacune des sources du réseau. Ce *champ initial de réseau* a été mis en uvre en utilisant le modèle déquation parabolique RAM. Les prédictions du champ acoustique générées en utilisant cette technique sont comparées aux solutions exactes des modes normaux pour un réseau de sources calculées avec le modèle ORCA. Des exemples de calculs de forme dondes synthétiques obtenues avec le *champ initial de réseau* sont également présentés. La méthode décrite dans cet article peut être utilisée pour prédire avec précision les formes donde de pression dun réseau de canons à air dans lenvironnement marin, à condition que le modélisateur connaisse (ou puisse calculer) les signatures en champ lointain de chacun des canons à air du réseau.

1 INTRODUCTION

Modern ocean acoustic modeling codes are capable of accurately predicting sound propagation in real ocean environments; however, special treatment is required for modeling directional sources, like airgun arrays, since most available codes solve the wave equation for isotropic (non-directional) sources on a finite range/depth grid. When modeling sound propagation from a strongly directional source, like an airgun array, the modeler must take care to properly couple the directionality function of the source to the pressure field computed by the propagation model. Previous efforts at modeling an airgun array using the parabolic equation (PE) method, by DeRuiter *et al.* [1], assumed an isotropic source and focused on reproducing the time arrival structure of received pulses while ignoring directionality. Accurate modeling of both the amplitude and frequency structure of airgun array sound emissions requires, however, a rigorous treatment of the frequency-dependent directionality function of the source.

Coupling a directional source to a raytrace code is straightforward: each ray is weighted by the far-field directionality function of the source according to the ray launch angle. Coupling a directional source to a purely harmonic propagation modeling code—i.e., using wavenumber integration, normal modes or parabolic equation method—is not so straightforward. In this case, one can generally simulate a directional source by summing together the fields from an array of discrete isotropic sources located near the origin [2]. The amplitudes and phases of the array elements must be chosen to replicate the far-field directionality pattern of the source under investigation. Even so, airgun arrays (and horizontal arrays in general) present a computational problem because the array elements are not all located at the zero-range of the modeling grid. As shown in the next section, this problem can be overcome in normal mode theory by invoking the far-field approximation for an array source. This, in turn, motivates our solution for an array starter for the PE method.

2 THEORY

Consider a N-element planar array situated at depth z_s with its geometric centre at $x = y = 0$. In the plane $z = z_s$, the array elements are located at the coordinates

$$\boldsymbol{\Delta r}_m = (x_m, y_m), \qquad m = 1, 2 \ldots N.$$

Each element of this array has complex amplitude/phase A_m at some frequency f. We seek an expression for the far-field acoustic pressure from such an array in an arbitrarily stratified, range-independent environment where the acoustic pressure can be computed from the normal mode solution to the Helmholtz equation:

$$p(r, z; z_s) = \sqrt{\frac{2\pi i}{r}} \sum_{n=1}^{\infty} \psi_n^*(z_s)\psi_n(z) k_n^{-1/2} e^{ik_n r}, \qquad (1)$$

where $\psi_n(z)$ are the normal modes, k_n is the horizontal wavenumber of mode n, z_s is the source depth, and r and z are the usual cylindrical coordinates.

In the horizontally-stratified, range-independent case, the solution to the wave equation is symmetrical with respect to the azimuth angle, θ. Due to the intrinsic directionality of the array, however, the acoustic field is not generally symmetrical with respect to θ. The total field from this array at location $(\boldsymbol{r}, z) = (r, \theta, z)$ is given by

$$p_\Sigma(\boldsymbol{r}, z) = \sum_{m=1}^{N} A_m p(|\boldsymbol{r} - \boldsymbol{\Delta r}_m|, z). \qquad (2)$$

Let us define the far-field of the array as the region where $|\boldsymbol{r}| \gg |\boldsymbol{\Delta r}|$. Beyond this range, the separation of the array elements perpendicular to the direction of propagation (i.e., out of the r/z plane) becomes unimportant and we need only consider the position of each array element projected onto the r/z plane:

$$\Delta r_m = \boldsymbol{\Delta r}_m \cdot \frac{\boldsymbol{r}}{|\boldsymbol{r}|} = x_m \cos\theta + y_m \sin\theta. \qquad (3)$$

In the far-field of the array, the spreading loss terms for the different array elements are approximately the same (i.e., $\sqrt{r - \Delta r_m} \approx \sqrt{r}$). From Equation 1 we obtain the following expression for the total field of the array in terms of the normal modes:

$$\begin{aligned} p_\Sigma(r, z) &= \sqrt{\frac{2\pi i}{r}} \sum_{n=1}^{\infty} \psi_n^*(z_s)\psi_n(z) k_n^{-1/2} e^{ik_n r} \\ &\quad \times \left[\sum_{m=1}^{N} A_m e^{-ik_n \Delta r_m}\right]. \end{aligned} \qquad (4)$$

The physical interpretation of Equation 4 is straightforward: in the far-field of the array, the normal modes are weighted by the vertical array directionality (the bracketed term) according to the grazing angle $\phi_n = \cos^{-1}(k_n c/\omega)$.

Equation 4 could be used for computing the field from a horizontal array using normal modes; in particular, it would be useful for computing the initial field for an array using one-way coupled or adiabatic modes. Equation 4 could also be used for constructing a PE starting field from the normal modes (i.e., for generating a modal starter). In a range-independent environment, however, there is no computational advantage to Equation 4 since Equation 2 gives the exact answer and is just as easy to compute given the mode functions, ψ_n (this fact is exploited to validate the array starter approach in Section 3). Instead, for the general case of range-dependent problems, we seek to rewrite Equation 4 in terms of the parabolic equation solution to the Helmholtz equation and solve the inhomogeneous initial value problem for an array source at $z = z_s$. We do so in terms of Collins' PE self-starter.

Following Collins [3]l, recall that the normal modes in Equation 1 satisfy the eigenvalue equation, which we write using operator notation as follows:

$$k_0^2(1 + X)\psi_n = k_n^2\psi_n, \qquad (5)$$

where k_0 is some reference wavenumber, ρ is the density of the medium, and the depth operator X is defined to be

$$X = k_0^{-2}\left(\rho\frac{\partial}{\partial z}\frac{1}{\rho}\frac{\partial}{\partial z} + k^2 - k_0^2\right). \qquad (6)$$

This is the same eigenvalue equation that we obtain from the separation of variables solution of the Helmholtz equation, but this particular form is useful for deriving PE approximations. Equation 4 can be rewritten in terms of the depth-operator, X, as follows:

$$\begin{aligned} p_\Sigma(r, z) &= \sqrt{\frac{2\pi i}{r}} \sum_{m=1}^{N} A_m e^{-ik_0 \Delta r_m \sqrt{1+X}} \\ &\quad \times \left[k_0^{-1/2}(1+X)^{-1/4} e^{ik_0 r\sqrt{1+X}} \delta(z - z_0)\right], \end{aligned} \qquad (7)$$

where the completeness relation for the normal modes has been used to obtain the delta function $\sum \psi_n^*(z_0)\psi_n(z) = \delta(z - z_0)$.

The term in brackets in Equation 7 is actually the PE self-starter field for a point-source, $p_s(r, z)$ [3, Eq. 7], with a cylindrical spreading term ($r^{-1/2}$) factored out. If we denote the range-factored (i.e., multiplied by $r^{1/2}$) self-starter as

$$\begin{aligned} p_s'(r, z) &= \sqrt{r} p_s(r, z) \\ &= \sqrt{\frac{2\pi i}{k_0}}(1+X)^{-1/4} e^{ik_0 r\sqrt{1+X}} \\ &\quad \times \delta(z - z_0), \end{aligned} \qquad (8)$$

then we obtain the following result for the PE starting field at range r_s from an array:

$$p_\Sigma(r_s, z) = \frac{1}{\sqrt{r_s}} \sum_{m=1}^{N} A_m p_s'(r_s - \Delta r_m, z). \qquad (9)$$

That is, the array starting field in Equation 9 is obtained by summing together the N point-source, range-factored starting fields together at range r_s, each displaced by distance Δr_m from the origin. The resulting starting field may then be propagated forward from range r_s in the usual fashion.

Although Equation 9 was derived for the far-field case, there is no requirement that the starter range, r_s, be in the far-field of the array. This is because the starting field, $p_\Sigma(r_s; z)$, exhibits the same far-field radiation pattern as the source array in the Fraunhofer zone. Thus, even if the starting field is computed in the near-field, the array starter solution will converge to the correct far-field solution as the PE is marched out in range.

In order to avoid having to perform back-propagation, the range of the starting field, r_s, must be greater than the maximum value of Δr_m. The starting range must also be sufficiently large so that the numerical computation of the self-starter is stable for the smallest value of $r - \Delta r_m$. In the authors' experience, a suitable value for r_s may be obtained by adding at least half the horizontal computation grid spacing to the maximum value of Δr_m. Also, if the array spacing is larger than the computation grid spacing (e.g., at high frequencies), then it is acceptable to take multiple PE range steps to arrive at r_s. Finally, note that r_s may be different for different frequencies and azimuth angles.

Even though it was derived for the range-independent case, the array starter can be applied equally well to a range-dependent environment. This is because the normal modes that contribute to the starting field are excited according to the vertical wavenumber spectrum of the source array (i.e., the vertical directionality), as can be seen by inspection of Equation 4. As a consequence, the array starter can be used to compute the field from an array in a range-dependent environment as long as the environment is at least approximately range-independent near the source (i.e., within range r_s of the source).

3 VALIDATION

Provided the modeler has access to an existing PE self-starter code—such as the one in RAM—numerical implementation of the array starter (Equation 9) is straightforward. The array starter code need only invoke the self-starter as a subroutine to generate multiple vertical starting fields (i.e., $p(r_{s\,m}, z)$) at N ranges

$$r_{s\,m} = r_s - \Delta r_m, \qquad m = 1 \ldots N.$$

The resulting collection of starting fields must then be range-factored and summed together with the appropriate frequency-domain complex amplitudes $A_m(f)$ to yield the array starting field. The array starter has been implemented here using the RAM split-step Padé PE code [4], version 1.5g.

In order to validate the present implementation of the array starter, a range-independent benchmark test scenario was created using the ORCA normal-mode code [5], version 2.0. In a range-independent environment, Equation 2 is an exact expression for the pressure field from an array source, which

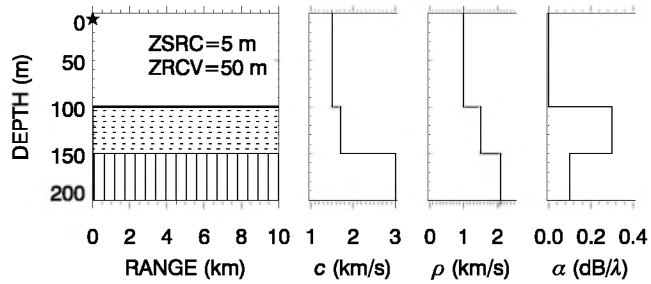

Figure 1: Diagram showing acoustic properties of the range-independent test case used for validating the array starter. Acoustic parameters are sound speed, c, density, ρ, and attenuation, α. The source depth for the test case was 5 m and the receiver depth was 50 m.

is valid even in the near-field (the array starter is only valid in the far-field). Thus benchmark reference solutions were generated for the array starter by using Equation 2 with the normal modes computed by ORCA.

The benchmark test case consisted of a planar array source in a shallow, range-independent ocean waveguide. The water depth in the waveguide was taken to be 100 m and the bottom consisted of a single 50 meter sediment layer over a semi-infinite basement. A diagram showing the acoustic properties of the test environment is presented in Figure 1. For simplicity, sound speed gradients were not used in each layer in order to avoid difficulties associated with the different sound speed interpolation methods used by RAM and ORCA (i.e., c-linear versus $1/c^2$-linear interpolation).

The source, shown in Figure 2, was taken to be a 16 element planar array consisting of two identical sub-arrays separated by 10 metres. The sub-array elements were separated by 3 m and the tow depth of the array was taken to be 5 m. This particular layout, with equally spaced elements divided into linear sub-arrays, was chosen because it is similar to commonly used airgun array configurations. The array elements all had identical amplitude and phase so that the main lobe of the array was in the vertical ($\phi = \pm 90°$) direction. Additionally, the source level of each element was taken to be $SL = -10 \log N$ dB @ 1 m ($N = 16$) so that the vertical far-field source level of the array was 0 dB @ 1 m (unity amplitude). The propagation direction was taken to be $\theta = 45°$, as indicated by the arrow in Figure 2; this direction was purposely chosen to be at an angle with respect to the array axis so as to increase the complexity of the vertical directionality function and thus provide a more rigorous test case.

Figure 3 shows benchmark transmission loss comparisons for a receiver at 50 m depth. The transmission loss comparisons were run at two frequencies, 125 Hz and 500 Hz, which correspond to quarter-wavelength and single-wavelength multiples of the sub-array element spacing. The plots show excellent agreement between the transmission loss computed using RAM and ORCA, indicating that the array starter is valid and that it was implemented correctly.

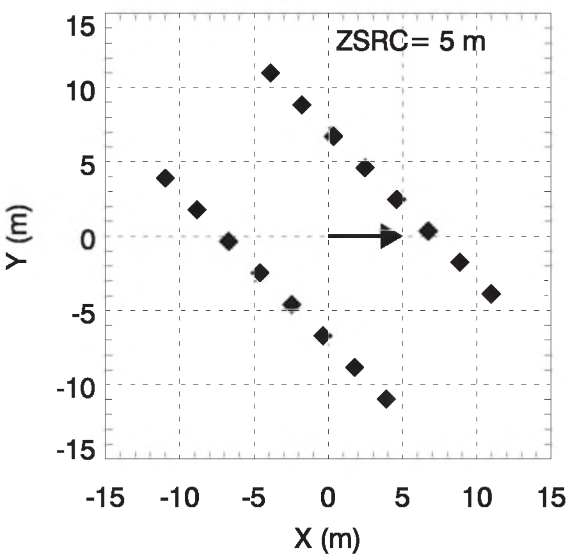

Figure 2: Diagram of the 16 element planar array used for the benchmark test scenario (the tow depth of the array is 5 m). The diamonds indicate the locations of the array elements and the arrow shows the direction of sound propagation (i.e., increasing r).

Figure 3 also shows the transmission loss for an isotropic point source with $SL = 0$ dB @ 1 m, for comparison. Although the isotropic source has the same source level as the 16 element test array in the vertical direction ($\phi = \pm 90^{\circ}$) the transmission loss for the point source is ≈ 12 dB less than for the array source in the horizontal direction. This example shows that, when modeling sound propagation from an array source, it is important to take directionality into account in order to to avoid substantial errors in the received sound level estimates.

4 SYNTHETIC WAVEFORM EXAMPLE

This section gives an example of a synthetic waveform calculation in a range-dependent test environment in order to demonstrate how the array starter method may be applied to a real airgun modeling problem. For this example calculation, a set of notional airgun signatures has been computed using a physical modeling approach. The source model employed here predicts notional airgun signatures by modeling the oscillation and radiation of a collection airgun bubbles and was developed by one of the authors as part of a thesis project [6]. In addition to the bubble oscillation physics, the source model includes non-linear pressure interaction between bubbles, port throttling and thermodynamic heat transfer across the bubble wall. The output of the airgun model has been validated against a large collection of source signature data for Bolt 600/B airguns [7]. The model physics are based on the work of investigators such as Ziolkowski [8, 9], Laws *et al.* [10], and Landrø [11]. Note that, although modeled signatures have been used here, notional signatures for the array starter method could also be obtained from near-field acoustic measurements of an airgun array. When using measured signatures, however, it is important to remove pressure interaction effects from near-field measurements to obtain the notional far-field signatures [12].

A typical 16-gun, two-string, 1500 in^3 (24.6 liter) airgun array was chosen for the example synthetic waveform calculation, as shown in Figure 4. The nominal tow depth of the example airgun array was taken to be 6 m and the firing pressure was taken to be 2000 psi (13.6 MPa). Figure 5 shows the notional source signatures for this array as computed by the airgun source signature model. Distortion of the bubble pulses, particularly noticeable in the signatures of the 80 in^3 guns, is due to non-linear pressure interaction effects between airguns in the array [12]. Note that Figure 5 only presents source signatures for half of the guns in the array (i.e., a single string); the source signatures for the other eight guns are identical due to the symmetry of the array. The sampling interval of the synthetic source signature data presented in Figure 5 is $\Delta t = 100\ \mu$s.

In order to perform waveform modeling using the Fourier synthesis method, a discrete frequency grid is employed

$$f_k = k\Delta f, \quad k = 1, 2 \ldots M,$$

where Δf is the frequency spacing of the field calculations and $f_{max} = M\Delta f$ is the maximum field computation frequency. Recall that the frequency spacing also determines the length of the synthetic data window according to the relation $T = 1/\Delta f$. For the example calculation presented here, $\Delta f = 0.5$ Hz and thus the length of the synthetic data window is $T = 2$ s. The maximum computation frequency must be selected based on the power spectrum of the source waveforms; for the present example, $f_{max} = 1024$ Hz, which encompasses over 99.9% of the signal energy in the synthetic airgun waveforms shown in Figure 5.

In addition to the bandwidth of the field calculation, f_{max} also dictates the required frequency resolution for the source waveforms according to the relation $\Delta f = f_{max}/M$. Thus, one must generally resample the airgun source signatures in the frequency domain so that their Discrete Fourier Transforms (DFT's) have the same frequency resolution as the field calculations. This is most simply accomplished by padding or truncating the source signature data in the time domain before taking the DFT. Once the source signatures have been resampled to the correct frequency spacing, the DFT coefficients correspond to the complex phase/amplitude terms, $A_m(k\Delta f)$, at each model frequency. Equation 9 may then be used to compute the starting field, at frequency f along azimuth θ, from the DFT coefficients and the projected airgun coordinates, $\Delta r_m(\theta)$. Consistent spatial sampling is also important: at each frequency, the range and depth spacing of the PE grid is taken to be an integer multiple of the smallest value, to ensure that the computation points are coincident.

Figure 6 shows the range-dependent test environment that has been used for the example waveform synthesis calculation. Acoustic propagation has been modeled along a downward sloping bottom, with water depth varying from 50 m

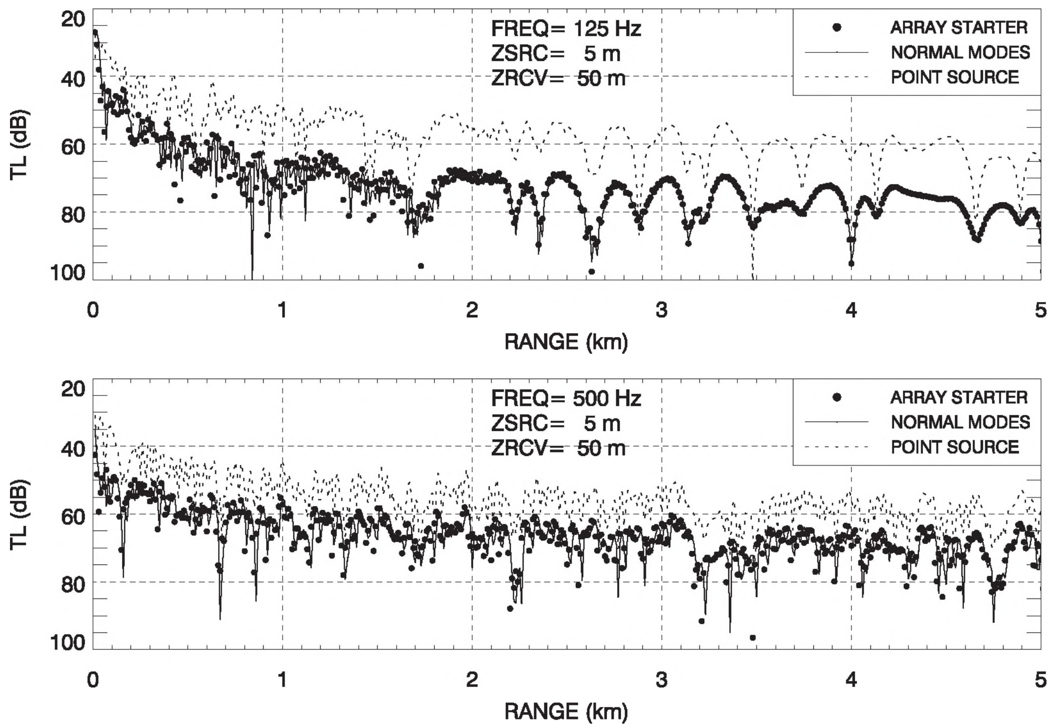

Figure 3: Benchmark comparison plots of transmission loss versus range for ORCA (solid line) and RAM seeded with the array starter (circles). Benchmark plots are presented for 125 Hz (top) and 500 Hz (bottom). For reference, the plots also show transmission loss for an isotropic point source.

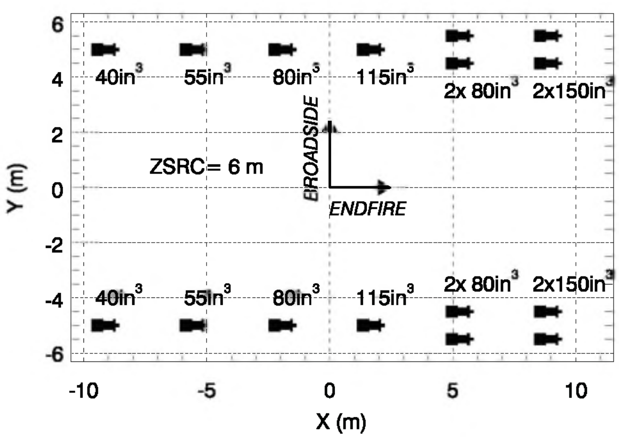

Figure 4: Plan-view diagram of the 16 airgun array used for the example calculation (total volume 1500 in^3); the nominal tow depth of the array was taken to be 6 m. The plot annotations indicate the volume of each airgun and the arrows show the broadside and endfire directions from the array.

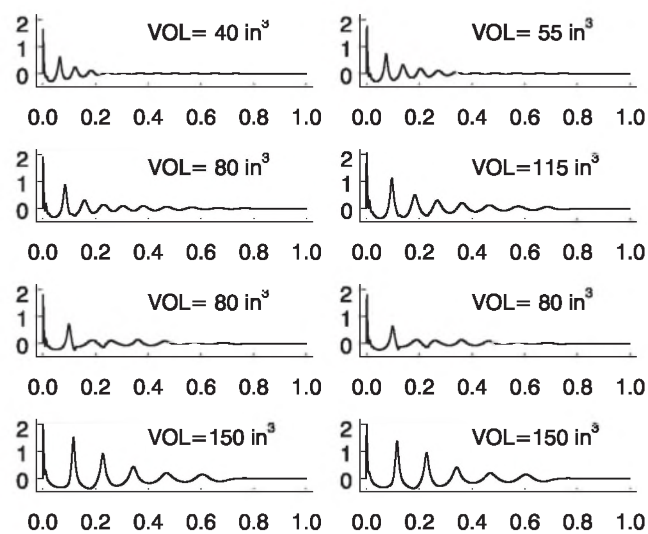

Figure 5: Notional source signatures for 8 of 16 guns in the 1500 in^3 example array, as computed by the source signature model. Pressure units (vertical axes) are in bar·m (1 bar=10^5 Pa) and time units (horizontal axes) are in seconds. The plot annotations indicate the volumes of individual guns. The source signatures for the remaining eight guns are identical to the ones presented here due to the symmetry of the array.

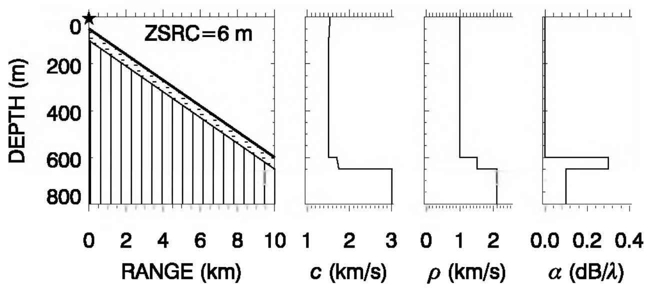

Figure 6: Diagram showing acoustic properties of the range-dependent environment used for the example waveform calculation. Acoustic parameters are sound speed, c, density, ρ, and attenuation, α. Note that the sound speed profile in the water column is downward refracting.

at the source to 600 m at 10 km range (3.15° slope). The sound speed profile in the water column is downward refracting, varying from 1.54 km/s at the sea-surface to 1.49 km/s at 600 m depth. The sub-bottom, which runs parallel to the bathymetry, consists of a 50 meter sediment layer over a semi-infinite basement. The sound speed in the sediment layer is upward refracting with a vertical gradient of 1/m ($c = 1.70$–1.75 km/s) and the sound speed in the basement is homogeneous ($c = 3$ km/s).

Figure 7 shows synthetic airgun pulse waveforms computed using the array starter method at r =10 km for the range-dependent test environment of Figure 6. Two cases are presented: one with array endfire ($\theta = 0°$) oriented in the downslope direction and the other with array broadside ($\theta = 90°$) oriented in the downslope direction. The plots show comparisons of airgun pulses at multiple receiver depths, from 50 m to 550 m in 100 m increments. Although the waveform data in Figure 7 are synthetic, they can be used to compute standard marine mammal noise exposure metrics, such as peak and *rms* sound pressure level, and sound exposure level (SEL), versus depth and range from the array, just as with acoustic data measured *in situ*.

The example waveforms presented in Figure 7 were computed assuming strictly two-dimensional sound propagation and also neglecting back-scattered energy from upslope of the array. Three-dimensional effects are unimportant for the example case presented here because the propagation plane is oriented directly downslope and so there is no horizontal coupling from adjacent azimuths [13]. The contribution of upslope back-scatter is expected to be negligible for the present example case, based on the work of Westwood [14] who showed that back-scattered energy was insignificant for penetrable wedge environments similar to the one considered here. Thus these two approximations are not expected to introduce significant errors into the waveform calcuations.

The synthesized waveforms in Figure 7 contain a considerable amount of structure due to the rich frequency content of the sound emissions from the airguns. From the figure, one can see that airgun pulses in the lower part of the water column ($z > 200$ m) have the greatest amplitudes and are much more sharply peaked than airgun pulses in the upper part of the water column ($z < 200$ m). This is because high frequencies, which carry the energy from the sharp initial peaks in the airgun source signatures, are trapped in the bottom duct created by the down refracting sound speed profile. In the high frequency raytrace approximation, the sound rays "skip" down the seabed slope creating a shadow zone near the sea-surface. At low frequencies, on the other hand, the long wavelength normal modes span the whole water column, thus leaking low frequency sound energy out of the bottom duct. The low frequencies, however, only carry energy from the lower amplitude airgun bubble pulses, rather than the peaks.

Inspection of the waveforms in Figure 7 shows that levels in the broadside direction of the array are louder, and contain more high-frequencies, than levels in the endfire direction. This is because, for each of the two subarrays, all sound wavelengths add constructively in the broadside direction, whereas only those wavelengths that are integer multiples of the gun spacing (or are substantially larger than the gun spacing) add constructively in the endfire direction. This kind of directivity, with maximum levels measured at array broadside, is typical of seismic airgun arrays, which often consist of several gun strings towed in parallel behind the survey vessel. This example shows that the direction of sound propagation (i.e., the azimuth angle, θ) is an important determiner of both the intensity and frequency content of the received pulse from an airgun array.

5 CONCLUSION

This article has presented an "array starter" technique for modeling sound propagation from an airgun array using the parabolic equation method. The array starter fully accounts for the vertical and horizontal directionality of an array source; it is computed by summing together phase-shifted, range-factored replicas of the PE self-starter for each array element. Field predictions computed using the array starter are valid in the far-field of the array, including those regions where the acoustic field is dominated by steep propagation angles. A numerical implementation of the array starter was validated against exact (range-independent) field solutions for an array source computed using the ORCA normal mode model. An example was also presented of how the array starter may be combined with the Fourier synthesis technique to generate synthetic airgun waveform data in a range-dependent environment. Synthetic airgun pulses, computed using the array starter technique, can be used for predicting common noise exposure metrics for marine mammals, including peak and *rms* sound pressure level, and sound exposure level. Although the array starter was devised with airgun arrays in mind, this technique can be used for modeling sound propagation for any kind of horizontal or volumetric array source using the parabolic equation method.

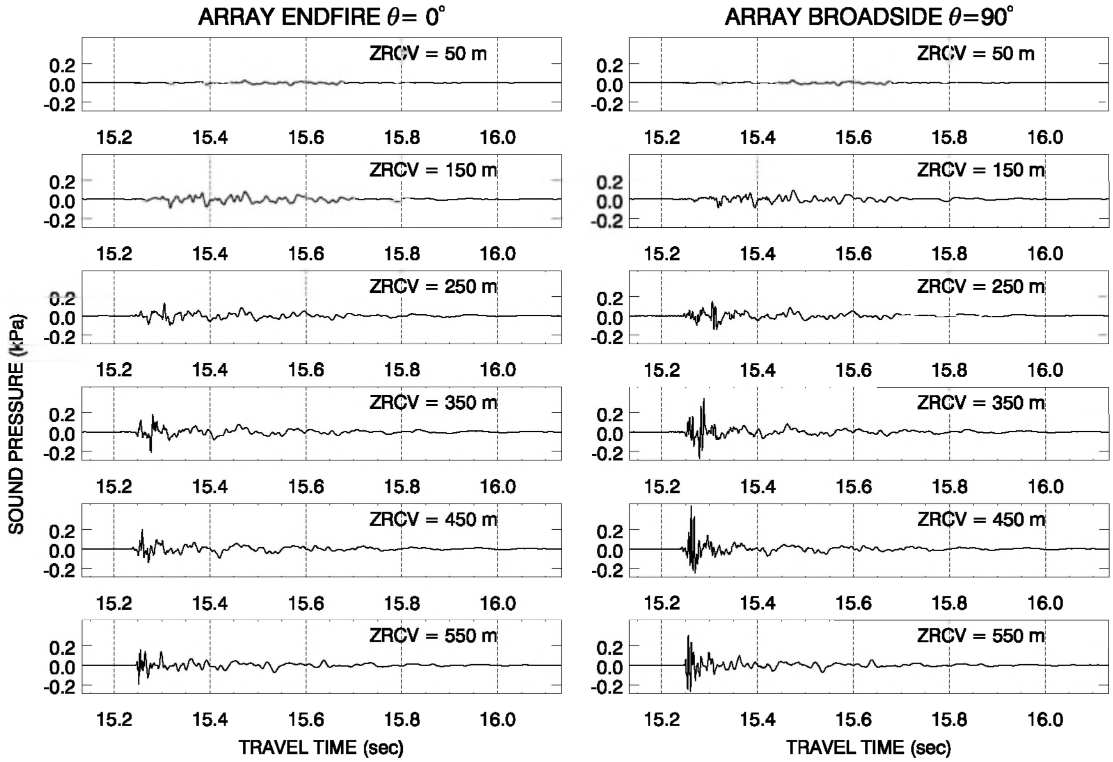

Figure 7: Synthetic airgun pulses at 10 km range, as computed in the range-dependent test environment of Figure 6, (left) for array endfire oriented downslope and (right) for array broadside oriented downslope. The receiver depth of each waveform is shown in the plot annotation. All waveforms are presented using the same time and pressure scales.

REFERENCES

[1] S. L. DeRuiter, P. L. Tyack, Y. T. Lin, A. E. Newhall, J. F. Lynch, P. J. O. Miller, "Modeling acoustic propagation of airgun array pulses recorded on tagged sperm whales (*Physeter macrocephalus*)" J. Acoust. Soc. Am. **120** 4100–4114 (2006).

[2] H. Schmidt and F. B. Jensen, "A full wave solution for propagation in multilayered viscoelastic media with application to Gaussian beam reflection at fluid-solid interfaces" J. Acoust. Soc. Am. **77** 813–825 (1985).

[3] M. D. Collins, "The stabilized self-starter" J. Acoust. Soc. Am. **106** 1724–1726 (1999).

[4] M. D. Collins, "A split-step solution for the parabolic equation method" J. Acoust. Soc. Am. **94** 1736–1742 (1993).

[5] E. K. Westwood, N. R. Chapman, and C. T. Tindle, "A normal-mode model for acousto-elastic ocean environments" J. Acoust. Soc. Am. **100** 3631–3645 (1996).

[6] A. O. MacGillivray, "An acoustic modelling study of seismic airgun noise in Queen Charlotte Basin" M. Sc. Thesis, University of Victoria (2006).

[7] R. G. Racca and J. A. Scrimger, "Underwater acoustic source characterization of air and water guns" DREP Technical report No. 06SB 97708-5-7055, Defense Research and Development Canada (1986).

[8] A. Ziolkowski, "A method for calculating the output pressure waveform from an air gun" Geophys. J. Int. **21** 137–161 (1970).

[9] A. Ziolkowski and G. Metselaar,"The pressure wave field of an air gun array" SEG Expanded Abstracts **3** 274–276 (1984).

[10] M. Laws, L. Hatton, and M. Haartsen, "Computer modelling of clustered airguns" First Break **8** 331–338 (1990).

[11] M. Landrø, "Modelling of GI gun signatures" Geophysical Prospecting **40** 721–747 (1992).

[12] A. Ziolkowski, G. Parkes, L. Hatton, and T. Haugland, "The signature of an air gun array: computation from near-field measurements including interactions" Geophysics **47** 1413–1421 (1982).

[13] F. Sturm and J. A. Fawcett, "On the use of higher-order azimuthal schemes in 3-D PE modeling" J. Acoust. Soc. Am. **113** 3134–3145 (2003).

[14] E. K. Westwood, "Ray model solutions to the benchmark wedge problems" J. Acoust. Soc. Am. **87** 1539–1545 (1990).

ACOUSTIC TRANSMISSION LOSS MEASUREMENTS IN QUEEN CHARLOTTE BASIN

Melanie E. Austin[1,2], Alexander O. MacGillivray[1] and N. Ross Chapman[2]
[1]JASCO Applied Sciences, Victoria, BC, CANADA
[2]School of Earth and Ocean Sciences, University of Victoria, Victoria, BC, CANADA

ABSTRACT

A transmission loss experiment was carried out during the winter in south Hecate Strait using a small airgun array source. Airgun pulses were recorded at horizontal receiver ranges between 20 m and 10 km using a bottom-mounted hydrophone recorder. Transmission loss values were computed by subtracting measured source levels from received sound levels in 1/3-octave bands. Transmission loss data were compared to predictions from a parabolic-equation (PE) sound propagation model coupled with an airgun array source level model. The measured transmission loss was characteristic of cylindrical spreading, with very little additional loss attributable to non-geometric terms. Mid-frequency (100-400 Hz) sound propagation was found to be best supported by the environment. The PE model predictions showed good agreement with the experimental data.

RÉSUMÉ

Une expérience ayant pour but de calculer les pertes de transmission acoustique a été menée au cours de l'hiver dans le sud du Détroit d'Hecate à l'aide d'un petit réseau de canons à air. Les impulsions des canons ont été mesurées par des enregistreurs posés sur le fond marin à des distances horizontales allant de 20 m à 10 km. Les valeurs de perte de transmission ont été calculées en soustrayant les niveaux sonores mesurés à la source de ceux reçus aux enregistreurs (niveaux exprimés en tiers d'octaves). Les résultats de perte de transmission obtenus ont été comparés aux prédictions d'un modèle de propagation du son utilisant l'équation parabolique. Les pertes de transmission mesurées étaient caractéristiques d'une propagation cylindrique avec une très faible contribution de termes supplémentaires non-géométriques. Il a également été trouvé que l'environnement facilitait la propagation du son en moyennes fréquences (100-400 Hz). Les prédictions issues du modèle d'équation parabolique concordaient avec les résultats expérimentaux.

1. INTRODUCTION

There is currently a moratorium on offshore oil and gas development in British Columbia, due to the environmental concerns associated with hydrocarbon exploration and extraction. In 2004, the Royal Society of Canada prepared a report [1] identifying knowledge gaps in science related to oil and gas development in the BC offshore. The impact of man-made noise on marine mammals and fish was identified as one key area of concern associated with offshore exploration activities. Underwater sound generated by seismic airgun surveys has the potential to negatively impact marine mammals and fish in the surrounding environment [2]. The need to further investigate the potential impacts of noise associated with seismic surveying was identified as a significant knowledge gap in the Royal Society report.

Assessing the potential impact of seismic exploration on marine mammals and fish requires estimates of the acoustic footprint of airgun survey activities. Acoustic propagation models—particularly those based on the parabolic-equation (PE) method—can be used to estimate the noise footprint of seismic surveys [3]. The accuracy of numerical models is limited, however, by environmental uncertainty. Required model inputs include the defining properties of the water column and ocean bottom that impact the sound transmission characteristics of the environment (bathymetry, sound speed profile, geoacoustics, etc.). When available, field measurements can be used to characterize the acoustic properties of specific environments helping to calibrate model inputs and serving as a means to validate model estimates.

This paper presents results of an airgun transmission loss study that was carried out in Hecate Strait in December 2006 to characterize airgun sound transmission in the BC offshore and to assess the accuracy of PE model estimates for this environment [3]. The goals of the study are as follows:

1. To measure source and received levels for airgun pulses at various source-receiver separations.

2. Determine the characteristic transmission loss in the environment from the airgun measurements.

3. Examine the sound transmission characteristics at the location as a function of sound frequency.

2. METHODS

2.1 Transmission Loss Experiment

The transmission loss experiment was carried out in Hecate Strait on 4 December 2006 at a location near a number of historical oil and gas exploration well sites (Figure 1). A small airgun array source was towed behind the study vessel (Silver Dawn I) along a transect that provided received level measurements at various source-receiver separation distances. An ocean bottom hydrophone (OBH) recorder system was used to collect transmission loss data as the vessel traversed the track.

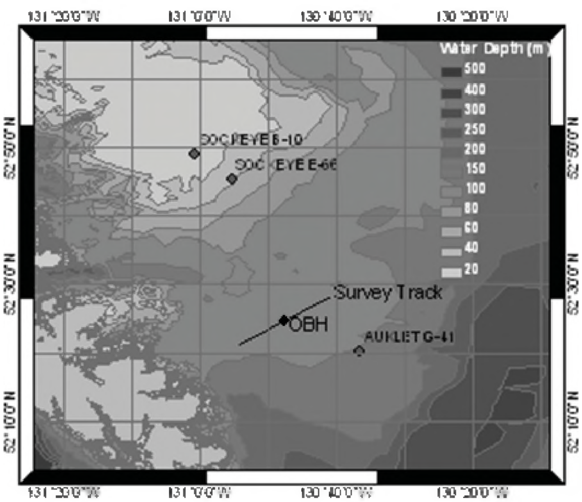

Figure 1. Map of study area showing OBH position (diamond) and survey track (line). Locations of historical oil and gas exploration wells are also indicated.

The towed acoustic source was a 30 in^3 airgun array consisting of two airguns (10 in^3 and 20 in^3) mounted side by side on a custom built frame, separated horizontally by 1 m. The array was towed at a depth of 4 m and the depth was monitored using an underwater depth sensor (JASCO AIM 2000). A calibrated reference hydrophone (Reson TC4034 with nominal sensitivity -218 dB re 1 V/μPa) mounted 1 m in front of the airgun array provided source level measurements. The signal from the source hydrophone was recorded at 25 kHz using a 16-bit laptop-based acquisition system (Quatech DAQP-16). This airgun array was much smaller than a typical industry array; however, the experiment was not intended to mimic a production seismic survey, but rather to characterize the sound transmission of a source signal characteristic of airgun pulses.

Acoustic data were collected using an OBH recorder system that was deployed on the seafloor (114 m depth). The system was mounted with a calibrated Reson TC4043 hydrophone (nominal sensitivity of -201 dB re V/μPa). A Sound Devices 722 24-bit digital hard-drive recorder inside the OBH pressure housing recorded data at 32 kHz during the experiment while the source vessel sailed along the a track that passed directly over the recorder. The source vessel travelled from southwest to northeast along one track, 20 km in length, providing measurements of airgun signals at horizontal ranges between 20 m and 10 km range to each side of the OBH. A dedicated marine mammal observer was on board the source vessel throughout the study. There were no marine mammal sightings reported while the airguns were active.

A CTD (conductivity-temperature-depth) cast was performed at the OBH location prior to the transmission loss experiment, using a Seabird SBE-19 profiler. Temperature and salinity measurements were used to derive the sound speed profile in the water column as a function of depth (Figure 2). The sound speed profile was an upward refracting profile, typical for this environment in winter conditions [4].

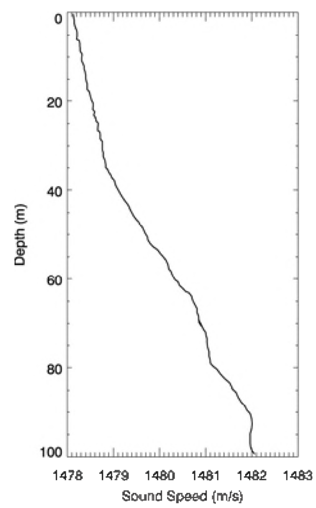

Figure 2. Sound speed profile at OBH location as computed from CTD cast data.

2.2 Data Processing

Acoustic data were processed using customized analysis software to obtain peak and rms sound pressure level (SPL) in dB re 1 μPa and sound exposure level (SEL) dB re 1 $\mu Pa^2 \cdot s$ for each airgun pulse. The source-receiver separation for each pulse was computed by matching the shot times with the vessel GPS navigation logs. Each pulse was transformed to the frequency domain to obtain the energy density spectrum ($\mu Pa^2 \cdot s$) in 1-Hz bins. The spectrum was integrated inside standard 1/3-octave bands from 10 Hz to 2 kHz to obtain 1/3-octave band SEL values for each airgun pulse. Transmission loss versus range (in decibels) was computed by subtracting the SEL received at the OBH from that received at the 1 m reference range for each pulse.

The received sound level at distance r from an underwater sound source can be approximated by a simple transmission loss equation expressed in decibels that incorporates geometrical spreading, reflections from the surface and seafloor, and attenuation within the water column and sea bed as follows [5]:

$$RL = SL - n \log r - \alpha r. \qquad (1)$$

In Equation (1), *RL* is the received sound level, *SL* is the source level (referenced to 1 metre), *n* is a geometric spreading constant, *r* is the source-receiver separation in meters, and α is a general attenuation coefficient. The last two terms in Equation (1) describe the transmission loss. The geometric spreading term has a value of 10 for conditions of cylindrical spreading and a value of 20 for spherical spreading.

Transmission loss estimates as a function of range were computed directly by subtracting the measured received levels from measured source levels.

2.3 Acoustic Modelling

Acoustic transmission loss was modelled using the RAM split-step Pade PE code, version 1.5g [6]. RAM was configured to estimate transmission loss along the experimental track in a reciprocal sense, meaning that for the purposes of the modelling, the source was placed at the seafloor and the receiver was modeled at the true source depth. The reciprocity principle of acoustics permits this transposition [7].

The transmission loss model required a description of the bathymetry, sound speed profile, and geoacoustics along the survey track. Bathymetry data were interpolated from a high-resolution (100 m) dataset provided by the Canadian Hydrographic Service (Figure 3). The sound speed profile in water was computed from the CTD profiler data. Based on surficial geology maps published by the Geological Survey of Canada, the seabed type at the study location was estimated to be sand and gravel [8]. Seabed geoacoustic properties for this bottom type (sound speed, density and attenuation versus depth) were based on profiles derived from a prior modelling study of sound propagation in Hecate Strait [3, Tab. 4.4].

Airgun source levels used for the model-data comparisons were computed using JASCO's calibrated airgun array source model (AASM) that estimates directional sound levels based on the volume, depth, and position of the individual airguns in an array [3].

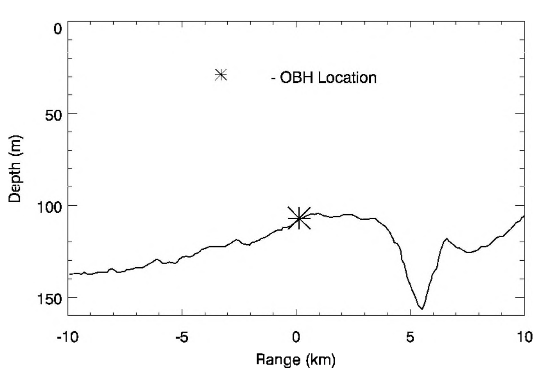

Figure 3. Bathymetry along experiment track. OBH recorder was deployed on the seabed at zero range, as indicated by the star symbol.

Modelled sound levels (SEL) were computed by combining source level estimates with computed 1/3-octave band transmission loss for each source-receiver pair. Broadband sound levels were computed by summing together the modelled 1/3-octave band levels.

5 RESULTS AND DISCUSSION

5.1 Airgun Source Levels

Source levels for the experiment were computed from the data received on the source hydrophone mounted on the airgun frame. Each individual airgun pulse was analyzed and the mean sound level over all shots was used to estimate the source characteristics (Table 1). The standard deviations show that the source level of the array was very consistent throughout the study. Using 1 second time windows, average 1/3-octave band source levels (dB re 1 μPa @ 1 m) were also computed for the airgun array (Figure 4). The dominant 1/3-octave band was observed to be at 20 Hz.

Table 1. Mean sound level of the 30 in^3 airgun array (± 1 standard deviation) as computed from the airgun pulses recorded at 1 m range.

Peak SPL (dB re 1 μPa @ 1 m)	rms SPL (dB re 1 μPa @ 1 m)	SEL (dB re 1 μPa^2·s @ 1 m)
231.5 ± 1.2	214.5 ± 0.7	206.1 ± 0.7

5.2 Transmission Loss Measurements

Transmission loss values were computed from the measured data in 1/3-octave bands from 20 Hz to 5 kHz (Figure 5). The data show that 1/3-octave bands with centre frequencies between 315–500 Hz exhibited the least transmission loss. The relatively high optimum frequency band for the transmission loss suggests that the bottom supports efficient shear wave propagation that increases the loss at low frequencies (< ~ 200 Hz) [9].

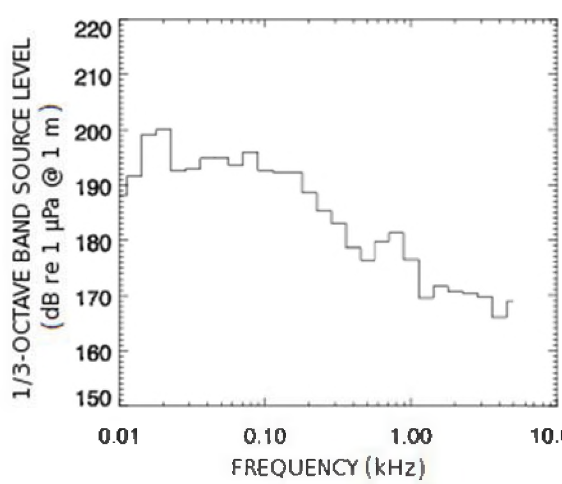

Figure 4. Mean 1/3-octave band source levels for the 30 in^3 airgun array.

The highest frequency bands (>1 kHz) showed the greatest loss at ranges less than approximately 3 km, beyond which the greatest loss was observed in the very low frequency bands (below approximately 100 Hz for the departure and below 50 Hz for the approach). Even though the propagation of low frequencies was not well supported in this environment, these bands contributed strongly to the received levels, since the source contained significant energy in these bands.

The empirical transmission loss equation (1) was separately fit to the transmission loss curves for 0.1 and 5 kHz, to derive the best least-squares fit for each band (Table 2). The spreading coefficient, n, was similar across the bands and the main difference arose in the α term, with the 2-5 kHz bands being well approximated by geometric spreading. The broadband transmission loss trend best matched the loss exhibited by the dominant 100–315 Hz bands.

Table 2. Least-squares coefficients for third-octave bands centred at 0.1 and 5 kHz.

Track		0.1 kHz	5 kHz
	SL	179	142
Approach	n	13.4	13
	α	0.001	0
	SL	175	143
Departure	n	10.8	11.7
	α	0.003	0

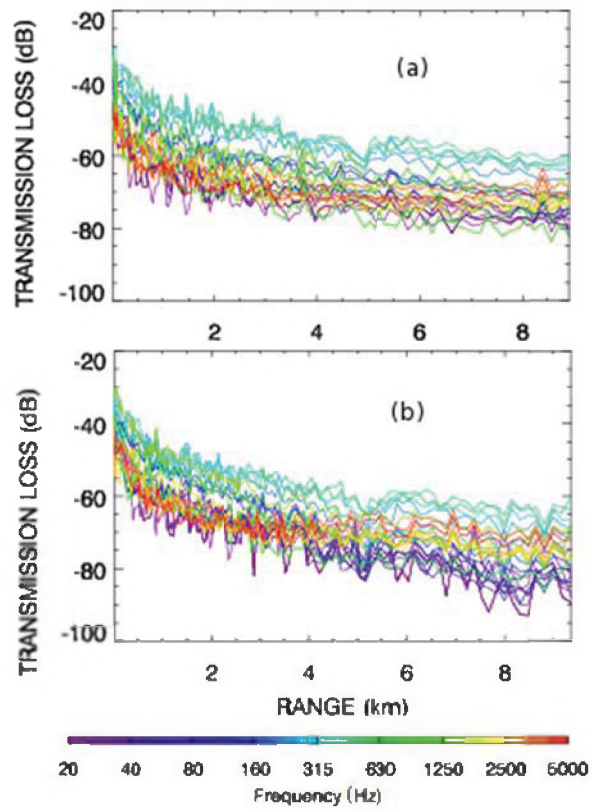

Figure 5. Transmission loss versus horizontal source-receiver separation, in 1/3-octave bands, as the vessel approached (a) and departed from (b) the OBH position.

5.3 Model Data Comparison

Figure 6 presents a comparison of 1/3-octave band levels versus range, as predicted by the PE model, to data measured along the approach track. The overall features are in excellent agreement between the model and the hydrophone data. Both the model and the data indicate dominance of the mid-frequency components at long ranges. The model predicted slightly higher received levels in the 0.5–1 kHz range than was measured in the experiment. Along the departure track (not shown) the model data agreement was also good for most frequencies, however excess long range attenuation at 10-40 Hz was not reproduced by the PE model.

Comparison of the broadband received levels (Figure 7) showed the data and model were in good agreement along the approach track to the OBH location. The model-data agreement was also very good for the departure track until approximately 5 km range, beyond which the measured data exhibited stronger transmission loss than predicted by the model. This may have been due to potential three-dimensional effects from the bathymetry, as the sound traveled cross-slope, that the two-dimensional transmission loss model did not account for. This may have also been due to a range-dependent transition in the seabed geoacoustics along the departure track, which was not accounted for by the PE model.

6. CONCLUSIONS

Acoustic measurements for south Hecate Strait showed that transmission loss in this environment is generally described as cylindrical spreading with very little additional loss attributable to non-geometric terms. Mid-frequency (100-400 Hz) sound propagation was found to be well supported in this depth regime (100-150 m). Comparison of the airgun measurements with sound levels predicted by the PE model showed good agreement between the model and the measured data. Both the model and the measurements indicated that the dominant sound transmission frequencies were between 100-400 Hz. The model slightly overestimated levels between 500 Hz and 1 kHz compared with the data, and did not predict the long range attenuation of some very low frequency energy as the sound traveled over a more complicated bathymetry along the departure track. The model-data mismatch along the departure track was attributed to environmental uncertainty and neglect of out-of-plane transmission loss effects by the two-dimensional PE model.

ACKNOWLEDGEMENTS

This work was funded by the British Columbia Ministry of Energy and Mines. We would like to acknowledge Roberto Racca for his participation in the field study. We thank Bob

MacDonald for his expert services operating the airguns during the survey, our Marine Mammal Observer Scott Toews, and Michel Jutras and the crew of the Silver Dawn I for their tremendous assistance working in this challenging environment.

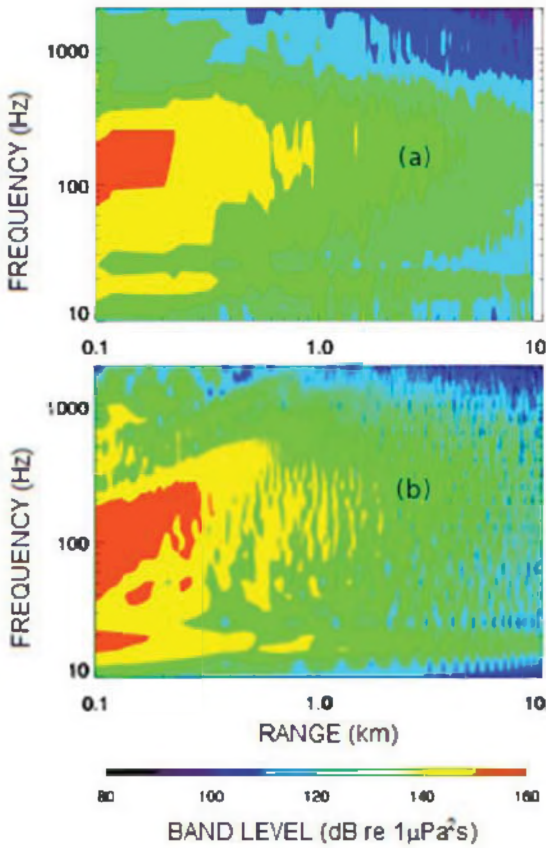

Figure 6. Contours of 1/3-octave band received levels (SEL) versus horizontal range and frequency, as calculated from the measurements (a), and as predicted by the PE model (b) for the approach track.

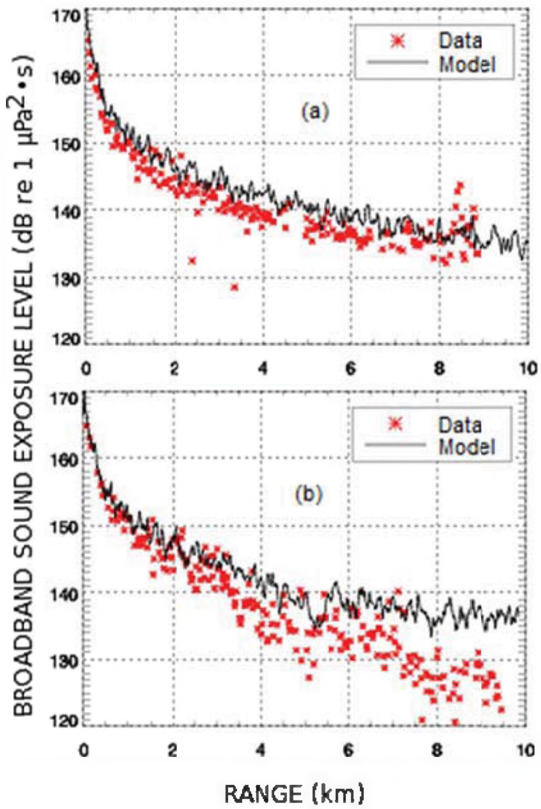

Figure 7. Broadband received levels (SEL) versus horizontal source-receiver separation as estimated by the PE model (line) and as measured in the experiment (star symbols), for the approach track (a) and the departure track (b).

REFERENCES

1. Royal Society of Canada (RSC). The Royal Society of Canada Report of the expert panel on science issues related to oil and gas activities, offshore British Columbia. RSC EPR 04-1 (2004).

2. W.J. Richardson, C.R. Greene Jr., C.I. Malme and D.H. Thomson. *Marine Mammals and Noise*. Academic Press, San Diego, CA (1995).

3. A.O. MacGillivray. An acoustic modelling study of seismic airgun noise in Queen Charlotte Basin. M.Sc. Thesis, University of Victoria (2006).

4. W. R. Crawford. Oceans of the Queen Charlotte Islands. Canadian Technical Report of Fisheries and Aquatic Sciences No. 2383, Institute of Ocean Sciences, Department of Fisheries and Oceans, (2001).

5. R.J. Urick. *Principles of Underwater Sound for Engineers*. McGraw-Hill, New York (1967).

6. M. D. Collins. A split-step Pade solution for the parabolic equation method. Journal of the Acoustical Society of America, 93:1736–1742, (1993).

7. F. B. Jensen, W. A. Kuperman, M. B. Porter, and H. Schmidt. Computational Ocean Acoustics. AIP Press, Woodbury, NY (1994).

8. J. V. Barrie, J. L. Luternauer, K. W. Conway, and A. Caltagirone. Surficial geology of the Queen Charlotte Basin. GSC Open Files 2193, 2195, 2196, 2197, Geological Survey of Canada (1990).

DEVELOPMENT OF DIGITAL ACOUSTIC SENSOR FOR REMOTE APPLICATIONS

Duane B. Watson, P.Eng, Greg VanSlyke, P.Eng
Omnitech Electronics, 1-10 Akerley Blvd, Dartmouth NS, Canada B3B1J4

ABSTRACT

Centralized sampling acquisition systems are commonly used to acquire and digitize data from arrays of acoustic sensors. These systems have centralized/co-located connection points for multiple sensor channels and contain digitization and processing electronics that can be shared across these inputs. While this system architecture can simplify the electronics design, it has several intrinsic properties that degrade the data quality and increase system complexity for certain application parameters. Advancements in high speed, low power electronics have made distributed sensor digitization feasible for applications with limited available power such as remote underwater surveillance and autonomous underwater vehicle systems. This paper explores some limitations of centralized systems in underwater acoustic applications and presents some examples of where the benefits of distributed digital sensors were realized.

RÉSUMÉ

Les systèmes centralisés d'acquisition d'échantillons sont couramment utilisés afin d'obtenir et de numériser les données en provenance des réseaux de capteurs acoustiques. Ces systèmes sont dotés de prises centralisées/adjacentes pour de multiples canaux de capteurs et contiennent des électroniques de traitement et de numérisation auxquels tous ces canaux ont accès. Tandis que ce système d'architecture peut simplifier la conception électronique, il possède plusieurs propriétés intrinsèques qui dégradent la qualité des données et accroissent la complexité du système pour certaines applications. Des avancements au niveau de l'électronique à haute vitesse à faible puissance ont permis la numérisation à partir de capteurs décentralisés pour des applications ayant une puissance restreinte, telles que la surveillance sous-marine à distance et les systèmes de véhicules sous-marins autonomes. Cet article examine certaines limites des systèmes centralisés dans des applications acoustiques sous-marines, et présente quelques exemples de situations où les avantages des capteurs numériques décentralisés ont été réalisés.

1. INTRODUCTION

Acoustic sensor arrays are used in a variety of complex underwater applications from static environmental monitoring antennas to non-linear towed hydrophone arrays.

In centralized sampling systems, piezo-electric acoustic sensors are distributed throughout the array and wired on individual electric pairs to a central data acquisition unit. In analog piezo-electric arrays, signals from the sensors are typically transmitted as analog current through a dedicated loop or as a pre-amplified voltage on a differential pair.

Within the past decade, high speed digital sampling, processing and transmission electronics have been relatively high cost and have had relatively high power consumption. This limited the use of sensor-integrated digitization to systems with high capacity power sources and large budgets. The proliferation of portable, battery powered handheld computing devices and phones has led to rapid advancements in low power, small, cost effective electronics well suited for acoustic data acquisition and processing. Distributed digital sensor arrays today can be designed and manufactured with little or no design overhead and similar, or even reduced, circuit complexity. Digital sensors can achieve advantages over analog equivalents in many areas. High level concept comparisons and application examples where digital acoustic sensor arrays have been successfully deployed are given in the following sections.

2. ELECTRO-MAGNETIC NOISE

Electro-magnetic interference (EMI) is a common source of signal noise in measurement systems. The magnitude and spectrum of the interference depends on several factors that are often outside the control of the acoustic system engineer or scientist. Influence on analog signals from EMI generated from external sources can be minimized by electrical shielding, shortened cable runs,

and other techniques. Often acoustic sensors are integrated into existing systems or spaces where removal of noise sources or relocating sensors is not possible. The levels and sources of EMI are not known as systems are designed for use in a multitude of spaces, locations and installations. EMI is not limited to high frequencies or nearby sources. Power line frequencies from high voltage transmission lines and electric railways can produce detectable interference over large distances in sensitive electronics. This interference can be detectable on analog acoustic arrays deployed in near littoral waters and in harbors.
When the acoustic system has to operate in environments with potential sources of EMI, digital data transmission from sensors ensures data collected at the sensors is not degraded and removes a variable error source from the system.

3. SMALLER CABLES AND CONNECTORS

Omnitech Electronics has designed acoustic arrays with more than 60 digital hydrophones over lengths greater than 1 km using fewer than five conductor pairs. If these arrays were built using analog sensors, the cable would require more than 120 conductors and connector pins. The number of conductors in a cable increases the size and weight of the cable which makes transport, handling and deployment of the array more difficult.

Since digital hydrophones can share power and data wires, the number of required conductors can be as few as four (two pairs) depending on the length of the array, sampling rate, and data capacity of the cable and transceivers. Fewer conductors allows for smaller, lighter, lower cost, and more flexible cable as well as simpler, smaller and less expensive connectors. In bottom deployed acoustic arrays, the smaller, lighter cables can be deployed from small vessels without any handling equipment. For AUV and other applications, small cables and connectors are more easily integrated into, and routed through, existing spaces.

4. RELIABILITY AND REDUNDANCY

All else equal, a cable with fewer conductors and connector pins has fewer points of failure and is more reliable than an equally made cable with more connections [1] . In addition, a digital signal is more easily paralleled to allow for redundancy. Omnitech has added redundant digital communication and power to systems where customers were worried about possible cable damage, a feature not economically possible with high sensor count analog arrays.

The level of EMI adds to the noise floor and reduces the effective dynamic range of the sensors. Relative immunity to EMI is a major advantage of digital signal transmission. In distributed digital systems, all acoustic signals are digitized as close to the analog sensor as possible thereby reducing the susceptibility to EMI. Digital data is transmitted to a central processing and/or data recording unit. As a digital signal, the data is immune to small signal EMI.

5. PRICE PER PERFORMANCE

As sensor count and cable distances increase so does the cost of cabling and connectors. In analog sensor arrays the cost of long cables can be the most significant cost of the system. With digital sensors, the cable cost represents a much lower portion of the total system thus significantly reducing the cost of large systems allowing a redistribution of funds away from costly cables to improved sensor performance. Funds that would be spent on passive cabling can be better spent on increased sensitivity, additional sensors, higher sample rates, increased processing, etc.

6. LOSS-LESS REPEATERS

Cable lengths on a digital data bus can be extended through the use of repeaters or optical converters without any additional signal loss or distortion. With analog sensors, adding cable length adds output capacitance, resistance and inductance and will affect the signal properties and frequency response of the sensors. Analog repeaters add signal distortion and increase power consumption and ultimately limit the performance of systems with long cable runs.

7. INTEGRATED ACOUSTIC CALIBRATION

Digital acoustic sensors can be made ‘smarter’ than analog sensors. Each individual sensor in an array can be configured with a unique identification number that allows that particular sensor to be tracked and correlated to recorded data without any error prone external data records. Furthermore, Omnitech’s implementation of the digitalization circuitry allows for in-sensor acoustic calibration. Coefficients for calibrated sound pressure levels, in engineering units, can be stored in each sensor and all acoustic outputs adjusted ‘in-sensor’. In this approach, calibration factors remain with the sensor wherever that sensor is used and requires no externally stored information. This feature is impractical to implement and error prone in a centralized system in which the analog array can be detached and interchanged with the digitization circuitry and/or calibration software.

8. Mixed Signal Sensors

Some detection, monitoring, diagnostic and classification applications benefit from simultaneously sampled, mixed signal sensors. With distributed digital arrays, multiple types of sensors can be integrated into the acoustic array and simultaneously sampled on a signal cable. Omnitech has successfully integrated both magnetic and electric field sensors along with high resolution pressure, heading, optical and temperature sensors in to acoustic arrays. Digital sensors can be configured with sensor identification data and parameters. Upper level systems and software can read this data from the sensors thus reducing the amount of user entered information in reconfigurable and traceable systems.

9. Sensor Design and System Flexibility

Omnitech has been developing distributed digital sensors for acoustic and mixed sensor systems and arrays since 2001. Initial arrays were developed to be disposable, and rapidly deployable in shallow water (< 200 m depth). These systems were used in technology demonstration projects with Defence Research and Development Canada as part of Underwater Canadian Acoustic Research Arrays (UCARA) and Rapidly Deployable Systems (RDS)[2] projects. Omnitech continues to make significant improvements to design concepts from these projects and has demonstrated the benefits of distributed digital sensors in a variety of custom applications. Since 2007, Omnitech has refined system components to create a flexible platform for highly customizable systems. The power efficiency achieved through use of new advances in power efficient electronics allows these digital systems to be used in applications with limited available power.

The advantages of distributed sensors systems can be realized in more than just underwater applications. Any system with multiple analog sensors and central data collection can benefit. Example applications include building monitoring, seismic surveys, microphone arrays, large area surveillance, noise source localization and diagnostic measurements.

10. Real-Time Gain Control

Most acoustic sensors in conventional arrays have a fixed gain preamplifier that drives signals to the central digitizer. If this preamplifier gain is too low, small signals will be lost in the system noise whereas if it is too high, larger signals are distorted by clipping.

With Omnitech's distributed digital sensors, all gain stages can be adjusted in real-time to maximize the dynamic range of the system according to the optimal settings required for the given measurement. For example, Omnitech's 24-bit deep water hydrophone has real-time gain control settings from 0 – 90 dB in 10 dB steps. This flexibility allows the same system to measure very small and very large sound pressure levels without hardware changes in the array. The same digital array can be deployed for measuring seismic blasting or ambient noise without modifications.

11. Low Cost Monitoring Arrays

Omnitech has designed and built low cost shallow water (< 200 m) arrays for use in harbour and coastline surveillance[3] and asset protection. In these arrays, sensor elements and digitization electronics are molded directly into the cabling as shown in Fig. 1. The resulting arrays are light weight, rugged and can be deployed by hand from small vessels and connected to surface, shore or small underwater data collection and/or processing units. Omnitech has delivered these arrays with various sensor configurations of 48 single frequency or mix sampling rate acoustic, environmental, and orientation sensors and with connector breakouts and for customized low frequency and high frequency electro-magnetic sensors.

Figure 1. Low cost acoustic array, elements (darker), molded directly into the cable

12. Long Range Acoustic Bearing for AUVs

Omnitech has used digital hydrophones to create a long range acoustic bearing system (LRAB) using a three axis direction acoustic array. LRAB designed for under-ice operation in an AUV and was used in DRDC's project Cornerstone in support of the United Nations Convention on the Laws of the Sea (UNCLOS) data collection for Natural Resources Canada. These arrays were able to accurately calculate a homing bearing to a 190 dB, 1350

Hz sound source at ranges of more than 50 km and survive to depths greater than 3 km under the ice in the Canadian Arctic. A photo of the AUV under the ice during Cornerstone is shown in Fig. 2.

Figure 2. AUV under the Canadian ice sheet, using LRAB acoustic bearing array

The arrays had to function in close proximity to high power bottom sounding sonar and electronics and relatively high levels of vehicle noise. Each array is paired with a custom low power embedded processing board that runs the array data collection and processing software and communicates with the vehicle control computer via Ethernet. The entire system uses less than 2 W from the AUV power supply. The array used in the Project Cornerstone AUV, is 17.5 inches in diameter and uses seven (7) digital hydrophones connected to a 4-wire connector through the AUV pressure hull. This array is shown mounted in an AUV nosecone in Fig. 3. Omnitech has also developed a reconfigured version that is 5.8 inches in diameter for smaller AUVs with shorter homing range and reduced depth requirements. Fig. 3 shows

Figure 3. Digital LRAB Array mounted in AUV nose cone (left), Deep water digital hydrophone (right)

13. ARCTIC SURVEILLANCE

Arctic sovereignty has become a high profile priority for Canadian and international governments, companies and communities. Omnitech has developed acoustic arrays designed for multi-year deployment in remote arctic locations.

Figure 4. DRDC Artic Research Camp, Devon Island, NU

These arrays are part of a technology demonstration project with DRDC Atlantic[3] . A photo of the remote camp for these trials is shown in Fig. 4. The low power design of Omnitech's digital arrays is critical in remote locations such as the Arctic. Even when arrays are tethered to shore, power over long-term, unmanned deployments is limited and must be supplied by onsite power generation that can survive and operate through Arctic winters.

14. AUV TOWED ARRAYS

Digital distributed sensors have a significant advantage over analog hydrophones in AUV applications in several regards. Digital arrays can make use of smaller connectors through bulkheads to dry bays in the AUV since data from dozens of sensors can be multiplexed onto a signal communications data bus. Electronic components required for filtering and sampling the acoustic data are distributed into the hydrophones rather than located in the dry bay of the AUV. With all else equal, this reduces the required size of the internal electronics and saves space that is often at a premium within the vehicle. All sensitive analog electronics are located in the array, away from potential EMI sources in the AUV such as switching power supplies, pulse-width modulation (PWM) based servo motor controllers and partial duty cycle sounders or sensors that create periodic power loads. Modern digital electronic components are small compared with the low-noise, high-sensitivity piezo-electrical hydrophones elements. As a result., integrating the digitization circuitry with the analog amplifier can be done with only a marginal increase in the size of the sensing element in the array.

15. DEEP WATER ACOUSTIC ARRAYS

In water depths greater than approximately 1000 m, the hydro static pressure becomes too high for encapsulated electronic components to survive without being enclosed in a pressure vessel versus epoxy or urethane encapsulation often used for shallow water sensors. In Omnitech's deep water products all electronic components are enclosed in connectorized pressure vessels and all individual hydrophones are pressure tested before integration into the overall system. Digital data from deep water sensors can be transmitted to shore, surface buoy, or stored in underwater data collection units. Omnitech's deep water array and data collection unit can operate for up to six weeks recording continuous data from 64, 24-bit digital hydrophones at 5 kSp/s plus a high frequency hydrophone at 40 kSp/s.

16. CONCLUSION

Distributed digital sensors offer significant advantages over centralized sampling of analog sensors in multi sensor systems common to underwater acoustic and other applications. These advantages have been realized in many successful projects that would not have been manageable or cost effective using distributed analog arrays. Low power modern electronics allow digitization and communication circuitry to be integrated into sensing elements with minimal increase in size. Smaller cables and reduced connector pin counts reduce the handling requirements, weight and cost of wiring while also increasing reliability of connections. The advantages of distributed digital sensors should be considered when designing any acoustic or mixed signal measurement system.

17. REFERENCES

[1] Military Standard, MIL-HDBK-217F Notice 2, (1995) "Military Handbook – Reliability Prediction of Electronic Equipment", Section 17.1., US Department of Defence.

[2] Rapidly Deployable Systems Array Technology. Defence Research and Development Canada Atlantic Fact Sheet NO. NetALS0108, 2008.

[3] G.J. Heard, N. Pelavas, C.E. Lucas, I. Peraza, D. Clark, C. Cameron, V. Shepeta ,"Development of Low-cost Underwater Acoustic Array Systems for the Northern Watch Technology Demonstration Project"., , Canadian Acoustics Vol. 39(3), pp 200 - 201, (Sept. 2011).

SPARSE BROADBAND ACOUSTIC RESPONSE ESTIMATION VIA A GAUSSIAN MIXTURE MODEL WITH APPLICATION TO M-ARY ORTHOGONAL SIGNALING

Paul J. Gendron
Maritime Surveillance Division, Code 56490
Space and Naval Warfare Systems Center Pacific, San Diego CA, USA.
paul.gendron@navy.mil

ABSTRACT

Shallow water acoustic response functions at high frequencies and large bandwidths exhibit spatio-temporal variability that depends greatly on the propagation media's volume and boundary conditions as well as system source-receiver motion. For this reason practical acoustic systems invariably must operate without perfect knowledge of the space-time state of the ocean media. Considered here is a Gaussian mixture assignment over Doppler and channel bandwidth employed to describe the amplitude and phase of such acoustic response functions over signal duration and bandwidth that can serve in many scenarios to replace recursive least squares and Kalman-like algorithms. The mixtue Gaussian model of channel dynamics allows for the accurate and adaptive description of the response function. The model is flexible and naturally accommodates varying degrees of observed channel sparsity. Posterior expectations are derived and shown to be soft shrinkage operators over Doppler-channel frequency. The model allows for novel and accurate estimates regarding the aggregate acoustic path dilation process that serve to replace conventional phase locked loops. This adaptive filtering scheme with aggregate path dilation estimation and compensation is tested on M-ary orthogonal signals at both 1 and 2 bits per symbol during the Unet08 acoustic communication experiments. These tests took place in the downward refracting, lossy bottom environment of St. Margaret's Bay Nova Scotia off of the R/V Quest. Receiver algorithms based on this approach were applied to a single element acoustic time series and empirical bit error rates demonstrate a 4 dB improvement over rank based maximal path combining methods. For a single hydrophone at 2 bits per symbol a bit error rate of less than 10^{-4} is observed at received SNR < -10 dB corresponding to an SNR/bit < 14 dB.

1 INTRODUCTION

This work is concerned with the basic problem of accurately estimating the time varying broadband acoustic Green's function in dynamic shallow water environments from observed measurements at very low signal to noise ratios (SNRs). The methods are fundamentally adaptive filtering schemes and constitute an essential component to a wide range of signal analysis methods from medical diagnostics [16] and classification of volume density from ultrasound backscatter [8] to acoustic communications applications [11][18] . Conventional approaches in the context of acoustic communications include variants of least mean square, recursive least squares and the Kalman filtering algorithm[2][10][15]. These approaches fundamentally leverage the temporal coherence of the Green's function through appropriate averaging to ensure that the resulting estimates are statistically efficient. One shortcoming of these algorithms is that they are typically employed in a look-back framework, only exploiting preceeding observations to make inferences regarding the present time sample. By marching forward in time and leveraging a Markov assumption regarding the process, these algorithms exploit a temporal model of the dynamics of the response process to make an estimate of the present state. For the case of observations over a finite duration window, more data can be brought to bear on the estimation problem and greater statistical efficiency can be attained. The time-recursive Gauss-Markov framework is capable of being adapted to such scenarios by employing forward-backward methodologies to fully exploit the temporal dependencies.

This article develops and demonstrates an estimation scheme based on a mixture-Gaussian model over time/Doppler and frequency/selectivity such that the Green's function at any instant can be estimated given all of the data over the entire duration and bandwith of the signal[9]. The resulting mixture-Gaussian framework allows for a level of flexibility in the regularization that is not as easily accomplished with Gauss-Markov models short of full forward-backward recursions. The latent parameters of the mixture model succinctly and parsimoniously capture the degree of sparsity encountered in underwater acoustic environments. Presented here is a modeling framework for time varying acoustic response functions that can serve the practical needs of acoustic parameter estimation as well as coherent underwater acoustic communications. Much like forward-backward recursions the proposed adaptive filtering method allows for the efficient use of all of the observations within the signaling epoch to make inferences regarding each time instant within that epoch.

1.1 Joint channel and symbol estimation

The specific application to be explored here is that of adaptive filtering applied to underwater acoustic communication receivers where estimates of the acoustic response enable coherent multipath combining. Let the measurements at the acoustic receiver be represented by $\mathbf{r}$, the acoustic response over the broadband channel as $\mathbf{h}$ and let $\mathbf{b}$ represent the symbols sent. An acoustic communication receiver can be broadly described as a set of symbol decision rules $\hat{\mathbf{b}} = D_{\mathbf{h}}[\mathbf{b}|\mathbf{r}]$ that extract the relevant information regarding the symbols from the received data. However since the prior constraints on the acoustic response function are not easily analytically averaged out over the conditional density of the data the optimal solution

$$\begin{aligned} \hat{\mathbf{b}} &= \arg\max_{\mathbf{b}} \int p(\mathbf{r}|\mathbf{h},\mathbf{b}) \times p(\mathbf{h})\; d\mathbf{h} \\ &= \arg\max_{\mathbf{b}} \;\; E_{\mathbf{h}}\; [p(\mathbf{r}|\mathbf{h},\mathbf{b})] \end{aligned} \tag{1}$$

can be unwieldy. While the conditional model of the received data $p(\mathbf{r}|\mathbf{h},\mathbf{b})$ will almost invariably be a multivariate Gaussian density and the bit coding scheme allows $p(\mathbf{b}|\mathbf{h},\mathbf{r})$ to be well specified [15] the marginal $p(\mathbf{b}|\mathbf{r})$ is an average over an acoustic channel of high dimension residing in a much higher dimensional (> 1000) delay-Doppler space. This makes computing $\hat{\mathbf{b}}$ a significant challenge. For this reason it is useful to break up the problem into a few simpler ones that are more easily handled and for which tractable and computationally less burdensome solutions can be derived. The solution $\hat{\mathbf{b}}$ can be well approximated by solving a sequence of conditional optimization problems in the parameters of $\mathbf{h}$. The result is a set of estimators for the channel parameters and a set of decision rules conditioned on those channel estimates.

$$\begin{aligned} \hat{\mathbf{h}}^i &= E_{h|b=\hat{b}}[\mathbf{h}|\mathbf{r},\mathbf{b}=\hat{\mathbf{b}}^{i-1}] \\ \hat{\mathbf{b}}^i &= \arg\max_{\mathbf{b}} p(\mathbf{b}|\mathbf{r},\mathbf{h}=\hat{\mathbf{h}}^i) \;\; . \end{aligned} \tag{2}$$

This sequence characterizes the channel estimation based receiver approach taken here. Various optimization schemes for each conditional density may be chosen and associated algorithms follow. More accurate rules can be derived, for instance the channel conditional expectation based on the symbol decision could rather be weighted over symbol probabilities,

$$\hat{\mathbf{h}}^i = E_{b|r} E[\mathbf{h}|\mathbf{r},\mathbf{b}]$$

rather than simply conditioned on the argmax: $\hat{\mathbf{b}}^i$. Use of such $soft$ decision rules would lead to weighted averages with added computational costs but no greater conceptual hurdle. The receiver structure takes advantage of the analytic simplicity of the conditional densities of the channel and symbol parameters to approximate the maximizing argument of the marginal density. Adaptive filtering, the estimation of the channel state, is therefore critical for coherent multipath combining in time varying environments.

1.2 Organization of this article

The remaining sections of this article are organized as follows: Section 2 presents the salient features of shallow water acoustic response functions and associates the dynamic parameters with the delay-Doppler acoustic response. Section 2 then goes on to present the Gaussian mixture model as a means of describing the sparse delay-Doppler arrivals of acoustic response functions. The section goes on to derive estimators for the acoustic response function given a received time series. Section 3 presents an aggregate path dilation process model and shows how accurate estimates of the acoustic response function can be used to unravel bulk correlated path delay time processes. Section 4 presents various acoustic communication receiver algorithms for M-ary orthogonal signaling based on the proposed adaptive filtering scheme. Section 5 presents results from an M-ary orthogonal signaling experiment taken during at-sea tests in St. Margaret's Bay. Section 6 presents summarizing statements, conclusions and future work.

2 MODEL OF UNDERWATER ACOUSTIC RESPONSE

Each acoustic path linking source and receiver exhibits geometric spreading and frequency dependent volume attenuation [12][20]. Let $l_{m,t}$ represent the acoustic path length of the m^{th} acoustic path at time t and let $\tau_{m,t} = \int_{l_{m,t}} d\mathbf{s}/c(s,t)$ represent its propagation delay. The amplitude and phase contribution of the pressure field at the receiver due to the m^{th} path is

$$\begin{aligned} h_{m,t,f} &= l_{m,t}^{-1+\epsilon_m} \times e^{-\alpha(\omega) l_{m,t} + \sum_k \gamma_{m,k}(\omega)} \times e^{-j\omega\tau_{m,t}} \\ &= a_m(t,f) \times e^{-j\omega\tau_{m,t}} \qquad\qquad \omega = 2\pi f. \end{aligned} \tag{3}$$

The first term captures attenuation due to geometric spreading and with $|\epsilon_m| << 1$ the refractive effects through the volume. The second term summarizes the volume attenuation due to sea-water absorption losses [12][20]. The term $\sum_k \gamma_{m,k}(\omega)$ summarizes the boundary interactions where Re$\{\gamma\}$[nepers], Im$\{\gamma\}$[radians]. Here $\gamma_{m,k}$ is the reflection coefficent of the k^{th} boundary interaction along the m^{th} acoustic path. The final term captures the aggregate phase rotation associated with propagation over the acoustic path. The phase rotation is a linear funtion of frequency as the sound speed and thus $\tau_{m,t}$ is not a function of frequency. The aggregate acoustic response function is the superposition of these M_{path} acoustic contributions

$$h_{t,f} = \sum_{m}^{M_{path}} h_{m,t,f}. \tag{4}$$

The inverse Fourier transform of Eq. (4) is the response function over path-delay and geo-time and can be expressed as

$$\begin{aligned} h_{t,\tau} &= \textstyle\sum_m^{M_{path}} \psi_{m,t}(\tau - \tau_{m,t}) \\ \psi_{m,t}(\tau) &= (2\pi)^{-1} \textstyle\int a_m(t,\omega/2\pi) \times e^{j\omega\tau} \;\; d\omega. \end{aligned} \tag{5}$$

Here notation is simplified by retaining h as the response function regardless of the basis functions or domain over which it is defined. The response function can likewise be represented over the delay-Doppler domain with

$$\begin{aligned} h_{\Delta,\tau} &= \sum_{m}^{M_{path}} \psi_{m,\Delta}(\tau) \\ \psi_{m,\Delta}(\tau) &= \int_{I_T} \psi_{m,t}(\tau - \tau_{m,t}) e^{-j\Delta t} dt. \end{aligned} \tag{6}$$

The total delay spread of the multi-path channel is

$$\tau_{max} = \max_{m,t}\{\tau_{m,t}\} - \min_{m,t}\{\tau_{m,t}\}. \tag{7}$$

Underwater acoustic response functions can vary greatly across ocean environments as well as over time in a given ocean environment. Certain bottom materials and roughness, water sound speed and surface wave spectra imply certain acoustic response functions and these can vary greatly spatially and temporally. Given the environmental conditions numerical solutions to acoustic propagtion can be useful in revealing the characteristics of broadband acoustic channel conditions [12] however acoustic receiver algorithms must be robust to spatial and temporally varying channel conditions with limited or no prior information regarding any of the acoustic environment parameters. The algorithms must effectively construct the essential parameters of the response from the measured pressure field. Because of the unknown and diverse range of channel conditions a significant hurdle in underwater acoustic receiver algorithms is that the underlying model must not place severe restrictions on the temporal or spatial variations of the functions $\{\psi_m, \tau_m\}_{m\leq M_{path}}$ between communication epochs while simultaneously parsimoniously allowing for their variation within a signaling epoch. Such parsimonious representation allows for the low variance estimation of the response function while giving flexibility to handle quite different environments.

In the approach presented here two features of shallow water acoustic response function are exploited. First, their sparsity, the interarrival durations on average exceed the delay bandwidth of the intra-path spreading functions $\psi_m(\tau)$. Explicitly, with $\hat{\psi}_m(\tau) = \psi_m(\tau)/\sum \psi_m(\tau)$ it is postulated that $E[\sqrt{\int \tau^2 \hat{\psi}_m(\tau) d\tau}] < E[|\tau_m - \tau_n|])$ where the expectation operator $E[\cdot]$ is over the observed sample space of environments. Secondly it is postulated that the arrival delay processes $\tau_m(t)$ of the various paths for a given signaling epoch exhibit significant temporal correlation. This assumption is attributed to the fact that angle spreads of propagating paths in ocean waveguides are very small, typically less than 20^o often less than 5^o so that the dominant motion within the horizontal plane couples similarly to all coherent delay paths.

2.1 Model of passband frequency translated underwater acoustic response

Using the passband basis functions $\{e^{j\omega_c t}\phi(t - n/W)\}_{n\in I}$ of bandwidth W, centered at time n/W and frequency $f_c = \omega_c/2\pi$, express the M-ary orthogonal spread spectrum communication signal as

$$s_t = e^{j\omega_c t} \sum_n c_n^{\mathbf{b}} \phi(t - n/W). \tag{8}$$

Here the notation $c_n^{\mathbf{b}} = c_{<n>_{N_s}}^{b_{\lfloor n/N_s \rfloor}}$ is employed allowing the sent signal to be unencumbered with the specification of the duration N_s of the signaling frame. At the receiver the signal is

$$Hs(t) = \int h_{t,\tau} s_{t-\tau} d\tau$$

and with the simplified broadband channel model (4) express this time-frequency distorted signal as

$$\begin{aligned} Hs(t) \times e^{-j\omega_c t} = \sum_{m,n} c_n^{\mathbf{b}} e^{-j\omega_c \tau_{m,t}} \int \psi_{m,t}(\tau - \tau_{m,t}) \\ \times e^{-j\omega_c(\tau - \tau_{m,t})} \phi(t - \tau - n/W) d\tau. \end{aligned} \tag{9}$$

Expressing the baseband translated and filtered acoustic response function for the m^{th} path as

$$\tilde{\psi}_{m,t}(\tau) = \int \psi_{m,t}(\tau') \times e^{-j\omega_c \tau'} \phi(\tau - \tau') d\tau'$$

results in

$$Hs(t) \times e^{-j\omega_c t} = \sum_n c_n^{\mathbf{b}} \times h_{t,t-n/W} \tag{10}$$

$$h_{t,\tau} = \sum_m e^{-j\omega_c \tau_{m,t}} \tilde{\psi}_{m,t}(\tau - \tau_{m,t}).$$

The key features of the acoustic response (11) are now identified. First, time variations in the acoustic path delays $\tau_{m,t}$ imply both time varying phase modulations ($e^{j\omega_c \tau_{m,t}}$) and time varying arrival times of the phase-fronts ($\tau_{m,t}$). As previously mentioned the phase fronts are not dispersed since sound speed is not a function of frequency. Most of the energy is captured in a small set of delay times and therefore acoustic response functions are generally sparse with dominant arrivals occupying a relatively small proportion of the τ_{max} duration delay band. Secondly since angle spreads are small in the horizontal ocean waveguide the temporal process of the delay times exhibit considerable correlation.

The linear model (10) can be expressed as a sampled discrete time $t = \rho \times n'/W$ version as

$$Hs(n') \times e^{-j\rho\omega_c n'/W} = C_{\mathbf{b}}\mathbf{h} \ . \tag{11}$$

and letting $I_T = \{0 < t < T\}$ be the $K \times N_s/W + \tau_{max}$ duration communication packet interval and I_τ = [max$\tau_m(t)$, min$\tau_m(t)$] the passband translated acoustic response function can be represented in the delay-Doppler domain as,

$$h_{\Delta,\tau} = \sum_m \int_{I_T} e^{-j2\pi\Delta t - j\omega_c \tau_{m,t}} \times \tilde{\psi}_{m,t}(\tau - \tau_{m,t}) dt$$

which is simply expressed as,

$$h_{\Delta,\tau} = U_\Delta h_{t,\tau} \tag{12}$$

where U_Δ is the Fourier transform from geo-time to Doppler frequency. The channel response function can likewise be represented in the Doppler[Hz]-selectivity/frequency[Hz] domain via

$$h_{\Delta,f} = \int_{I_\tau} e^{-j2\pi f\tau} h_{\Delta,\tau} \quad d\tau$$
$$\Leftrightarrow \quad h_{\Delta,f} = U_{\Delta,f} h_{t,\tau} \tag{13}$$

where $U_{\Delta,f}$ is the 2-D Fourier transform from geo-time[sec] and delay[sec] to Doppler[Hz] and selectivity[Hz]. Likewise the passband filtered and baseband translated acoustic response function can be represented in the time-frequency domain as

$$h_{t,f} = \sum_m \phi(f) a_m(t, f + f_c) e^{-j2\pi(f+f_c)\tau_{m,t}}$$
$$\Leftrightarrow \quad h_{t,f} = U_{t,f} h_{t,\tau} \tag{14}$$

where it is understood that the argument denotes the Fourier transform, $\phi(f) = \int \phi(t)e^{-j2\pi ft}dt$.

2.2 Prior density for acoustic response function

Underwater acoustic response functions can vary considerably as a function of the environment. In order to capture this prior variability or uncertainty in the acoustic response function in such a way that variations are modeled in a parsimonious and yet flexible and accommodating way consider the use of an adaptive scheme suited for sparse time-varying channels. The notion of sparsity simply captures the fact that typical acoustic response functions obey the rule: $M_{path} < W\tau_{max}$. It is useful to view each delay-Doppler slot therefore as a possible ensonified acoustic path between source and receiver. Each of these slots will have a prior probability of being acoustically occupied, coherently linking source and receiver. Acoustic path occupation likelihood at a given delay-Doppler is set by a probability $\pi_{\Delta,\tau}$ that is a function of the Doppler frequency. The amplitude and phase of the occupied Doppler-frequency slot will be hypothesized as Gaussian with zero mean and a known variance. For the unoccupied slots it is also postulated that the amplitude and phase are Gaussian however the unoccupied slots are naturally associated with a much smaller variance. The probability density function of the channel's amplitude and phase at any given slot is therefore modeled by a binary mixture Gaussian model that is fully specfified by two variances and a probability that the slot is in one of the given states. These prior assumptions are captured in the following hierarchical Bayesian model,

$$h_{l,k}|z_{l,k} \sim N_{h_{l,k}}^{z_{l,k}}(0, \lambda_k^2) \times N_{h_{l,k}}^{1-z_{l,k}}(0, \epsilon_k^2) \tag{15}$$

$$z_{\Delta,\tau} \sim Ber(\pi_{\Delta,\tau}), \quad \pi_{\Delta,\tau} = \pi_0 D(\Delta) \times U_{0,\tau_{max}}(\tau)$$
$$\int_I D(\Delta) d\Delta = 1.$$

The factor π_0 is the a priori sparsity. The factor $D(\Delta)$ is a marginal or average Doppler spectrum and captures the prior likelihood of the ensonified channel paths' scatterers possessing a given aggregate velocity $v = c_{speed} \times \Delta/f_c$. This average Doppler spectrum has the interpretation of a probability density function. Given τ_{max} the delay profile U is a uniform density. Regarding Doppler spread, two physical processes are worth considering. First there is the Doppler offset associated with initialization and estimation of source and receiver clock rate offsets and relative platform speeds. This spread can be quite large and will depend on both the time-bandwidth product of the initializing synchronization waveform and the acceleration rate of the platforms. The second is the inherent Doppler spread associated with the acoustic response function and captures for instance the different path dilation rates. It is accepted that actual acoustic path amplitudes and phases with their times of arrival known do not necessarily obey a Gaussian density. While propagation modeling over actual underwater environments and geometries could provide insight into the actual densities of the channel coefficients it would require environmental information that is not availale to most underwater systems. The proposed model is useful because it allows for the parsimonious treatment of sparse time varying arrivals and the analytic solution of all posterior moments leading to computationally reasonable solutions. The mixture weights π and spectrum $\bar{\lambda}, \bar{\epsilon}$ could likewise be tuned with dependencies across delay-Doppler. For now it is accepted that the model, while not proved from propagation physics, offers an inductive framework that captures the essential spectral features of shallow water acoustic response functions. It thereby provides a useful adaptive structure for estimation of the response from observations.

It is also useful to consider a similar Gaussian mixture model on the Doppler-selectivity domain

$$h_{l,k}|z_{l,k} \sim N_{h_{l,k}}^{z_{l,k}}(0, \lambda_k^2) \times N_{h_{l,k}}^{1-z_{l,k}}(0, \epsilon^2)$$

$$z_{\Delta,f} \sim Ber(\pi_{\Delta,f}), \quad \pi_{\Delta,f} = \pi_0 D(\Delta) \times S(f). \tag{16}$$

The parameters π, $\bar{\lambda}$, and $\bar{\epsilon}$ can be estimated from the data as in [9].

2.3 Posterior inference for acoustic response function

Under the assumption that the acoustic noise is Gaussian and its covariance is known it can be whitened and the likelihood function is therefore Gaussian. It follows that the posterior density of the acoustic Green's function over the symboling epoch is

$$p(\mathbf{h}|\mathbf{r}, \mathbf{b}) \propto N_{\mathbf{r}}(C_{\mathbf{b}} \underbrace{U_{\Delta,\tau}^{-1}\mathbf{h}}_{\mathbf{h}_{t,\tau}}, I) \times$$
$$\prod_{l,k} \left(\pi_\Delta N_{h_{l,k}}(0, \lambda_{l,k}^2) + (1 - \pi_\Delta) N_{h_{l,k}}(0, \epsilon_{l,k}^2)\right). \tag{17}$$

Assume that the symbols exhibit orthogonality over the delay, i.e. $C_{\mathbf{b}}$ satisfies $C_{\mathbf{b}}' C_{\mathbf{b}} = I$ recalling that the Fourier transform U is unitary we have

$$p(\mathbf{h}|\mathbf{r},\mathbf{b}) \propto N_{\mathbf{h}}(\check{\mathbf{h}}, I) \times \prod_{l,k} \pi_\Delta N_{h_{l,k}}(0,\lambda_{l,k}^2) + (1-\pi_\Delta) N_{h_{l,k}}\left(0,\epsilon_{l,k}^2\right)$$

and refactoring the product of Gaussian densities implies

$$p(\mathbf{h}|\mathbf{r},\mathbf{b}) \propto \prod_{l,k} (\pi_{\check{h}_{l,k}} N_{h_{l,k}}(\gamma(\lambda_{l,k})\check{h}_{l,k}, \gamma(\lambda_{l,k})) + (1-\pi_{\check{h}_{l,k}}) N_{h_{l,k}}(\gamma(\epsilon_{l,k})\check{h}_{l,k}, \gamma(\epsilon_{l,k}))) \quad (18)$$

where the least squares estimates are

$$\check{\mathbf{h}}_{\Delta,\tau} = U_{\Delta,\tau}\check{\mathbf{h}}_{t,\tau} \quad , \quad \check{\mathbf{h}}_{t,\tau} = C'_{\mathbf{b}}\mathbf{r}$$

and

$$\pi_{\check{h}_{l,k}} = \left(1 + \frac{1-\pi_\Delta}{\pi_\Delta} \frac{N_{\check{h}_{l,k}}(0,\epsilon_{l,k}^2+1)}{N_{\check{h}_{l,k}}(0,\lambda_{l,k}^2+1)}\right)^{-1}$$

$$\gamma(x) = \frac{x^2}{x^2+1} .$$

Since mixture Gaussian priors are conjugate for Gaussian likelihood functions the posterior density (18) is also a mixture Gaussian. The posterior mean is a weighted average of each model's average and since the posterior model probabilities π are also functions of the data the result, while akin to a classic Wiener filter, has an additional adaptable feature in the mixture weights. The result is a shrinkage operator of the raw delay-Doppler measurements $\check{\mathbf{h}}_{\Delta,\tau}$,

$$E[h_{l,k}|\mathbf{r},\mathbf{b},\hat{\epsilon},\hat{\lambda}] = \left(\pi_{\check{h}_{l,k}}\gamma(\lambda_{l,k}) + (1-\pi_{\check{h}_{l,k}})\gamma(\epsilon_{l,k})\right)\check{h}_{l,k}$$

which is written in compact form with S denoting the soft shrinkage rule

$$\hat{\mathbf{h}}_{\Delta,\tau} = S_{\check{\mathbf{h}}}(\check{\mathbf{h}}_{\Delta,\tau}). \quad (19)$$

This posterior expectation greatly attenuates smaller, noise-like coefficients while leaving the larger coefficients unchanged. The γ's are Wiener-like gains over each delay-Doppler element. The variance is

$$\begin{aligned} \hat{v}_{l,k} = var[h_{l,k}|\mathbf{r},\mathbf{b},\hat{\epsilon},\hat{\lambda}] \\ = \left(\pi_{\check{h}_{l,k}}\gamma(\lambda_{l,k}) + (1-\pi_{\check{h}_{l,k}})\gamma(\epsilon_{l,k})\right) \\ +\pi_{\check{h}_{l,k}}(1-\pi_{\check{h}_{l,k}})(\gamma(\lambda_{l,k})-\gamma(\epsilon_{l,k}))^2 \times \check{h}_{l,k}^2 \end{aligned} \quad (20)$$

and can be understood as $\mathrm{var}[h_{l,k}] = E_{z_{l,k}}\mathrm{var}[h_{l,k}|z_{l,k}] + \mathrm{var}_{z_{l,k}}E[h_{l,k}|z_{l.k}]$. The parameters $\{\lambda_{l,k},\epsilon_{l,k},\pi_\Delta\}$ allow for adaptation of the model to the observations and they, like the gains, are estimated from the data, see for instance[9]. The Laplace approximation to the posterior distribution of the acoustic response function in the delay-time domain is therefore

$$p(\mathbf{h}_{t,\tau}|\mathbf{r},\mathbf{b},\hat{\epsilon},\hat{\lambda}) \approx N_{\mathbf{h}}(U_{\Delta,\tau}^{-1}\hat{\mathbf{h}}_{\Delta,\tau}, U_{\Delta,\tau}^{-1}\Upsilon U_{\Delta,\tau}^{-1}) \quad \Upsilon = \mathrm{Diag}(\hat{v}). \quad (21)$$

A computationally reasonable approximation to $E[\mathbf{h}|\mathbf{r}] = E_{\mathbf{b}}E[\mathbf{h}|\mathbf{r},\mathbf{b}]]$ is

$$E[\mathbf{h}|\mathbf{r},\mathbf{b}]] \approx U_\Delta^{-1}S_{E_{\mathbf{b}|\mathbf{r}}[\check{\mathbf{h}}]}(E_{\mathbf{b}|\mathbf{r}}[\check{\mathbf{h}}_{\Delta,\tau}]) \quad (22)$$

where

$$E_{\mathbf{b}|\mathbf{r}}[\check{\mathbf{h}}_{t,\tau}] = \sum \check{\mathbf{h}}_{t,\tau}(\mathbf{b})p(\mathbf{b}|\mathbf{r}) \ .$$

Figure 1 displays and comparse the least squares channel estimate and the posterior mean estimate based on the proposed mixture Gaussian model for an acoustic response function taken in St. Margaret's Bay. These are both for the same 2-ary spread spectrum signal set at -14 dB received SNR. The least square estimate is to the left and the MMSE posterior mean estimate based on the proposed mixture Gaussian model is to the right. Figure 2 shows a similar result for 4-ary signal epoch at a received SNR of -9 dB. In both figures 1 and 2 the power of the posterior mean to denoise dominant and faint arrivals as well as null the delay bands that are dominated by noise is apparent.

3 ESTIMATION OF AGGREGATE PATH DILATION

One of the critical advantage of accurate coherent estimates of the acoustic response function is that the bulk (aggregate, shared or common) dilation process associated with the acoustic arrival delay times can be estimated and factored out of the Green's function by "un-dilating" the received acoustic waveform. These path delay time processes are driven largely by source receiver motion in the case of mobile communicators but also by common ocean volume forces. For many underwater acoustic applications platform velocity is relatively minimal in the vertical direction as vehicles typically transit at a constant depth. For small acoustic angle spreads in shallow water, less than 15° range rate is a dominant factor in the shared delay time process. These arrival time variations for horizontally moving platforms are correlated having common time varying components that can be factored out to increase effective channel coherence. These facts account for the efficacy of phase tracking algorithms and the phase locked loop [15] for mobile commmunications and underwater acoustic communications[18] in particular. Here a subtly different approach is taken; the acoustic response function captures all delay-Doppler behavior over the signaling epoch up to the resolution of the symbol duration and the aggregate arrival time variations are then deduced from this estimate. The bulk path dilation estimate defines a natural (time-varying) sampling rate for the acoustic response that nearly "straightens out" or compenstates for the shared time variation of the acoustic paths. The remaining time variations of the acoustic arrivals constitute the natural coherence time of the ocean acoustic response function.

The Doppler bandwidth $1/2N_sW$ associated with the symbol interval determines the bandwidth of the final estimate and this is set by the processing gain and signaling bandwidth. Consider the two cases: 1) Time invariance dilation, that is, the shared component of the delay paths is a

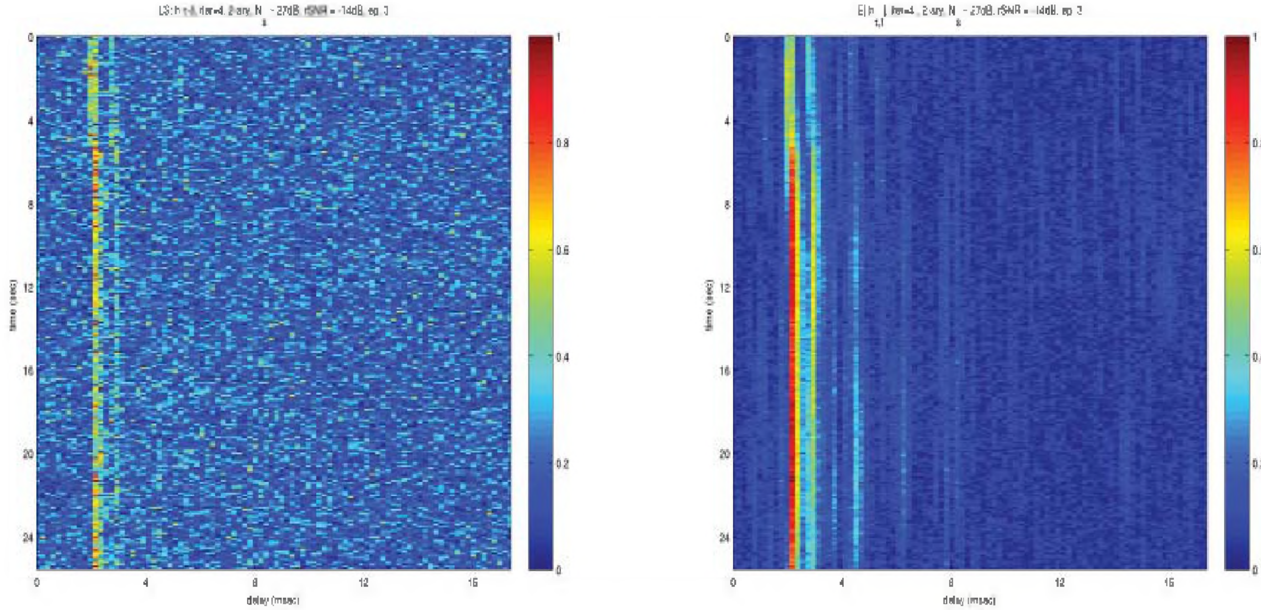

(a) (b)

Figure 1: Qualitative performance comparison of least squares channel estimate (left) with MMSE channel estimate based on Gaussian mixture model. Received SNR is -14 dB. Both are from the same 2-ary orthogonal spread spectrum data set.

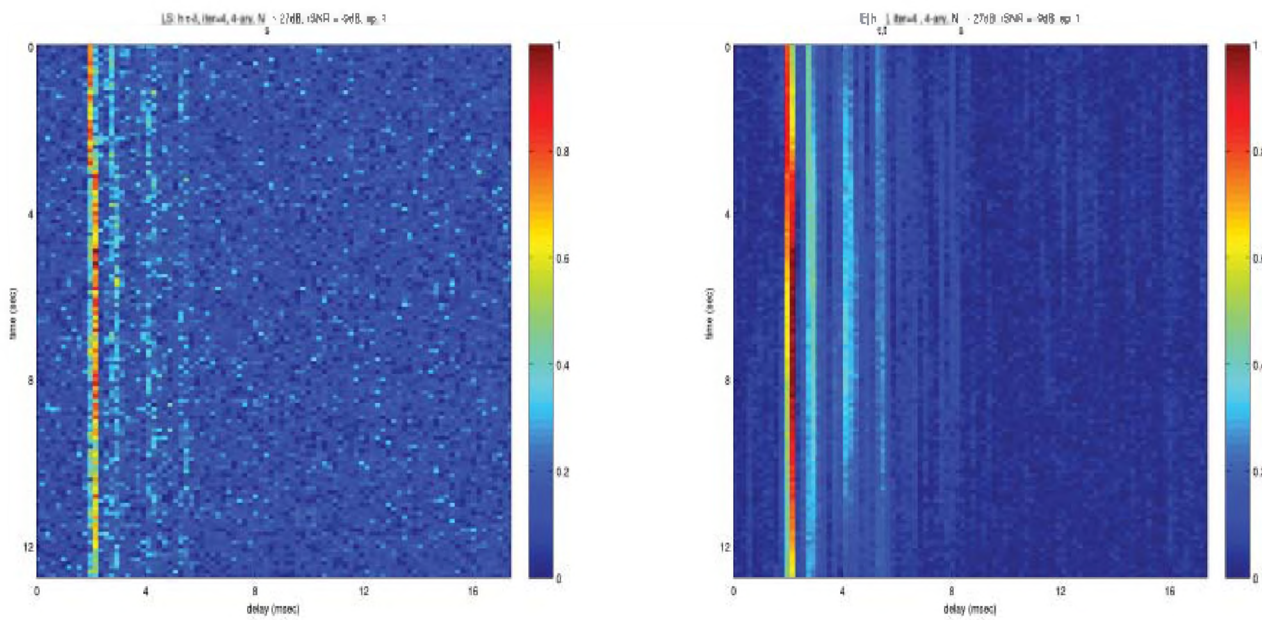

(a) (b)

Figure 2: Qualitative performance comparison of least squares channel estimate (left) with MMSE channel estimate based on Gaussian mixture model. Received SNR is -9 dB. Both are from the same 4-ary orthogonal spread spectrum data set.

simple linear function of time synonymous with a constant Doppler offset for all paths. 2) Time varying dilation. Allow for a common, shared temporal variation in the acoustic arrival times over the symboling interval. In the following subsections each of these is considered and suitable estimators are developed.

3.1 Time invariant path dilation rate

Factoring out a common linear delay drift, consider the model of the M_{path} dimensional arrival process as

$$\tau_m(t) = \delta_o \times t + \delta\tau_m(t) \ \ , \ m = \{1, \dots M_{path}\} \qquad (23)$$

where δ_o is a shared dilation rate among all of the paths. This factoring is obviously not unique and therefore we will seek to specify it in such a way that an appropriately weighted combination of the $\delta\tau_m(t)$ are minimized. To do this express the channel of Eq. (14) over Doppler frequency Δ, and channel frequency f, as

$$h_{\Delta,f} = \phi(f) \sum_m \int e^{-j2\pi(\Delta+(f+f_c)\delta_o)t} \times a_m(t, f+f_c) e^{-j2\pi(f+f_c)\delta\tau_m(t)} dt. \qquad (24)$$

Let

$$\tilde{\psi}^o_{m,\Delta,f} = \phi(f) \int e^{-j2\pi\Delta t} a_m(t, f+f_c) \times e^{-j2\pi(f+f_c)\delta\tau_m(t)} dt \qquad (25)$$

denote the m^{th} residual acoustic arrival response demodulated by frequency δ_o. Express the channel response, frequency shifted by δ_o, as

$$h_{\Delta-(f+f_c)\delta_o,f} = \sum_m \psi^o_{m,\Delta,f} \quad . \qquad (26)$$

The Doppler spread for this particular acoustic response can be defined as

$$\int \Delta^2 |h_{\Delta-(f+f_c)\delta_o,f}|^2 d\Delta \quad .$$

Choose as an estimate of δ_o the value that minimize the total Doppler spread of the Doppler shifted version:

$$\hat{\delta_o} = \arg\min_{\delta_o} \int \Delta^2 |\hat{h}_{\Delta-(f+f_c)\delta_o,f}|^2 d\Delta df \quad . \qquad (27)$$

This implies that the solution obeys

$$\int \Delta |\hat{h}_{\Delta-(f+f_c)\hat{\delta_o},f}|^2 d\Delta df = 0, \qquad (28)$$

which can be interpreted as the expectation or the average over the Doppler spectral density $|\hat{h}_{\Delta-(f+f_c)\hat{\delta_o},f}|^2$. The Doppler offset for the given δ_o is proportional to the channel frequency $(f+f_c)$. The solution for a given f is

$$(f+f_c)\hat{\delta_o}(f) = \frac{\int \Delta |\hat{h}_{\Delta,f}|^2 d\Delta}{\int |\hat{h}_{\Delta,f}|^2 d\Delta}$$

and averaged over the entire bandwidth is

$$\hat{\delta_o} = \int \frac{\Delta}{(f+f_c)} \frac{|\hat{h}_{\Delta,f}|^2}{\int |\hat{h}_{\zeta,\xi}|^2 d\zeta d\xi} d\Delta df. \qquad (29)$$

3.2 Time-varying path dilation rate

Consider now factoring out a common time-varying delay process from each of the path arrival times. Doing so leads to a model of the M_{path} arrival time processes as

$$\tau_m(t) = \tau_o(t) + \Delta\tau_m(t) \ \ , \ m = \{1, \dots M_{path}\}. \qquad (30)$$

As a function of $\tau_o(t)$ the acoustic response function Eq. (11) is

$$h_{t,\tau} = e^{-j\omega_c\tau_o(t)} \sum_m e^{-j\omega_c\Delta\tau_{m,t}} \times \tilde{\psi}_{m,t}(\tau - \tau_{m,t}) \qquad (31)$$

and recalling that the conditional mean of the response function in delay-time is $\hat{\mathbf{h}}_{t,\tau}$ a computationally efficient estimation method for $\tau_o(t)$ is to consider the Laplace approximation to the density of $\mathbf{h}|\mathbf{r}$ and find its maximum with respect to $\tau_o(t)$. Define the bandwidth associated with the bulk dilation process as W_o and further let the bandlimited version of $\hat{h}_{t,\tau}$, the posterior mean estimate of the channel from data be denoted as

$$\hat{h}^o_{t,\tau} = \int_{W_o} \hat{h}_{\Delta,\tau} e^{j2\pi\Delta\times t} d\Delta. \qquad (32)$$

Approximate the bulk dilation process with

$$\begin{aligned} \hat{\tau_o}(t) &= \arg\max_{\tau_o(t)} < \hat{h}_{t,\tau}, h_{t,\tau}(\tau_o(t)) > \qquad (33) \\ &= \arg\max_{\tau_o(t)} Re\{\int \hat{h}_{t,\tau} \times h'_{t,\tau}(\tau_o(t)) d\tau\} \end{aligned}$$

leading to

$$\hat{\tau_o}(t) = \arg\max_{\tau_o(t)} \quad e^{+j\omega_c\tau_o(t)} \int |\hat{h}_{t,\tau}| e^{j\angle\hat{h}_{t,\tau}} \times \sum_m e^{+j\omega_c\Delta\tau_{m,t}} \tilde{\psi}'_{m,t}(\tau - \tau_{m,t}) d\tau. \qquad (34)$$

To average out the $\tilde{\psi}'_{m,t}(\cdot)$ and $\Delta\tau_{m,t}$ assume that the remaining time varying phase variations $\{e^{+j\omega_c\Delta\tau_{m,t}}\}$ are negligibly small. This crude assumption allows us to approximate

$$\sum_m e^{+j\omega_c\Delta\tau_{m,t}} \tilde{\psi}'_{m,t}(\tau - \tau_{m,t}) = |\hat{h}_{t,\tau}| e^{j\angle h(0,\tau)}.$$

It follows that

$$\begin{aligned} \hat{\tau_o}(t) &= \arg\max_{\tau_o(t)} Re\{e^{+j\omega_c\tau_o(t)} \times \qquad (35) \\ &\int |\hat{h}_{t,\tau}|^2 \times e^{j(\angle\hat{h}_{t,\tau} - \angle\hat{h}_{0,\tau})} d\tau\} \end{aligned}$$

so that a nearly maximum likelihood solution to $\tau_o(t)$ is

$$\hat{\tau_o}(t) = \omega_c^{-1} arg \left[\int |\hat{h}_{t,\tau}|^2 \times e^{j\angle\hat{h}_{t,\tau} - \angle\hat{h}_{0,\tau}} d\tau \right]. \qquad (36)$$

This estimator weighs the phase rotation rate at each delay in proportion to it's energy so that the dominant arrivals dominate the estimate.

3.3 Inversion of the aggregate time dilation function

The proposed mixture Gaussian adaptive filtering scheme and the associated estimate of the bulk diation rate enable an increase in the effective channel coherence by unraveling the effect of the aggregate dilation, $\tau_o(t)$. This is accomplished by re-sampling the received data at a time-varying rate associated with the inverse of $u(t) = t - \tau_o(t)$. Recalling Eq. (10), note that

$$\begin{aligned} Hs(t) = \sum_n c_n^{\mathbf{b}} \times e^{-j\omega_c u(t)} \sum_m e^{-j\omega_c \Delta\tau_m(t)} \times \\ \tilde{\psi}_{m,t}(u(t) - \Delta\tau_{m,t} - n/W) \\ u(t) = t - \tau_o(t). \end{aligned}$$

Since the dilation rates are much smaller than the acoustic propagation speed the function $u(t)$ is a monotonically increasing function with a unique inverse $t = \nu \circ u \circ t$ and therefore Hs can be expressed as a function of u the natural time variable for the acoustic observations,

$$\begin{aligned} Hs(v \circ u) = \sum_n c_n^{\mathbf{b}} \times e^{-j\omega_c u} \sum_m e^{-j\omega_c \Delta\tau_m(\nu\circ u)} \times \\ \tilde{\psi}_{m,\nu\circ u}(u - \Delta\tau_m(\nu \circ u) - n/W). \quad (37) \end{aligned}$$

This is done to specify the inverse of the time dilation operator u. To do this, note that incremental differences in the two sampling grids are: $t - u = \tau_o(t)$, exactly the time varying dilation rate. Now approximate $\tau_o(t)$ as a function of u by a first order Taylor expansion $\tau_o(t) \approx \tau_o(u) + \partial_u \tau_o(u)(t - u)$ so that

$$\begin{aligned} t - u &\approx \tau_o(u) + \partial_u \tau_o(u)(t - u) \\ \tau_o(u) &= (t - u)(1 - \partial_u \tau_o(u)) \\ t &= u + \frac{\tau_o(u)}{1 - \partial_u \tau_o(u)}, \end{aligned}$$

and it follows that

$$\nu \circ u(t) = t \quad , \quad \nu(x) = x + \frac{\tau_o(x)}{1 - \partial_x \tau_o(x)} \quad . \qquad (38)$$

The estimate of the resampling operator ν is derived from the estimated bulk dilation rate $\tau_o(t)$ via a one to one map. The estimation process conditioned on the previous estimate of the symbol set can be summarized as follows:

$$\underset{E[\cdot|r,b]}{\hat{\mathbf{h}}} \Longrightarrow \underset{\approx \arg\max p[\cdot|r,b]}{\hat{\tau}_o(t)} \underset{one-to-one}{\Longrightarrow} \hat{\nu} \quad \hat{\nu} \circ \hat{u} = t \quad (39)$$

3.4 Effect of resampling operator on acoustic response function

Considering again the model of the received pressure imparted from the information bearing source (37) on the receiver element as

$$\begin{aligned} Hs \circ \nu(u) = e^{-j\omega_c u} \sum_n c_n^{\mathbf{b}} \sum_m e^{-j\omega_c \Delta\tau_m \circ \nu(u)} \times \\ \tilde{\psi}_{m,\circ\nu(u)}(u - \Delta\tau_m \circ \nu(u) - n/W) \end{aligned}$$

the baseband demodulated and resampled acoustic response function can be identified as

$$\begin{aligned} h^\nu(u,\tau) = \sum_m e^{-j\omega_c \Delta\tau_m^\nu(u)} \times \tilde{\psi}_{m,u}^\nu(\tau - \Delta\tau_m^\nu(u)) \quad (40) \\ \Delta\tau_m^\nu(u) = \Delta\tau_m \circ \nu(u) \quad , \quad \tilde{\psi}_m^\nu(\tau) = \tilde{\psi}_{m,\circ\nu(u)}(\tau). \end{aligned}$$

Since Eq. (40) is of the same form as (10) the resampling operator can be decomposed into a set of composite resampling operators consistent with an iterative joint estimation based receiver. If the function $\nu(t)$ is well estimated from the data the bandwidth of the residual channel response parameterized by $\psi_{m,u}, \Delta\tau_m^\nu$ will on average be less than that of the original sampled processes.

To illustrate the value of the proposed scheme as a means to focus coherent acoustic energy dispersed in Doppler bandwidth by source-receiver motion consider the application of the proposed dilation compensation method. Figure 3 presents an example of an acoustic Green's function in Doppler[Hz] and channel frequency[kHz] comparing time-invariant dilation and time varying dilation. In both cases the results are taken from a joint symbol and channel estimation procedure associated with an acoustic communications signal. The estimator on the left is that of one iteration after initial channel and symbol estimates. The estimator to the right is that of the third iteration following time varying Doppler compensation. The significant focusing and narrowing of the Doppler bandwidth of the response function is observed.

4 AN M-ARY ORTHOGONAL SIGNALING FOR UNDERWATER ACOUSTIC COMMUNICATIONS

The signaling scheme that is used to test these proposed adaptive filtering schemes is similar to that of the M-ary Walsh/m-sequence signaling tested by Iltis [11]. Performance bounds have been derived for M-ary orthogonal spread spectrum signaling through fading channels for the case of independent channel gains [17][1][6][7][14] and specific algorithms for diversity combining of M-ary orthogonal signals have been explored [19]. In this present study it is assumed that the symbol sets have good orthogonal properties over the multipath spread of the acoustic channel. The essential feature of such an M-ary signal set is that the symbol sequences $\mathbf{c}_m$, $m = 1, ...M$, obey

$$C_k' C_l = I \times \delta_{k-l} + E_{k,l} \qquad (41)$$

where C_m is the convolution operator associated with the code word $\mathbf{c}_m$. The matrix E has all coefficients less than $1/N_s$ where N_s is the sequence length. The receiver estimates the bit stream sent by

$$\begin{aligned} \hat{\mathbf{h}}^i &= E_{h|b=\hat{b}}[\mathbf{h}|\mathbf{r}, \mathbf{b} = \hat{\mathbf{b}}^{i-1}, \tau_o = \hat{\tau_o}^{i-1}] \\ \hat{\mathbf{b}}^i &= \arg\max_{\mathbf{b}} p(\mathbf{b}|\mathbf{r}, \mathbf{h} = \hat{\mathbf{h}}^i, \tau_o = \hat{\tau_o}^i) \qquad (42) \\ \hat{\tau_o}^i &= \arg\max_{\tau_o} p(\mathbf{h}_{\tau_o}|\mathbf{r}, \mathbf{b} = \hat{\mathbf{b}}^{i-1}). \end{aligned}$$

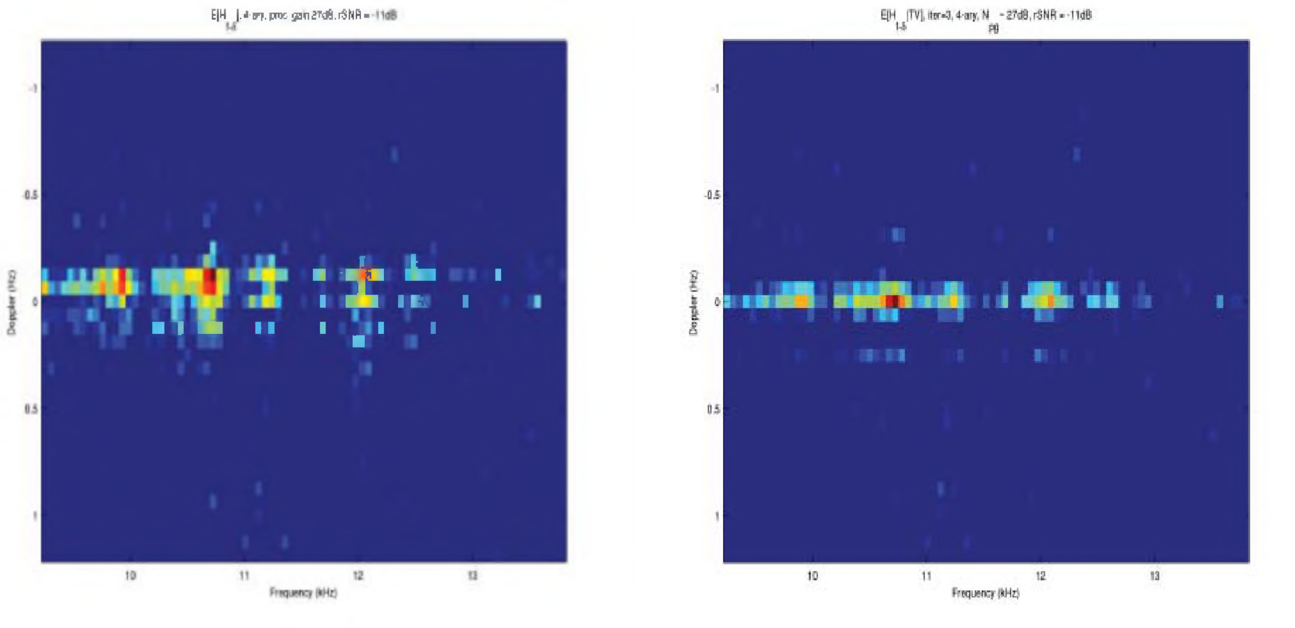

(a) (b)

Figure 3: Display of acoustic response functions demonstrating the focusing of energy in Doppler that attends time varying dilation estimation and compensation (40). Channel estimates were taken from the same 4-ary orthogonal data sets. Left, with only time invariant Doppler compensation. Right, with time-varying Doppler compensation.

Here, as previously, $\mathbf{h}$ represents the double spread channel function, $\mathbf{b}$ represents the sent bit stream of interest and τ_o represents the aggregate time varying dilation rate. Iterative receiver structures can now be constructed from any of the various conditional estimators of channel and dilation rate coupled to symbol decisions conditioned on those estimates. In this section a few such receivers that provide a good compromise between accuracy and computational cost are discussed. Coherent and non-coherent symbol decisions are considered but only of the hard decision type.

4.1 Symbol decision rules

In this channel estimation based scheme symbol decisions are made conditioned on the data $\mathbf{r}$ and the channel parameter estimates which of course are functions of the data. For simplicity we ignore the variance of the channel estimates in the decision process. The likelihood function for each symbol is of the form

$$\mathbf{r}_t|\mathbf{h}_t, b_t \sim N_{\mathbf{r}}(C_{b_t}\mathbf{h}_t, I) \qquad b_t \in \{1, 2 \dots M\}$$

where b_t specifies the sent codeword at the t^{th} symboling frame determining the $N_s + L - 1 \times L$ convolution operator C_{b_t}.

4.2 Coherent soft and hard decisions

With equally probable and equal energy symbols the probability of $b = m \in$ and ignoring the variance of the channel function estimation errors approximate as $P(b = m|\mathbf{r}, \mathbf{h} = \hat{\mathbf{h}}) = p(\mathbf{r}|b = m, \mathbf{h}) / \sum_{m'} p(\mathbf{r}|b = m', \mathbf{h} = \hat{\mathbf{h}})$. The results is

$$P(b_t = m|\mathbf{r}, \mathbf{h}) \approx \frac{e^{2Re[\hat{\mathbf{h}}' C'_m \mathbf{r}_t]}}{\sum_l e^{2Re[\hat{\mathbf{h}}' C'_l \mathbf{r}_t]}} \tag{43}$$

and approximate ML decisions conditioned on the channel iteration estimate are

$$\hat{b}_t \approx \arg\max_m \quad Re[\tilde{\mathbf{h}}'_t C'_m \mathbf{r}_t] \quad (\mathrm{WPC-C}). \tag{44}$$

We denote this symbol decision rule as weighted path combining with coherent decisions (WPC-C).

4.3 Noncoherent soft and hard decisions

Likewise non-coherent symbol estimates and decisions are based on $|\hat{\mathbf{h}}' C'_m \mathbf{r}_t|^2$. Assume perfect orthogonality of the symbol code words over the L lag delay band $C_m C_{m'} = I_L \delta_{m-m'}$ and for simplicity in what follows define $\tilde{\mathbf{h}} = \mathbf{h}/|\mathbf{h}|^2$ and noting that the M statistically independent $\tilde{\mathbf{h}}' C'_k \mathbf{r}_t$ complex scalar variables are Gaussian distributed

$$\begin{aligned}\tilde{\mathbf{h}}'_t C'_m \mathbf{r}_t | b_t = m &\sim N_x(|\mathbf{h}|_2, 1); \\ \tilde{\mathbf{h}}'_t C'_m \mathbf{r}_t | b_t \neq m &\sim N_x(0, 1)\end{aligned}$$

so that

$$\begin{aligned}x_m^2 = |\tilde{\mathbf{h}}' C'_m \mathbf{r}_t|^2 &\sim \chi_2^2(|\mathbf{h}|_2^2) \ , \\ x_{k|m}^2 = |\tilde{\mathbf{h}}' C'_k \mathbf{r}_t|^2 &\sim \chi_2^2\end{aligned} \tag{45}$$

Table 1: MPC receiver

MPC	
Parameter	Estimator
bulk path dilation: $\Delta\tau^o$	N/A
symbol decision:	Eq. (48)
channel estimate:	N/A

where $\chi_2^2(\lambda^2)$ represents a non-central chi-square random variable [13] with non-centrality parameter λ^2 and $\chi_2^2 = \chi_2^2(0)$ is the standard central chi-square random variable. Let $p_{\chi_2^2(\lambda)}(x)$ denote the density function of a non-central chi-square random variable with non-centrality parameter λ. It follows that symbol probabilities can be approximated by conditioning on the estimated channel response. It follows that $P(b_t = m|x_1^2, \ldots, x_M^2), \mathbf{h} = \hat{\mathbf{h}}) = p(\mathbf{r}|b = m, \mathbf{h})/\sum_{m'} p(\mathbf{r}|b = m', \mathbf{h} = \tilde{\mathbf{h}})$ and therefore

$$P(b_t = m|\mathbf{r}, \mathbf{h}) \approx \frac{p_{\chi_2^2(|\hat{\mathbf{h}}|^2)}(|\tilde{\mathbf{h}}' C_m' \mathbf{r}_t|^2)}{\sum_{k \in \mathcal{M}} p_{\chi_2^2(|\hat{\mathbf{h}}|^2)}(|\tilde{\mathbf{h}}' C_k' \mathbf{r}_t|^2)} \quad . \tag{46}$$

Hard decisions are simply

$$\hat{b}_t = \arg\max_m \; |\hat{\mathbf{h}}_t' C_m' \mathbf{r}_t|^2 \; (\mathrm{WPC-NC}). \tag{47}$$

Denote this symbol decision rule as weighted path combining with non-coherent decision (WPC-NC). These decision schemes will be compared to a maximal path combining (MPC) scheme that does not require channel estimation. While intuitively simple, the detail is worth stating. Let $\mathbf{x}^{(k)}$ be the kth ranked order statistic of $\mathbf{x}$ then choose the greatest L^* ranked outputs and sum. This can be expressed succinctly as

$$\hat{b}_t = \arg\max_m \sum_{(k)=1}^{L^*} \mathbf{x}_m^{(k)} \; , \; \mathbf{x} = \check{\mathbf{h}}_m^2 \; , \quad (\mathrm{MPC}). \tag{48}$$

$$\check{\mathbf{h}}_m = C_m' \mathbf{r}_t.$$

Table states the computationally fast maximal path combining (MPC) receiver where the decisions are based not on estimated $\mathbf{h}$ but on simply the L^* maximum coefficients of $\check{h}$, the matched filter outputs. Table 1 summarizes the maximal path combining receiver and Table 2 summarizes the channel estimation and dilation compensation based iterative receiver structures.

Figure 4 displays the performance of the proposed algorithm in terms of bit error rate as a function of iteration. Iteration one and iteration three are shown. Iteration one does not have time varying dilation estimation and iteration three does. The improvement by iteration three is approximately 2 dB, a significant performance gain. The results show that for 2-ary signaling at -12 dB received SNR the bit error rate is below 10^{-4}. For 4-ary signaling at -9 dB received SNR the bit error rate is below 10^{-6}. In each case the spreading gain is approximately 27 dB.

5 RESULTS.

The proposed adaptive filtering scheme was implemented in a channel estimation based communication receiver enabling coherent multipath combining of M-ary orthogonal signals and allowing the comparison with conventional schemes. The proposed iterative receiver structures were tested on signals of the Unet-08 M-ary orthogonal spread spectrum experiment of June 2008 taken in St. Margaret's Bay. Probability of bit error over a range of SNRs were computed by Monte-Carlo averaging of the receiver's error rate statistics. Presented here are comparisons of coherent channel estimate based results with maximal path combining, as well as coherent and non-coherent symbol decisions. All results are for single element reception. Array gain is not employed. The receivers tested are listed and described in Table 2. Rough synchronization and Doppler estimation are derived from short (1 symbol duration) broad band synchronization signals that initializes the algorithm. For all cases tested the received signal to noise ratio (rSNR) is measured as the in-band signal power average to the whitened noise power average over the entire signaling packet. Throughput rates for these schemes are as follows: 2-ary corresponds to 10 bps. 4-ary corresponds to 20 bps. Each communication packet employs 27 dB of processing gain, $N_s = 512$. Signal bandwidth is roughly 5.12 kHz corresponding to one symbol every 1/10 of a second. Higher throughput rates can be achieved by employing larger bandwidths, reduced procssing gain or larger alphabet sizes.

The performance of M-ary orthogonal signaling through a single element AWGN channel with coherent and noncoherent decisions is displayed on all figures for reference as a lower bound on error rate performance. Figure 4 displays the performance as a function of receiver iteration for 2-ary and 4-ary for 3 different channel epochs. The probability of error for two of the signaling epochs for 2-ary and 4-ary are shown in each panel. It is observed that refinement of the channel estimate leads to improved decisions. For the case of 2-ary we see roughly a .5 dB to 1.5 dB improvement from the first to the third iteration. Further iterations improve only slightly. For 4-ary we see a more significant 3 dB to 4 dB improvement from the first to the third iteration.

Consider a comparison of the proposed method with simple maximal path combining (MPC). Shown in figure 5, it is observed that coherent multipath combining outperforms MPC by greater than 2 dB regardless of the M, alphabet size. This is attributed to accurate channel estimation allowing the weighing of lower power coherent paths and the rejection of spurious noisey paths. By down weighting the acoustic inter-arrival times significant performance gains are observed. It should be mentioned that MPC using more than the $L = 8$ maximal delay lag coefficients does not lead to improved results. If L is chosen too large significant degradation in performance results as noise power is added to the decision statistic. Since MPC requires a prior information regarding the number of paths to combine it is clear that the channel estimation based schemes proposed here have an additional advantage of adaptability to channel conditions.

Table 2: Iterative receiver algorithms for M-ary orthogonal spread spectrum signaling

	Receiver 1	
	WPC w/ non-coh. decisions without symbol-aided timing estimation	
Parameter	Initialization	Iterative estimator
symbol decision: $\mathbf{b}^i$	$p(\mathbf{b}^0) = M^{-K}$ or (MPC)	Eq. (47)
acoustic response: $\mathbf{h}^i$	Eq. (22)	Eq. (19)
resampling operator: ν	N/A	N/A
	two iterations total	
	Receiver 2	
	WPC-non-coh. decisions with symbol-aided time-invariant timing estimation	
Parameter	Initialization	Iterative estimator
symbol decision $\mathbf{b}^i$	$p(\mathbf{b}^0) = M^{-K}$ or (MPC)	Eq. (47)
acoustic response: $\mathbf{h}^i$	Eq. (22)	Eq. (19)
bulk path dilation: $\Delta\tau^i$	Eq. (29)	Eq. (29)
resampling operator: ν	N/A	N/A
	three symbol decision iterations total	
	Receiver 3	
	WPC w/ coh. decisions with symbol-aided time-varying timing estimation	
Parameter	Initialization	Iterative estimator
symbol decision: $\mathbf{b}^i$	$p(\mathbf{b}^0) = M^{-K}$ or (MPC)	Eq. (44)
acoustic response: $\mathbf{h}^i$	Eq. (22)	Eq. (19)
bulk path dilation: $\tau^i(t)$	Eq. (29)	Eq. (36)
resampling operator: ν	N/A	Eq. (38)
	three symbol decision iterations total	

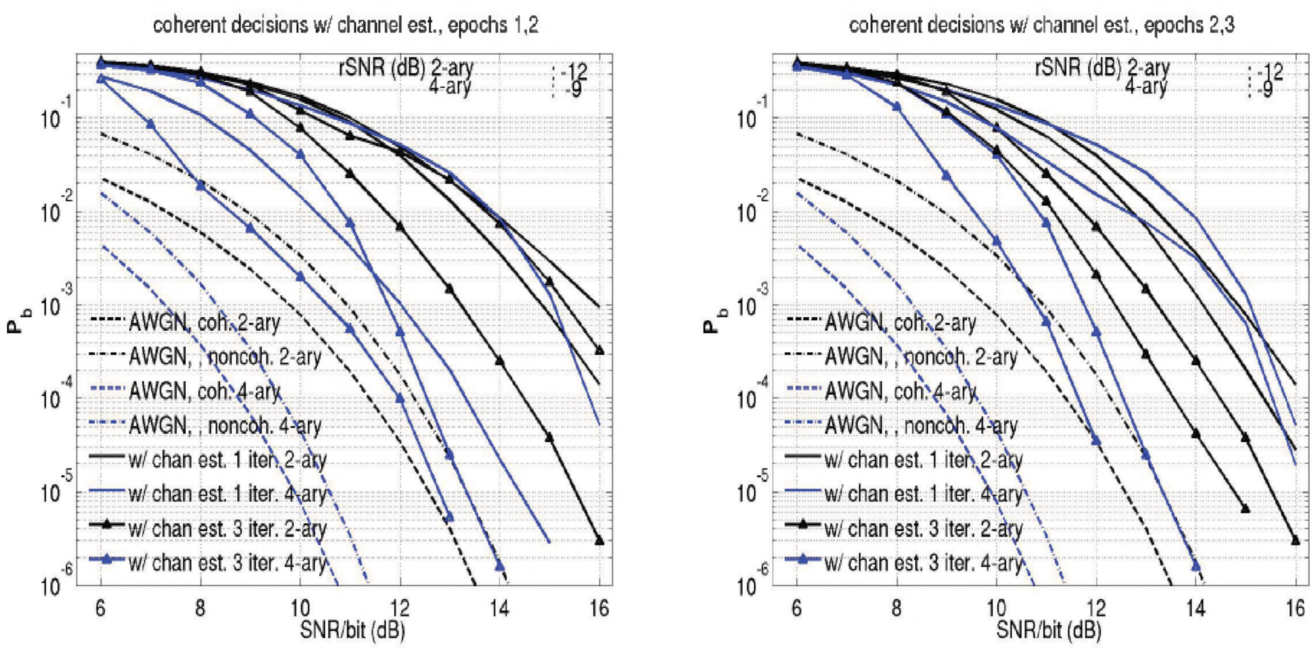

(a) (b)

Figure 4: Performance of coherent multipath combining for M-ary orthogonal signaling with proposed adaptive filtering scheme as a function of iteration. Results are shown for signaling epochs 1 and 2 in the lefthand (a) graph and for epochs 2 and 3 on the righthand (b) graph. Performance bound for AWGN channels is shown as a dashed line.

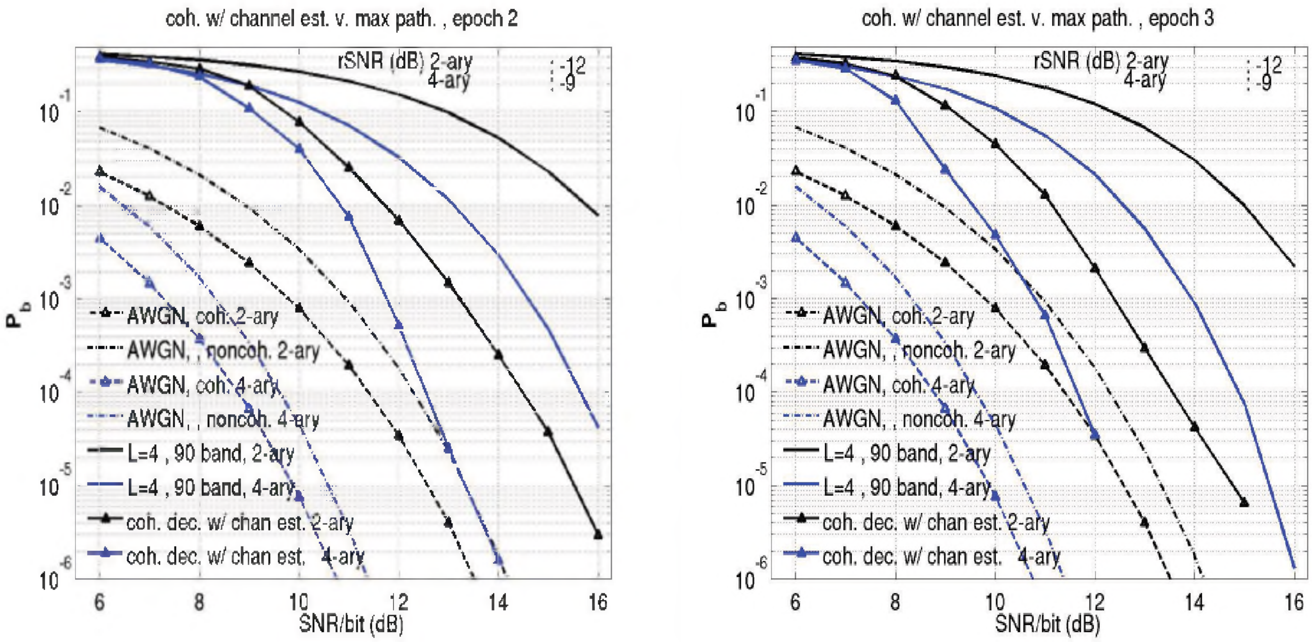

(a) (b)

Figure 5: Comparison of coherent combining of multipaths with channel estimation with that of maximal 4 paths combining (MPC) over a delay band of $W \times \tau_{max} = 90$. Improvement of 4 dB for 2-ary and 3 dB for 4-ary is apparent for all signaling epochs. AWGN bounds are shown as dashed lines.

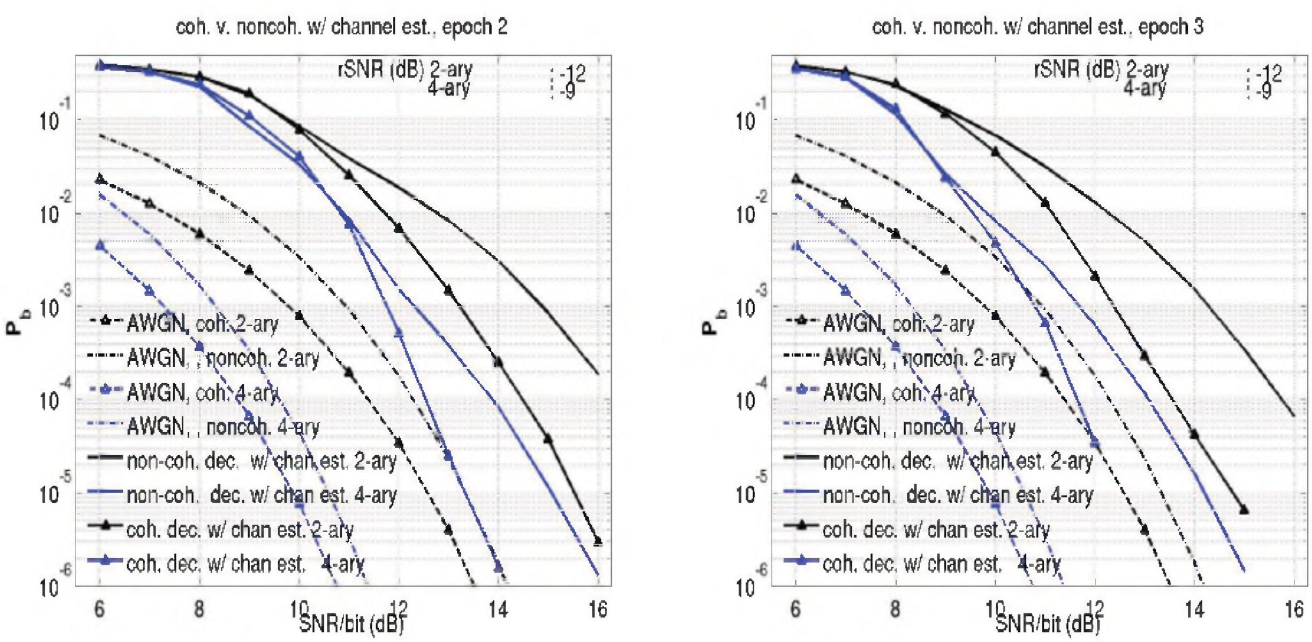

(a) (b)

Figure 6: Comparison of coherent decisions with channel estimation based coherent multipath combining with that non-coherent decisions. Improvements of up to 2 dB is observed for all signaling epochs for both 2-ary and 4-ary signaling is observed. AWGN bounds are shown as dashed lines.

It is worth comparing coherent decisions with non-coherent decisions. See Table 2 for the explicit computations with each. Figure 6 displays the performance of coherent channel estimation and multipath combining with coherent decisions against similar channel estimation with non-coherent decision. The receiver with Doppler compensation and coherent decisions outperforms that of non-coherent decisions over both signaling epochs and across signal to noise ratios. For 2-ary signaling a near 2 dB increase in performance is observed. For 4-ary the improvement with coherent decisions is also roughly 2 dB. It is observed that for 4-ary signaling an error rate of less than 10^{-4} is observed at -8 dB rSNR.

6 SUMMARY, CONCLUSIONS AND FUTURE WORK.

Mixture model based adaptive filtering schemes can incorporate all of the data in a signaling epoch to make accurate inferences regarding the acoustic response function at each symbol within the signaling epoch. These estimators enable iterative channel estimation based receiver algorithms for M-ary orthogonal communications in shallow water acoustic environments that can operatate at low SNR. Channel estimation is based on a Gaussian mixture model over Doppler and channel frequency that provides flexibility in the regularization of sparse acoustic channel estimates. The resulting estimator leaves acoustic arrivals that exhibit concentration of energy in Doppler unattenuated while greatly attenuating background noise and the incoherent highly dispersed low energy arrivals. This channel estimate forms the basis for time-varying aggregate path dilation estimation and resampling that effectively increases channel coherence to the natural coherence of the ocean media. Since signaling epochs can be quite long in duration reliable aggregate path dilation estimates require all of the data within a packet in order to operate efficiently at low SNR.

This scheme has been tested with a number of receiver implementations employing both coherent and non-coherent symbol decisions with the proposed channel estimation scheme. These novel channel estimation based weighted path combining schemes are compared to simple maximal path combining. The proposed receivers demonstrate between 3 and 4 dB of improvement over maximal path combining at received SNRs corresponding to a probability of error $< 10^{-5}$. For received SNRs of under -8 dB a probability of error of less than 10^{-4} for single element reception has been observed in the downward refracting environment of St. Margaret's Bay NS with a drifting source.

The schemes are well suited for low rate, low SNR underwater acoustic communications. They can be adapted to multi-user communications and MIMO applications. Future work will focus on modeling the dependence between delay-Doppler indicator variables $z_{k,l}$ for improved channel estimation and the extension of this mixture Gaussian model to beam angle for computationally fast beamforming for receiver arrays.

Acknowledgments

This work is supported by both the Office of Naval Research and by the Naval Innovative Science and Engineering Program. Thanks to Garry Heard of DRDC-Atlantic, for serving as Chief Scientist of the Unet08 experiments. Thanks to Dale Green of Teledyne Benthos for executing the Unet08 M-ary orthogonal acoustic experiments on the 4^{th} generation Teledyne Benthos modem.

REFERENCES

[1] V. Aalo, O. Ugweje, R. Sudhakar, "Performance analysis Analysis of DS/CDMA systems with noncoherent M-ary orthogonal modulation in Nakagami fading" *IEEE Trans. on Vehicular Technologies, Vol. 47, June 1999, pp 111-117.*

[2] P.J. Brockwell, R.A. Davis "Time Series: Theory and Methods, Second Edition", *Springer-Verlag*, ISBN 0-387-97429-6(USA), Springer Verlag, New York NY, 1991.

[3] Teledyne-Benthos, "Product Catalog 2010, Wireless Subsea Communications" *http://www.benthos.com/pdf/*

[4] P.J. Crepeau, "Asymptotic performance of M-ary orthogonal modulation in generalized fading channels" *IEEE Trans. Commun., Vol 36, No 11, November 1988, pp 1246-1249...*

[5] P. Dahl, et al., "Underwater Ambient Noise" *Acoustics Today*, Vol 3 Issue 1 pp 23-33. January 2007.

[6] A. Dekorsy, K.D. Kammeyer M-ary Orthogonal Modulation for Multi-Carrier Spread-Spectrum Uplink Transmission Proceedings of IEEE International Conference on Communications (ICC), Vol. 2 (June 1998), pp. 1004-1008.

[7] A. Dekorsy, S. Fischer, K. Kammeyer, Maximum likelihood decoding of M-ary orthogonal modulated signals for multi-carrier spread-spectrum systems Personal, Indoor and Mobile Radio Communications, 1998. The Ninth IEEE International Symposium on Boston MA, 8-11 Sep 1998, page(s): 538 - 543 vol.2, ISBN: 0-7803-4872-9 INSPEC Accession Number: 6275687, Digital Object Identifier: 10.1109/PIMRC.1998.734261

[8] N.R. Farnoud, M. Kolios and S. Krishnan, "Ultrasound Backscatter Signal Characterization and Classification Using Autoregressive Modeling and Machine Learning Algorithms", IEEE Conference Proceedings on Engineering in Medicine and Biology Society, vol. 3, pp. 2861 - 2864, Sep 17-21, 2003.

[9] P.J. Gendron, "An Empirical Bayes estimator for in-scale adaptive filtering" *IEEE Transactions on Signal Processing,* Vol. 56, No. 5, pp 1670-1683, May 2005.

[10] S. Haykin, "Adaptive Filter Theory", Prentice Hall Information and System Sciences Series, New Jersey, 2002.

[11] R. J. Iltis, "A Sparse Kalman Filter with Applicaiton to Acoustic Communications Channel Estimation" *IEEE/MTS OCEANS 2006*, ISBN 1-4244-0114-3, 18-21 September 2006.

[12] F.B. Jensen, W.A. Kuperman, M.B. Porter, H.Schmidt "Computational Ocean Acoustics", *AIP Press, AIP Series in Modern Acoustics and Signal Processing* ISBN 1-56396-209-8

[13] N.L. Johnson, S. Kotz, "Distributions in Statistics: Continuous univariate distributions-2," *John Wiley & Sons, Wiley Series in Probability and Mathematical Statistics, 1970.* ISBN 0-471-44627-0.

[14] I.D. Panagiotis, F-N. Pavlidou, DS/CDMA M-ary orthogonal signaling in shadowed Rayleigh channel for mobile communications, Wireless Networks, Vol. 2, pp 343-357.

[15] J. Proakis "Digital Communications", *McGraw-Hill, Inc.*, 1221 Avenue of the Americas, New York, NY 10020, 2000.

[16] M. de Oliveira Rosa, J.C. Pereira, M. Grellet, "Adaptive Estimation of Residue Signal for Vocal Pathology Diagnosis" *IEEE Trans. on Biomedical Engineering, Vol. 47, No. 1. January 2000, pp 96-104.*

[17] M.K. Simon, M.S. Alouini, "Bit error probability of noncoherent M-ary orthogonal modulation over generalized fading channels." *Int. J. Commun. and Networks, Vol 1, No 2. February 1998, pp 20-29.*

[18] M. Stojanovic, "Multichannel detection for wideband underwater acoustic CDMA communications" *Journal of Oceanic Engineering, 2006, Vol 31 No. 3 pp 685-695.*.

[19] J.S. Thompson, P.M. Grant, B. Mulgrew, "Algorithms for coherent diversity combining of M-ary orthogonal signals" *IEEE Journal on Selected Areas in Communications*, Vol 17, Issue 11, November 1999, pp 1886-1899.

[20] R. J. Urick, "Principles of Underwater Sound 3rd Edition" *Peninsual Publisher, 1996*. ISBN-13: 978-0932146625.

ICSV19 PRESS RELEASE

The 19th International Congress on Sound and Vibration (ICSV19), sponsored by the International Institute of Acoustics and Vibration (IIAV) and Vilnius University, will be held from 8 - 12 July 2012 at Vilnius University in Vilnius, Lithuania. Vilnius is the historical capital of Lithuania and dates back to the 14th century and has since been awarded the status of World Cultural Heritage by UNESCO. Vilnius University is one of the oldest universities in Eastern Europe and the friendly atmosphere of the modern city will mesmerize you and leave you with unforgettable memories.

Theoretical and experimental research papers in the fields of acoustics, noise, and vibration are invited for presentation. Participants are welcome to submit abstracts and companies are invited to take part in the ICSV19 exhibition and sponsorship. For more information, please visit < http://www.icsv19.org >.

For further details, please contact Malcolm J. Crocker at, crockmj@auburn.edu >.

Computational Ocean Acoustics

By Finn B. Jensen, William A. Kuperman, Michael B. Porter, and Henrik Schmidt
2nd Edition, Springer, 2011
List Price UD$185.00 (Hardcover)
630 Pages ISBN 9781441986771

Computational Ocean Acoustics is a textbook in Springer's Modern Acoustics and Signal Processing series. It provides a comprehensive review of computational techniques for numerical modeling of acoustic propagation in the ocean, by authors who are leaders in the field. It also discusses several applications of propagation modeling in ocean acoustics, in the modeling of ambient noise and in sonar signal processing in the presence of noise. The first edition of Computational Ocean Acoustics was published in 1994. This, the second edition, is for the most part an update rather than a reworking of the original. It is arranged in the same way, but with a number of modernized figures, new references, and new material in every chapter. The preface to the second edition handily describes where the most significant updates lie, some of which I will describe; however, many updates and improvements can be found throughout.

The first two chapters provide the required background for the in-depth coverage of propagation in the next part of the book. The first chapter, Fundamentals of Ocean Acoustics, covers most of the basics of underwater acoustics, updated from the original with descriptions of some of the more recent models for boundary interactions and a valuable discussion on units of power and intensity. One unusual aspect to the way the book is organized is that the sonar equation does not make an appearance until the final chapter, definitely a surprise to those used to seeing books structured after Urick's classic Principles of Underwater Sound.

The second chapter, Wave Propagation Theory, gives the mathematical background upon which the rest of the book depends. The wave equation and Helmholtz equation are derived, and the analytic approaches to solving them in homogeneous media and waveguides are examined, and related to the numerical methods described in the following chapters. A new section on waveguide invariants is included in the 2nd Edition, expanded upon with material in several later chapters.

Chapters 3 through 7 each deal with one of the methods for numerically solving the wave or Helmholtz equation – ray methods, normal modes, wavenumber integration, parabolic equations, and finite difference and finite element models. Each chapter follows a similar structure, with an introduction to the history and basic ideas of the method, followed by a mathematical derivation and techniques for numerical solution. The applications and limitations of each method are covered in depth, with a number of examples. Each chapter also includes some more advanced topics, many of which have been updated with results from current research. A number of other revisions have been made in these chapters, including a significant reworking of the chapter on ray methods and expansion of the section on Gaussian beams, and more information on scattering and propagation in elastic media throughout. One feature that I particularly like in these chapters are the "recipes" for simple propagation code, which make the book particularly well-suited to a course on computational acoustics.

Chapter 8, Broadband Modeling, covers the areas of direct time-domain modeling and Fourier synthesis of broadband pulses. As in the other chapters, details concerning the actual numerical implementation of the ideas presented form an important part of this chapter. A number of interesting numerical examples are also discussed that make use of the modeling methods described in the earlier chapters.

Chapters 9 and 10 deal with applications of the propagation methods previously discussed. Chapter 9 shows how noise can be modeled using the propagation concepts developed earlier, in both two and three dimensions. It also includes a new section on how noise can be used to extract the physics of the propagation in a waveguide. Chapter 10 extends this to look at beamforming, matched-field processing, and some more recent developments such as phase conjugation and time reversal. This chapter could potentially serve as an interesting introduction to an advanced signal processing course.

This book has many valuable features. The reference lists at the end of each chapter are extensive. As in the first edition, the problems at the end of each chapter are interesting and useful, and these have also been extended to cover the additional material in this edition. These, together with the code recipes at the end of each chapter, help make it suitable as a graduate-level or advanced undergraduate-level textbook. It is also a valuable reference for government, industry, or academic workers in the field of underwater acoustic propagation, and in fact should also hold a great deal of interest to those working in atmospheric acoustic propagation (for example, as a companion to Salomons' Computational Atmospheric Acoustics).

There are some minor issues with the second edition, where on occasion the updates are not entirely seamless. The use of colour figures is a definite improvement, particularly in the last two chapters, but strangely not all figures have been updated. As well, at times those sections that have not been revised can seem slightly dated (e.g. by referring to a 20-year old paper as recent).

Nevertheless, if you do not own the first edition of this book, I strongly recommend the second edition. Even if you do have a copy of the first edition, there are sufficient useful additions and updates that it is worth acquiring.

Sean Pecknold
Group Leader, Maritime Environmental Awareness
Defence Research and Development Canada – Atlantic
sean.pecknold@drdc-rddc.gc.ca

Acoustics and Audio Technology, Third Edition

By Mendel Kleiner

J. Ross Publishing's Acoustics: Information and Communication Series; Soft Cover, September 2011

List Price $69.95

480 Pages, ISBN: 978-1-60427-052-5

The Faithful reproduction of sound is a passion that I share with Mendel Kleiner. So it was with great enthusiasm that I accepted the task of reviewing the third edition of his text.

Mendel Kleiner obtained his Ph. D. in Architectural Acoustics in 1978, and is currently a Professor of Acoustics at Chalmers University of Technology in Gothenburg, Sweden. Dr. Kleiner is in charge of the Room Acoustics group. Not only is he well published, but he has also presented keynote lectures and has led international conferences on acoustics and noise control. His main research areas are computer simulation of room acoustics, electroacoustic reverberation enhancement, room acoustics of auditoria, and sound and vibration measurement technology. Dr. Kleiner is a fellow of the Acoustical Society of America, the Chair for The Audio Engineering Society's Technical Committee on Acoustics and Sound Reinforcement, and iIs also a member on it Standards Committee.

The book presents a basic course on acoustic fundamentals and sound propagation; along with architectural acoustics, technologies for adjusting room acoustics with absorbers as well as reflectors and diffusers. He also offers an overview of the electromechanical and the acoustic principals of loudspeakers and microphones; and discusses the properties of hearing and voice. The end of most chapters presents some sample problems for those willing to tinker.

Chapter 1 starts with a general discussion on sound and the wave equation. The book appears to tailor itself for audio and music enthusiasts who aspire to be acousticians. Kleiner uses analogies to circuits to illustrate acoustic concepts.

Chapter 2, Audio Signals covers the 'jw', or complex method of applying the Fourier transform to signal analysis theory. There is a lucid discussion on the term 'level' that compliments his presentation of filters, bandwidth and frequency range in aiming at a given sound level. His closing discussion elaborates on the ubiquitous equivalent level.

Chapter 3 examines hearing thresholds and equivalent loudness measures, as well as other subjective parameters (i.e. pitch/ timbre). The information presented on sound reproduction is not often found in an entry level acoustic textbook and this discussion will be appreciated by those that have entered the field of acoustics via the music and audio route. Of specific interest is the concept of how our brain can fill in the missing information in a given recording. One of the unique factors of the chapters is its discussion of the human emotional factors that differentiates between listening and hearing. The common misconception is to limit the hearing to a range of 20 Hz - 20 kHz. It is now widely accepted that this frequency range can be extended provided the 'levels' in a particular frequency range are of sufficient magnitude.

Chapters 4 to 6 deal with Kleiner's areas of specialty, in Room Acoustics; and his ability to merge acoustic and audio cultures shines through. Chapter 4 divides room acoustics into technical and psychological acoustics, or what happens in time and space and how we perceive the diverse range of sound fields. The chapter discusses Geometric acoustics and Fresnel zones as a set up to Ray Tracing. He then takes you through the journey of sound being generated in a room; from its inception, to build up, and eventual decay with time in rooms with a variety of shapes. The chapter ends with discussion on model density, "Q" (bandwidth or shape of resonance) and the significance of the Schroeder frequency in wave theory.

Chapter 5 similarly presents a journey of how sound such as music is perceived from many apparent source locations as it reaches our ear; and how this perception can be altered delay, echo and coloration. The strength of this chapter is the inclusion of contemporary room acoustic metrics as well as a discussion of early/late reverberation, coupled sub-spaces and subjective diffuseness.

Chapter 6, Room Acoustics Planning and Design outlines the importance of acceptably quiet levels, the need for clear, natural sound and intelligible speech, and the importance of early energy arriving to the listener for ensuring 'good' acoustics.

The chapter discusses appropriate reverberation for music and it outlines the various forms of treatment to enhance the acoustics of rooms that are used for Sound Reproduction, such as studios and control rooms. This chapter ends with an overview of tools for predicting room response such as scale modeling, optical modeling, and computer-coded techniques such as FEM (Finite Element). The advantages and disadvantages of each methods, including hybrid models, are also discussed. This chapter ends with a forward-thinking discussion on Electronic Architecture-Sound field synthesis and reverberation enhancement via a smart sound systems or Auralization, a term whose origin has been credited to Kleiner.

Chapter 7 looks at the various forms of treatments that are available for optimizing the acoustics of a room, as well as methods for determining the sound absorption provided by various absorbers. A caution is provided with respect to the re-radiation of sound via turbulence and the minimization of this effect with appropriate design. Reflectors, as required for optimal sound distribution and the implementation of barriers (to reduce sound level) are also discussed. The chapter closes with some basic thoughts on introducing diffusers to deal with sound reflection from planar surfaces to remove echo, reduce coloration and provide efficient scattering as required for studios and theatres.

Chapter 8 presents a discussion on Waves in Solids and this book keeps pace with other relevant texts on the subject. It provides clear illustrations along with discussions on the mechanics of solids and the wave equation to describe the significance of bending waves. Kleiner excels at presenting concepts such as damping with clear illustrations and photos to augment his derivations. This method of communicating with the reader is evident throughout the book, allowing the reader to engage the subject with a greater likelihood of retention.

Chapters 9, 10 and 11 respectively cover Sound Radiation and Generation, Sound Isolation and Vibration Isolation. Again, the use of photographs (some very nostalgic) is effective, allowing one to truly appreciate Kleiner's authenticity in the sharing of his knowledge. The various mechanisms by which sound is generated (i.e. flow, bending waves in structures, etc.) is described and provides a logical transition into noise control.

Sound Isolation (chapter 10) looks at building acoustics and deals with the transmission of sound through partitions, enclosures and openings. Again, the text provides excellent illustration to support mathematical derivation. This chapter covers the behavior of dual panel partitions and the concept of composite transmission loss. The real world in situ performance of building elements is not ignored; as crack, leaks and flanking transmission are recognized.

Vibration isolation is briefly covered in Chapter 11. Kleiner shares his own experience with the design of unique phonographs/ turntables for illustration. He draws on mechanical and electrical analogs to get his point across effectively. This chapter serves its purpose as an introduction to vibration isolation by recognizing that the subject warrants further study for the student wishing to advance in this area.

Chapters 12 through to 15 are compelling as they document the foundation of audio technology and the role it plays as it merges into acoustics. The discussion on microphones covers the properties, of how they function, the tradeoffs of various types of microphones, their susceptibility to wind noise, and means of overcoming this with wind shields.

Chapters 13 and 14 cover the electrodynamics of the turntable and loudspeaker and are a pleasure to read. The operation of both these devices touches on virtually every aspect of acoustics, vibration and audio engineering. The phonograph and cutting head recording process is clearly outlined along with an organized discussion on the engineering dynamics of the playback system; namely; phonograph, tonearm and, cartridge and stylus. Chapter 14 is about the loudspeaker and its characteristics (i.e. vibration velocity of the diaphragm and sound pressure from a circular piston), as well as radiation and directivity fundamentals. There is ample discussion of the various types of enclosure designs ranging from sealed and vented boxes to horn-loaded and electrostatic concepts. The discussion closes with the electronic compensation of non linearties and the room-loudspeaker interaction.

Chapter 15 covers many aspects of headphones/ earphones and provides commentary on their potential impact on our hearing. The design principles of electromagnetic, electrodynamic and electrostatic headphones variations are discussed, providing the reader with ample information to select a type, are based on the level of quality required. The chapter ends with a brief discussion on the noise cancelling headphone and its role on providing hearing protection.

The book ventures into the modern era of Digital sound reproduction and digitization in chapter 16, and covers A/D and D/A conversion, dither, compression and coding. There is an intriguing discussion on perceptual coding where masking effects can be introduced to create desired tonal playback effects in the decoded signal. Factors affecting audio quality and a mandate for listening tests with appropriate audio, protocol specifications, and trained listeners are put forth.

The final chapter of the book presents the highlight of Kleiner's research and is consistent with his acknowledgement of himself as the pioneer of auralization. Chapter 17 is aptly titled Audio Systems and Measurement and is the most detailed chapter in the book. The importance of binaural sound reproduction for our perception of the spatial properties of sound is discussed; along with crosstalk elimination and the challenges in faithful sound reproduction with conventional stereo using loudspeakers. A good portion of the Chapter also looks at audio quality and measurements that are required to achieve this goal. Concepts such as frequency response, phase response, group delay and distortion (i.e. harmonic, intermodulation etc.) are further developed.

In keeping with Kleiner's focus on sound reproduction in spaces, it is not a surprise that his discussion then moves into sound measurements in special chambers (i.e. audio testing, anechoic, reverberation, living room, etc.) and quantitative analysis. He then moves into subjective analysis again stressing the importance of using (unbiased qualified listeners). Having participated in such listening tests, it cannot be understated that there are numerous factors to consider and document, including the fact that listening results must be validated statistically, and expressed in terms of mean standard deviation and confidence interval.

In the preface, Kleiner sets out several objectives for his book. He accomplishes each goal admirably with this well organized and well thought out text. The benefactor of his work is the student and future audio/ acoustic practitioner.

There are several classic acoustic texts which may cover more material and in greater depth; however Kleiner's efforts in bringing together audio and acoustics makes this a "fun" read and a great choice as a university undergraduate text for the student willing to take his/ her experience with Audition, Protools and Garage Band to the next level.

Vince Gambino
Aercoustics Engineering Ltd.
vinceg@aercoustics.com

Worship Space Acoustics

Mendel Kleiner, David L. Klepper and Rendell R. Torres
J. Ross Publishing, 2010
List price: $89.95 USD (Hardcover)
311 pp., ISBN: 978-1-60427-037-2-5

Worship Space Acoustics is written by a practicing acoustician (strong academic qualification), a former acoustician who is undergoing rabbinical studies and a Roman Catholic priest. The imprint of each of the three authors is clearly obvious, in particular, when each of the three worship spaces, church, synagogue and a mosque, is being discussed.

The book is divided into main parts. Part I discusses the acoustical aspects and Part II presents the details of the three worship spaces. Part I is divided into ten chapters with a basic introduction – 1) Fundamentals –Nature of sound; 2) Hearing; 3) Room acoustic fundamentals; 4) Sound absorbing materials; 5) Metrics for room acoustics; 6) Simulation and prediction; 7) Planning for good room acoustics; 8) Quiet; 9) Sound isolation and other noise issues; and 10) Sound systems for clarity and reverberation. Part I has three sections: a) Synagogues; b) Churches; and c) Mosques. Each of the three sections of Part II has many subsections that discuss the details such as history, types and occupancy requirements.

Part II of the book describes the three worship spaces in some detail. Historical development of the three worship spaces, churches, synagogues and mosques and their functionality are well discussed in Part II. The architectural details of different kinds of synagogues and churches are highlighted. Basic acoustical requirements are touched upon through case studies. The only acoustical measure that was highlighted in Part II was the reverberation time. The other acoustical metrics discussed in Part II are not mentioned at all while presenting details of the three worship spaces. In addition, subjective perception from an acoustical point of view was not discussed at all. The above two points, if presented in some detail would have the book very useful for practioners. We suggest that the above two points are included in the future editions of this interesting book on *Worship Space Acoustics*.

Ramani Ramakrishnan
Department of Architectural Science
Ryerson University
rramakri@ryereson.ca


For Digital Recorders
Introducing
For USB A/D Systems
PHANTOM POWER
7052PH
Measurement Mic System
7052H Type 1.5TM
Titanium Diaphragm
3Hz to >20 kHz
<20 dBA > 140 dBSPL
MK224 (<14 dBA to >134 dBSPL) Optional
4048 Preamp
Superior
IEC 1094 Type 1
Long-term Stability
Temperature and Humidity
Performance
Now in Stock
Phantom
to IEPE/ICP
Adaptor
Supplies 3-4 mA
Power
Accelerometers
Microphones
ICP1248
ACOustics
Begins with ACO
TM
MATTtm
Family
MATT TM
Mic
Attenuator
Handle Higher Sound Pressure Levels
ACO Pacific, Inc., 2604 Read Ave., Belmont, CA 94002
Tel:(650) 595-8588 FAX: (650) 591-2891 E-Mail: sales@acopacific.com
Web Site: www.acopacific.com

Canadian Acoustical Association
Association Canadienne d'Acoustique

PRIZE ANNOUNCEMENT • ANNONCE DE PRIX

Prize

Edgar and Millicent Shaw Postdoctoral Prize in Acoustics
Alexander G. Bell Graduate Student Prize in Speech Communication and Hearing
Eckel Graduate Student Prize in Noise Control
Fessenden Graduate Student Prize in Underwater Acoustics
Raymond Hetu Undergraduate Student Prize in Acoustics

Prix

Prix Post-doctoral Edgar et Millicent Shaw en Acoustique
Prix etudiant Alexander G. Bell en Communication orale et audition (2^{e} ou 3^{e} cycle)
Prix etudiant Eckel en Controle du bruit (2^{e} ou 3^{e} cycle)
Prix etudiant Fessenden en Acoustique sous-marine (2^{e} ou 3^{e} cycle)
Prix etudiant Raymond Hetu en Acoustique (1^{er} cycle)

Deadline for Applications:
April 30^{th} 2012

Date limite de soumission des demandes:
30 Avril 2012

Consult CAA website for more information
Consultez le site Internet de l'ACA pour de plus amples renseignements
(http://www.caa-aca.ca)

Call for Papers

A Special Issue of the

International Journal of Industrial Ergonomics

OCCUPATIONAL NOISE EXPOSURE:EXPOSURE ASSESSMENT AND CONTROL

Exposure to occupational noise is related to hearing loss, discomfort, fatigue and several other health and safety risks among the exposed workers. Although the research efforts over the past few decades have evolved into valuable guidelines and standards to protect workers from excessive exposures to noise, the subject of health effects, assessment and control continues to pose an array of multi-disciplinary challenges. The objective of this special issue is to compile recent research and development efforts in the field, including characterization and assessments, industrial noise control, the state of the art in the associated supporting technologies, hearing protection and perspectives on future developments and applications.

The specific topics of interest within the scope of this special issue include (but not being limited) the following:

- Characterization and assessments of workplace noise environment and noise sources;
- Hearing protection;
- Audiological and non-audiological health risks;
- Communication in noisy environments and safety issues;
- Comfort and perception issues related to workplace noise and hearing protection;
- Epidemiology;
- Standards: applications and limitations;
- Ergonomic interventions for risk control;
- Techniques for noise mitigation and industrial noise control, active noise control;
- Effect of noise on human performance;
- Analytical and numerical methods for noise assessment and control.

Prospective authors are invited to submit their original works within the scope of the special issue. The authors should follow the journal guidelines (http://ees.elsevier.com/ergon/) for preparing their manuscripts, and submit electronically to the journal website using the web-based submission tools. Each manuscript will be reviewed in accordance with the journal requirements.

SCHEDULE FOR SUBMISSIONS (tentative)

Manuscript Submission Deadline:	15 March 2012
Reviewers' reports and decision:	30 April 2012
Final Manuscript Due on:	30 June 2012

GUEST EDITORS

R. Ramakrishnan, DSc., P.Eng
Associate Professor, Architectural Science
Ryerson University
350 Victoria Street
Toronto, Ontario, CANADA M5B 2K3
Email: rramakri@ryerson.ca

P. Marcotte, Ph.D.
IRSST, Research Department
505 boul. de Maisonneuve West
Montreal, Quebec H3A 3C2
Canada
Email: marcotte.pierre@irsst.qc.ca

Second Announcement

ACOUSTICS WEEK IN CANADA

Banff, Alberta, 10-12 Oct. 2012

Mount Rundle from Banff townsite.

Acoustics Week in Canada 2012, the annual conference of the Canadian Acoustical Association, will be held in the beautiful town of Banff, Alberta, from 10-12 Oct. 2012. This is the premier Canadian symposium in acoustics and vibration, and this year's exceptional Rocky Mountain setting in Banff National Park (a UNESCO World Heritage Site) will make it an event you won't want to miss. The conference will include three days of keynote talks and technical sessions on all areas of acoustics, an Exhibition of acoustical equipment and services, the Acoustical Standards Committee Meeting, a Welcome Reception, the Conference Banquet and more. In keeping with the mountain grandeur of Banff National Park, the Conference theme is "Sound and the Natural World".

Venue and Accommodation – The Conference will be held at the Banff Park Lodge Resort and Conference Centre, which offers state-of-the-art conference facilities in a mountain-lodge ambience. Accommodation is available at both the Banff Park Lodge (www.banffparklodge.com) and at the neighbouring Bow View Lodge (www.bowview.com), both of which boast an exceptional, quiet location on the banks of the glacier-fed Bow River, but just two blocks from the Banff dining/shopping/entertainment district. The Banff Park Lodge is a Canada Select four-star hotel with 200 luxurious guest rooms, each with balcony or patio and mountain views. The Bow View Lodge is a three-star hotel with 60 comfortable rooms. Participants booking rooms before 5 Sept. 2012 will receive the special conference rate of $127/night for the Banff Park Lodge or $108/night for the Bow View Lodge (single or double occupancy, including complimentary wireless internet and many other amenities).

Staying at these outstanding conference hotels will place you near your colleagues and all conference activities, and will help make the meeting a financial success to the benefit of future CAA activities. Reduced room rates are in effect from 7 to 14 October, so consider extending your visit to Banff for an autumn holiday! Registration details will be available soon at the conference website.

Moraine Lake, Banff National Park.

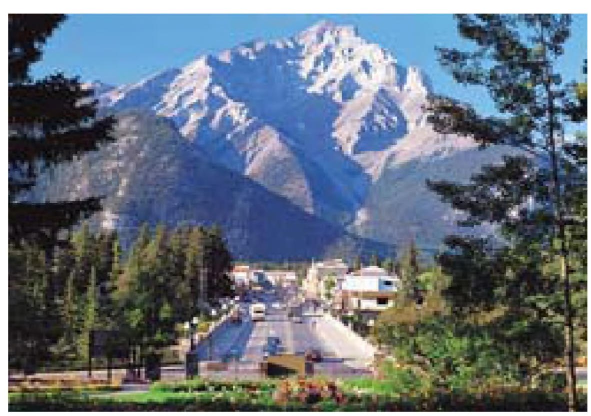

Main Street, Banff townsite

Banff Park Lodge, exterior and interior.

Plenary and Technical Sessions – Three keynote talks are planned in areas of broad interest and relevance to the acoustics community. Technical sessions are planned covering all areas of acoustics including:

- Acoustic Standards
- Architectural and Building Acoustics
- Bio-Acoustics and Biomedical Acoustics
- Engineering Acoustics
- Musical Acoustics
- Noise and Noise Control
- Physical Acoustics and Ultrasonics
- Psycho- and Physio-Acoustics
- Shock and Vibration
- Signal Processing
- Speech Sciences and Hearing Sciences
- Underwater Acoustics

If you would like to organize a session on a specific topic, please contact the Technical Chair.

Exhibition and Sponsorship – The conference will include an Exhibition of acoustical equipment, products and services on Thursday 11 Oct. 2012. If you or your company are interested in participating in the Exhibition or in sponsoring conference coffee breaks, social events and/or sessions, which provide excellent promotional opportunities, please contact the Exhibition Coordinator.

Students – Student participation is strongly encouraged. Travel subsidies and reduced registration fees will be available. Student authors are eligible to win industry-sponsored presentation awards.

Paper Submission – The abstract deadline is 15 June 2012. Two-page summary papers for publication in the proceedings issue of *Canadian Acoustics* are due 1 August 2012. Details of the submission procedure will be given at the conference website.

Registration – Registration details are available at the conference website. Early registration at a significantly reduced rate is available until 5 Sept. 2012 and is strongly encouraged.

Organizing Committee

- Conference Chair: Stan Dosso sdosso@uvic.ca
- Technical Chair: Roberto Racca roberto.racca@jasco.com
- Accounting and Registration:
  Clair Wakefield
  Lori Robson lori@wakefieldacoustics.com
- Exhibit and Sponsors: Lisa Cooper lisa.cooper@jasco.com
- Website: Brendan Rideout brendan.rideout@gmail.com
- Student Awards: Michael Wilmut mjwilmut@gmail.com

Hiking in Banff National Park.

Conference Website: www.caa-aca.ca

Mont Rundle vu de Banff.

SECONDE ANNONCE

SEMAINE CANADIENNE D'ACOUSTIQUE

Banff, Alberta, 10-12 Octobre 2012

La Semaine Canadienne d'Acoustique 2012, la conférence annuelle de l'Association Canadienne d'Acoustique, va prendre place à Banff, AB du 10 au 12 Octobre 2012. C'est le symposium majeur d'acoustique et de vibration au Canada, et cette année, le cadre exceptionnel du Parc National de Banff (site classé Patrimoine Mondial par l'UNESCO), au cœur des Rocheuses, va faire de cette conférence un évènement à ne pas manquer. La conférence inclura trois jours de présentations invitées et de sessions techniques dans tous les domaines de l'acoustique, une exposition d'équipements et services acoustiques, la réunion du Comité des Standards en Acoustique, une réception de bienvenue, le banquet de la conférence et bien plus encore. Inspiré par la splendeur du Parc National de Banff, le thème de cette conférence sera « Le son et le monde naturel ».

Centre de conférence et Hébergement – La conférence prendra place au Banff Park Lodge Resort and Conference Centre, qui offre des installations haut de gamme dans une atmosphère de chalet montagnard. Des logements sont disponibles au Banff Park Lodge (www.banffparklodge.com) ainsi qu'au Bow View Lodge (www.bowview.com), qui sont, tous les deux, des endroits exceptionnels et tranquilles situés sur la rivière Bow et à deux pas du quartier des restaurants/magasins/attractions. Le Banff Park Lodge est un hôtel quatre étoiles *Canada Select* qui offre 200 chambres luxueuses, chacune avec balcon ou patio et vue sur la montagne. Le Bow View Lodge est un hôtel trois étoiles avec 60 chambres confortables. Les participants réservant l'hôtel avant le 5 septembre 2012 recevront un tarif préférentiel de $127/nuit pour le Banff Park Lodge ou $108/nuit pour le Bow View Lodge (occupation simple ou double, incluant la connexion internet sans fil et de nombreux autres avantages). Un séjour dans cet hôtel extraordinaire vous placera au plus près de vos collègues et de toutes les activités de la conférence, et contribuera à faire de cette réunion un succès financier pour le bénéfice des activités futures de l'ACA. Les chambres à prix réduits sont disponibles du 7 au 14 octobre, donc n'hésitez pas à prolonger votre visite à Banff pour prendre quelques jours de vacances. Les détails d'inscription seront bientôt disponibles sur le site internet de la conférence.

Banff Park Lodge
RESORT HOTEL AND CONFERENCE CENTRE
ALBERTA, CANADA

Lac Moraine, Parc National de Banff.

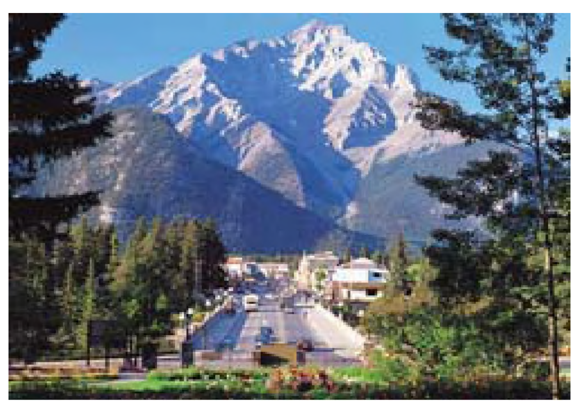

Main Street, Banff.

Banff Park Lodge, extérieur et intérieur.

Sessions scientifiques et plénières – Trois présentations invitées sont prévues dans des domaines d'intérêt général et pertinents pour la communauté d'acoustique. Des sessions techniques seront organisées dans tous les domaines principaux de l'acoustique, incluant les thèmes suivants:

- Standards en acoustique
- Acoustique architecturale et du bâtiment
- Bioacoustique et acoustique biomédicale
- Génie acoustique
- Acoustique Musicale
- Bruit et contrôle du bruit
- Physique acoustique et Ultrasons
- Psycho et Physioacoustique
- Chocs et Vibrations
- Traitement des signaux
- Sciences de la parole et Audition
- Acoustique sous-marine

Si vous désirez proposer et/ou organiser une session spéciale, veuillez contacter le président scientifique.

Exposition technique et commandite – Le congrès inclura une exposition d'équipements, produits et services acoustiques qui prendra place le jeudi 11 Octobre 2012. Si vous ou votre entreprise êtes intéressés à participer à l'exposition ou à commanditer les événements sociaux de la conférence et/ou les sessions, qui offriront d'excellentes opportunités promotionnelles, veuillez contacter le coordinateur de l'exposition.

Participation étudiante – La participation étudiante est fortement encouragée. Des subventions de voyages et des frais réduits d'inscription seront disponibles. Les étudiants donnant une présentation sont éligibles pour gagner des prix parrainés par l'industrie pour les meilleures présentations de la conférence.

Soumission d'articles – L'échéance pour la soumission des résumés est le 15 Juin 2012. Les résumés de deux pages pour publication dans le numéro d'actes de conférence d'*Acoustique Canadienne* sont dus pour le 1er août 2012. Les détails seront donnés sur le site internet de la conférence

Inscription – Les détails sur inscription sont disponibles sur le site internet de la conférence. La pré-inscription à prix réduits est disponible jusqu'au 5 septembre 2012 et est fortement encouragée.

Comité d'Organisation

- Président de la conférence: Stan Dosso sdosso@uvic.ca
- Président scientifique: Roberto Racca roberto.racca@jasco.com
- Trésorerie et inscription : Clair Wakefield
  Lori Robson lori@wakefieldacoustics.com
- Exposition et commandite: Lisa Cooper lisa.cooper@jasco.com
- Site internet : Brendan Rideout brendan.rideout@gmail.com
- Prix étudiants: Michael Wilmut mjwilmut@gmail.com

Site web de la conférence: www.caa-aca.ca

INSTRUCTIONS TO AUTHORS FOR THE PREPARATION OF MANUSCRIPTS

Submissions: The original manuscript and two copies should be sent to the Editor-in-Chief. The manuscript can also be submitted electronically.

General Presentation: Papers should be submitted in camera-ready format. Paper size 8.5" x 11". If you have access to a word processor, copy as closely as possible the format of the articles in Canadian Acoustics 39(1) 2011. All text in Times-Roman 10 pt font, with single (12 pt) spacing. Main body of text in two columns separated by 0.25". One line space between paragraphs.

Margins: Top - 0.75"; bottom - 0.75" minimum; sides - 0.75".

Title: Bold, Times New Roman 14 pt with 14 pt spacing, upper case, centered.

Authors/addresses: Names and full mailing addresses, 10 pt with single (12 pt) spacing, upper and lower case, centered. Names in bold text.

Abstracts: English and French versions. Headings, 12 pt bold, upper case, centered. Indent text 0.5" on both sides.

Headings: Headings to be in 12 pt bold, Times-Roman font. Number at the left margin and indent text 0.5". Main headings, numbered as 1, 2, 3, ... to be in upper case. Sub-headings numbered as 1.1, 1.2, 1.3, ... in upper and lower case. Sub-sub-headings not numbered, in upper and lower case, underlined.

Equations: Minimize. Place in text if short. Numbered.

Figures/Tables: Keep small. Insert in text at top or bottom of page. Name as "Figure 1, 2, ..." Caption in 9 pt with single (12 pt) spacing. Leave 0.5" between text.

Line Widths: Line widths in technical drawings, figures and tables should be a minimum of 0.5 pt.

Photographs: Submit original glossy, black and white photograph.

Scans: Should be between 225 dpi and 300 dpi. Scan: Line art as bitmap tiffs; Black and white as grayscale tiffs and colour as CMYK tiffs;

References: Cite in text and list at end in any consistent format, 9 pt with single (12 pt) spacing.

Page numbers: In light pencil at the bottom of each page. For electronic submissions, do not number pages.

Reprints: Can be ordered at time of acceptance of paper.

DIRECTIVES A L'INTENTION DES AUTEURS PREPARATION DES MANUSCRITS

Soumissions: Le manuscrit original ainsi que deux copies doivent être soumis au rédacteur-en-chef. Le manuscrit peut être aussi acheminé par voie électronique.

Présentation générale: Le manuscrit doit être soumis avec mise en page en format de publication. Dimension des pages, 8.5" x 11". Si vous avez accès à un système de traitement de texte, dans la mesure du possible, suivre le format des articles dans l'Acoustique canadienne 39(1) 2011. Tout le texte doit être en caractères Times-Roman, 10 pt et à simple (12 pt) interligne. Le texte principal doit être en deux colonnes séparées d'un espace de 0.25". Les paragraphes sont séparés d'un espace d'une ligne.

Marges: Haut - 0.75"; bas - minimum 0.75" ; côtés,- 0.75".

Titre du manuscrit: Caractères gras, Times New Roman 14 pt,avec espace interligne de 14 pt, lettres majuscules, texte centré.

Auteurs/adresses: Noms et adresses postales. Lettres majuscules et minuscules, 10 pt à simple (12 pt) interligne, texte centré. Les noms doivent être en caractères gras.

Sommaire: En versions anglaise et française. Titre en 12 pt, lettres majuscules, caractères gras, texte centré. Paragraphe 0.5" en alinéa de la marge, des 2 cotés.

Titres des sections: **T**ous en caractères gras, 12 pt, Times-Roman. Premiers titres: numéroter 1, 2, 3, ..., en lettres majuscules; sous-titres: numéroter 1.1, 1.2, 1.3, ..., en lettres majuscules et minuscules; sous-sous-titres: ne pas numéroter, en lettres majuscules et minuscules et soulignés.

Équations: Minimiser le nombre et les numéroter. Insérer directement dans le texte les équations très courtes.

Figures/Tableaux: De petites tailles. Les insérer dans le texte au haut ou au bas de la page. Les nommer "Figure 1, 2, 3,..." Légende en 9 pt à simple (12 pt) interligne. Laisser un espace de 0.5" entre le texte.

Largeur des traits: La largeur des traits sur les schémas techniques doivent être au minimum de 0.5 pt pour permettre une bonne reproduction.

Photographies: Soumettre la photographie originale sur papier glacé, noir et blanc.

Figures numérisées: Doivent être au minimum de 225 dpi et au maximum de 300 dpi. Les schémas doivent être en format bitmap tif. Les photos noir et blanc doivent en format tif sur une échelle de tons de gris et toutes les photos couleurs doivent être en format CMYK tif.

Références: Les citer dans le texte et en faire la liste à la fin du document, en format uniforme, 9 pt à simple (12 pt) interligne.

Pagination: Au crayon pâle, au bas de chaque page. Ne pas paginer si le manuscrit est envoyé par voie électronique.

Tirés-à-part: Ils peuvent être commandés au moment de l'acceptation du manuscrit.

The Canadian Acoustical Association
l'Association Canadienne d'Acoustique

Application for Membership

CAA membership is open to all individuals who have an interest in acoustics. Annual dues total $80.00 for individual members and $35.00 for Student members. This includes a subscription to ***Canadian Acoustics***, the Association's journal, which is published 4 times/year. New membership applications received before August 31 will be applied to the current year and include that year's back issues of ***Canadian Acoustics***, if available. New membership applications received after August 31 will be applied to the next year.

Subscriptions to *Canadian Acoustics* *or* Sustaining Subscriptions

Subscriptions to ***Canadian Acoustics*** are available to companies and institutions at the institutional subscription price of $80.00. Many companies and institutions prefer to be a Sustaining Subscriber, paying $350.00 per year, in order to assist CAA financially. A list of Sustaining Subscribers is published in each issue of ***Canadian Acoustics***. Subscriptions for the current calendar year are due by January 31. New subscriptions received before August 31 will be applied to the current year and include that year's back issues of ***Canadian Acoustics***, if available.

Please note that electronic forms can be downloaded from the CAA Website at **caa-aca.ca**

Address for subscription / membership correspondence:

Name / Organization ______________________________

Address ______________________________

City/Province ______________ Postal Code __________ Country ______________

Phone ______________ Fax ______________ E-mail ______________

Address for mailing Canadian Acoustics, if different from above:

Name / Organization ______________________________

Address ______________________________

City/Province ______________ Postal Code __________ Country ______________

Areas of Interest: (Please mark 3 maximum)

1. Architectural Acoustics
2. Engineering Acoustics / Noise Control
3. Physical Acoustics / Ultrasound
4. Musical Acoustics / Electro-acoustics
5. Psychological / Physiological Acoustic
6. Shock and Vibration
7. Hearing Sciences
8. Speech Sciences
9. Underwater Acoustics
10. Signal Processing / Numerical Methods
11. Other

For student membership, please also provide:

__________ __________ __________ __________

(University) *(Faculty Member)* *(Signature of Faculty Member)* *(Date)*

I have enclosed the indicated payment for:
[ ] CAA Membership $ 80.00
[ ] CAA Student Membership $ 35.00

Corporate Subscriptions:
[ ] $80 including mailing in Canada
[ ] $88 including mailing to USA,
[ ] $95 including International mailing

[ ] Sustaining Subscriber $350.00
includes subscription (4 issues /year)
to ***Canadian Acoustics.***

Payment by: [ ] Cheque
[ ] Money Order
[ ] Credit Card *(VISA only)*

Credit card number ______________________

Name on card ______________________

Expiry date ______________________

____

(Signature) (Date)

l'Association Canadienne d'Acoustique
The Canadian Acoustical Association

Formulaire d'adhésion

L'adhésion à l'ACA est ouverte à tous ceux qui s'intéressent à l'acoustique. La cotisation annuelle est de 80.00$ pour les membres individuels, et de 35.00$ pour les étudiants. Tous les membres reçoivent ***l'Acoustique Canadienne***, la revue de l'association. Les nouveaux abonnements reçus avant le 31 août s'appliquent à l'année courante et incluent les anciens numéros (non-épuisés) de ***l'Acoustique Canadienne*** de cette année. Les nouveaux abonnements reçus après le 31 août s'appliquent à l'année suivante.

Abonnement pour la revue *Acoustique Canadienne* et abonnement de soutien

Les abonnements pour la revue ***Acoustique Canadienne*** sont disponibles pour les compagnies et autres établissements au coût annuel de 80.00$. Des compagnies et établissements préfèrent souvent la cotisation de membre bienfaiteur, de 350.00$ par année, pour assister financièrement l'ACA. La liste des membres bienfaiteurs est publiée dans chaque issue de la revue ***Acoustique Canadienne***. Les nouveaux abonnements reçus avant le 31 août s'appliquent à l'année courante et incluent les anciens numéros (non-épuisés) de ***l'Acoustique Canadienne*** de cette année. Les nouveaux abonnements reçus après le 31 août s'appliquent à l'année suivante.

Pour obtenir des formulaires électroniques, visitez le site Web: **caa-aca.ca**

Pour correspondance administrative et financière:

Nom / Organisation ______________________________

Adresse ______________________________

Ville/Province ______________ Code postal __________ Pays ______________

Téléphone ____________ Téléc. __________ Courriel ______________

Adresse postale pour la revue Acoustique Canadienne

Nom / Organisation ______________________________

Adresse ______________________________

Ville/Province ______________ Code postal __________ Pays ______________

Cocher vos champs d'intérêt: (maximum 3)

1. Acoustique architecturale
2. Génie acoustique / Contrôle du bruit
3. Acoustique physique / Ultrasons
4. Acoustique musicale / Électro-acoustique
5. Physio / Psycho-acoustique
6. Chocs et vibrations
7. Audition
8. Parole
9. Acoustique sous-marine
10. Traitement des signaux /Méthodes numériques
11. Autre

Prière de remplir pour les étudiants et étudiantes:

__________ __________ __________ __________

(Université) (Nom d'un membre du corps professoral) (Signature du membre du corps professoral) (Date)

Cocher la case appropriée:
[ ] Membre individuel 80.00 $
[ ] Membre étudiant(e) 35.00 $
Abonnement institutionnel
[ ] 80 $ à l'intérieur du Canada
[ ] 88 $ vers les États-Unis
[ ] 95 $ tout autre envoi international
[ ] Abonnement de soutien 350.00 $ (comprend l'abonnement à *L'acoustique Canadienne*)

Prière d'attacher votre paiement au formulaire d'adhésion. Envoyer à :

Méthode de paiement:
[ ] Chèque au nom de l'Association Canadienne d'Acoustique
[ ] Mandat postal
[ ] VISA seulement

Numéro carte de crédit ______________

Nom sur la carte ______________

Date d'expiration ______________

____

(Signature) (Date)

The Canadian Acoustical Association
l'Association Canadienne d'Acoustique

SUSTAINING SUBSCRIBERS / ABONNES DE SOUTIEN

The Canadian Acoustical Association gratefully acknowledges the financial assistance of the Sustaining Subscribers listed below. Their annual donations (of $350.00 or more) enable the journal to be distributed to all at a reasonable cost.

L'Association Canadienne d'Acoustique tient à témoigner sa reconnaissance à l'égard de ses Abonnés de Soutien en publiant ci-dessous leur nom et leur adresse. En amortissant les coûts de publication et de distribution, les dons annuels (de $350.00 et plus) rendent le journal accessible à tous nos membres.

ACI Acoustical Consultants Inc.
Mr. Steven Bilawchuk - (780) 414-6373
stevenb@aciacoustical.com - Edmonton, AB

ACO Pacific Inc.
Mr. Noland Lewis - (650) 595-8588
acopac@acopacific.com - Belmont, CA

Acoustec Inc.
Dr. J.G. Migneron - (418) 834-1414
courrier@acoustec.qc.ca - St-Nicolas, QC

ACOUSTIKALAB Inc.
Jean Laporte - (514) 692-1147
jlaporte@acoustikalab.com - Montréal, QC

AECOM
Frank Babic - (905) 501-0641
frank.babic@aecom.com - Mississauga, ON

Aercoustics Engineering Ltd.
Mr. John O'Keefe - (416) 249-3361
johno@aercoustics.com - Toronto, ON

Bruel & Kjaer North America Inc.
Mr. Andrew Khoury - (514) 695-8225
andrew.khoury@bksv.com - Pointe-Claire, QC

Conestoga-Rovers & Associates
Tim Wiens - (519) 884-0510 x2352
twiens@craworld.com - Waterloo, ON

Dalimar Instruments Inc.
Mr. Daniel Larose - (514) 424-0033
daniel@dalimar.ca - Vaudreuil-Dorion, QC

Dessau Inc.
Jacques Boilard - (418) 839-6034
jacques.boilard@dessau.com - Lévis, QC

DuraSystems Barriers Inc.
Fred Woo - (905) 660-4455
fred.woo@durasystems.com - Vaughan, ON

Eckel Industries of Canada Ltd.
- (613) 543-2967
eckel@eckel.ca - Morrisburg, ON

ECORE International
Jocelyn L. Dillman - (717) 824-8203
jld@ecoreintl.com - Lancaster, PA

G.R.A.S. Sound & Vibration
- (330) 425-1201
sales@gras.us - Twinsburg, OH

Golder Associates Ltd.
Danny Da Silva - (905) 567-4444
dandasilva@golder.com - Mississauga, ON

H.L. Blachford Ltd.
Mr. Dalton Prince - (905) 823-3200
amsales@blachford.ca - Mississauga, ON

Hatch Associates Ltd.
Mr. Tim Kelsall - (905) 403-3932
tkelsall@hatch.ca - Mississauga, ON

HGC Engineering Ltd.
Mr. Bill Gastmeier - (905) 826-4044
bgastmeier@hgcengineering.com;janstey@hgcengineering.com - Mississauga, ON

Hydro-Québec TransÉnergie
M. Blaise Gosselin - (514) 879-4100 x5309
gosselin.blaise@hydro.qc.ca - Montréal, QC

Integral DX Engineering Ltd.
Mr. Greg Clunis - (613) 761-1565
greg@integraldxengineering.ca - Ottawa, ON

J.E. Coulter Associates Ltd.
Mr. John Coulter - (416) 502-8598
jcoulter@on.aibn.com - Toronto, ON

J.L.Richards & Assoc. Ltd.
Mr. Terry Vivyurka, P.Eng. - (613) 728-3571
mail@jlrichards.ca - Ottawa, ON

Jacobs & Thompson Inc.
Chris Brand - (416) 749-0600
cmaida@jacobs-thompson.com - Toronto, ON

Jade Acoustics Inc.
Ms. Dalila Giusti - (905) 660-2444
dalila@jadeacoustics.com - Concord, ON

JASCO Research Ltd.
Mr. Scott Carr - (902) 405-3336
scott@jasco.com - Dartmouth, NS

Kinetics Noise Control Inc.
Mr Mehrzad Salkhordeh - 905-670-4922
msalkhordeh@kineticsnoise.com - Mississauga, Ontario

Mc SQUARED System Design Group
Mr. Wade McGregor - (604) 986-8181
info@mcsquared.com - North Vancouver, BC

MJM Conseillers en Acoustique Inc.
M. Michel Morin - (514) 737-9811
mmorin@mjm.qc.ca - Montréal, QC

Novel Dynamics Inc.
Stan Thompson - (613) 598-0026
stan@noveldynamics.com - Ottawa, ON

Owens-Corning Canada Inc.
Mr. Salvatore Ciarlo - (800) 988-5269
salvatore.ciarlo@owenscorning.com - St. Leonard, QC

OZA Inspections Ltd.
Mr. David Williams - (800) 664-8263 x25
oza@ozagroup.com - Grimsby, ON

Peutz & Associés
M. Marc Asselineau - +33 1 45230500
m.asselineau@peutz.fr - Paris,

Pliteq Inc.
Wil Byrick - (416) 449-0049
wbyrick@pliteq.com - Toronto, ON

Pyrok Inc.
Mr. Howard Podolsky - (914) 777-7770
info@pyrok.com - Mamaroneck, NY

RWDI AIR Inc.
Peter VanDelden - (519) 823-1311
peter.vandelden@rwdi.com - Guelph, ON

Scantek Inc.
Mr. Richard J. Peppin - (410) 290-7726
peppinr@scantekinc.com - Columbia, MD

SNC-Lavalin inc., division Environnement
M. Jean-Luc Allard - (514) 393-1000
jeanluc.allard@snclavalin.com - Longueuil, QC

Soft dB Inc.
M. André L'Espérance - (418) 686-0993
contact@softdb.com - Sillery, QC

Sound & Vibration Solutions Canada, Inc.
Mr. Andy Metelka - (519) 853-4495
ametelka@cogeco.ca - Acton, ON

Soundtrap Inc.
Roger Foulds - (705) 357-1067
roger@soundtrap.ca - Sunderland, ON

Stantec Consulting Ltd.
Mrs. Zohreh Razavi - (604) 696-8472
zohreh.razavi@stantec.com - Vancouver, BC

State of the Art Acoustik Inc.
Dr. C. Fortier - (613) 745-2003
cfortier@sota.ca - Ottawa, ON

Swallow Acoustic Consultants Ltd.
Mr. John Swallow - (905) 271-7888
jswallow@jsal.ca - Mississauga, ON

Tacet Engineering Ltd.
Dr. M.P. Sacks - (416) 782-0298
mal.sacks@tacet.ca - Toronto, ON

True Grit Consulting Ltd.
Ina Chomyshyn - (807) 626-5640
ina@tgcl.ca - Thunder Bay, ON

Valcoustics Canada Ltd.
Dr. Al Lightstone - (905) 764-5223
solutions@valcoustics.com - Richmond Hill, ON

Vibro-Acoustics
Mr. Tim Charlton - (800) 565-8401
tcharlton@vibro-acoustics.com - Scarborough, ON

Wakefield Acoustics Ltd.
Mr. Clair Wakefield - (250) 370-9302
clair@wakefieldacoustics.com - Victoria, BC

Wilrep Ltd.
Mr. Don Wilkinson - (905) 625-8944
info@wilrep.com - Mississauga, ON

Xscala Sound & Vibration
Jim Ulicki - (403) 274-7577
info@xscala.com - Calgary, AB